



HAL
open science

Consequences of the photooxidation of polycarbonate and polyethylene: relating chemical and/or physical modifications to the change of their permeability

Zhouyun Chen

► **To cite this version:**

Zhouyun Chen. Consequences of the photooxidation of polycarbonate and polyethylene: relating chemical and/or physical modifications to the change of their permeability. *Polymers*. Université Clermont Auvergne, 2023. English. NNT : 2023UCFA0151 . tel-04624613

HAL Id: tel-04624613

<https://theses.hal.science/tel-04624613>

Submitted on 25 Jun 2024

HAL is a multi-disciplinary open access archive for the deposit and dissemination of scientific research documents, whether they are published or not. The documents may come from teaching and research institutions in France or abroad, or from public or private research centers.

L'archive ouverte pluridisciplinaire **HAL**, est destinée au dépôt et à la diffusion de documents scientifiques de niveau recherche, publiés ou non, émanant des établissements d'enseignement et de recherche français ou étrangers, des laboratoires publics ou privés.

UNIVERSITE CLERMONT AUVERGNE
ECOLE DOCTORALE DES SCIENCES FONDAMENTALES
THESE

présentée pour obtenir le grade de

DOCTEUR D'UNIVERSITE

Spécialité : Chimie des matériaux, nanomatériaux et procédés

Par **CHEN Zhouyun**

Master de l'Université de Strasbourg

**CONSEQUENCES OF THE PHOTOOXIDATION OF
POLYCARBONATE AND POLYETHYLENE: RELATING CHEMICAL
AND/OR
PHYSICAL MODIFICATIONS TO THE CHANGE OF THEIR
PERMEABILITY**

Soutenue publiquement le **20 décembre 2023**, devant le jury :

Président :	Christian Ley	Professeur des Universités Université de Haute Alsace
Rapporteur :	Pascal Wong Wah Chung	Professeur des Universités Aix-Marseille Université
Examineurs :	Angélique Bousquet	Maître de conférences Université Clermont Auvergne
	Fanny Coumes	Maître de conférences Sorbonne Université
Directeur de thèse :	Mohamed Sarakha	Professeur des Universités Université Clermont Auvergne
Co-directeur de thèse :	Julien Christmann	Maître de conférences Université Clermont Auvergne

UNIVERSITE CLERMONT AUVERGNE
ECOLE DOCTORALE DES SCIENCES FONDAMENTALES
THESE

présentée pour obtenir le grade de

DOCTEUR D'UNIVERSITE

Spécialité : Chimie des matériaux, nanomatériaux et procédés

Par **CHEN Zhouyun**

Master de l'Université de Strasbourg

**CONSEQUENCES OF THE PHOTOOXIDATION OF
POLYCARBONATE AND POLYETHYLENE: RELATING CHEMICAL
AND/OR
PHYSICAL MODIFICATIONS TO THE CHANGE OF THEIR
PERMEABILITY**

Soutenue publiquement le **20 décembre 2023**, devant le jury :

Président :	Christian Ley	Professeur des Universités Université de Haute Alsace
Rapporteur :	Pascal Wong Wah Chung	Professeur des Universités Aix-Marseille Université
Examineurs :	Angélique Bousquet	Maître de conférences Université Clermont Auvergne
	Fanny Coumes	Maître de conférences Sorbonne Université
Directeur de thèse :	Mohamed Sarakha	Professeur des Universités Université Clermont Auvergne
Co-directeur de thèse :	Julien Christmann	Maître de conférences Université Clermont Auvergne

看似寻常最奇崛，成如容易却艰辛。

王安石

This three-year PhD life in France has given me a wealth of educational and life experience, inseparable from the support and guidance of all the people I received. I want to take the chance to express my gratitude.

First, I would like to express my sincere gratitude to my thesis supervisors, Professor Mohamed Sarakha and Assistant Professor Julien Christmann from Université Clermont Auvergne, for their invaluable guidance throughout my thesis project. They have been like guiding lights in the fog, helping me navigate the complexities of my research. Whenever I faced crossroads, they provided me with signposts, allowing me to unravel the mysteries of my work. I am truly grateful for their passion and professionalism in science.

This thesis project was conducted full-time at the Institute of Chemistry Clermont Ferrand (ICCF), specifically within the Photochemistry team (together in the “Polymers, Photochemistry, Properties and Interfaces” and “Photochemistry, Reactivity and Environment” groups). I want to acknowledge Fabrice Leroux, the director of ICCF, and Sandrine Thérias, the director of the photochemistry team, for welcoming me into this organization.

I would also like to take this opportunity to extend thanks to the members of my jury for examining my work and providing valuable insights: Professor Christian Ley from the Université de Haute-Alsace, Professor Pascal Wong-Wah-Chung from the Université Aix-Marseille, Assistant Professor Fanny Coumes from Sorbonne Université, and Assistant Professor Angélique Bousquet from Université Clermont Auvergne.

I also thank Jean-Luc Gardette for the insightful discussions surrounding my thesis work.

Furthermore, I would like to express my appreciation to the individuals who contributed to obtaining experimental results at ICCF: Martin Lereboure for the chromatography experiments; Marine Benedict, a student from Gien, for advancing the project; Nicolas Batisse for sample

preparation; Jean-Michel Andanson for microscopy infrared experiments; David Bourgogne for the atomic force microscopy experiment.

I would also like to thank all the members of the photochemistry team, including permanent members, doctoral students, post-docs, and interns who were part of the team during these years—Albert, Mohammed, Emma, Nathan, Florian, Loélia, Luna, Floriane, and others. Thank you all for the memorable moments in the lab.

I would also like to thank the administrative staff of the ICCF and Université Clermont Auvergne: Stéphanie Bonnefoy, Aurélie Violette, and Emilie Habouzit for their efficiency and kindness.

I thank Covestro for generously providing the Polycarbonate films used in this study.

Furthermore, I wish to thank Université Clermont Auvergne and the Ministère de l'Enseignement Supérieur, de la Recherche et de l'Innovation (MESRI) for funding this research project titled 'Consequences of the photooxidation of polycarbonate and polyethylene: Relating chemical and/or physical modifications to changes in their permeability.'

Finally, I would like to express my profound gratitude to my family, girlfriend Delin, parents, and grandparents for all the motivation and encouragement they have provided me. Without their support, none of this would have been possible.

Publications and communications

Published Manuscripts

Zhouyun Chen, Mohamed Sarakha, Julien Christmann

"Consequences of sequential photooxidation of polycarbonate: Relating microscopic modifications to the change of oxygen permeability." *Journal of Applied Polymer Science*, 2023, 140(37): e54397.

doi.org/10.1002/app.54397

Zhouyun Chen, Julien Christmann*, Mohamed Sarakha

"Evaluating the effect of photoaging on polyethylene permeability: measurement of the transport properties in liquid phase." *ACS Applied Polymer Materials*, 2024, 6, 1, 496–503.

doi.org/10.1021/acscpm.3c02178

Oral presentations

2022 Jun. 7th - 8th

Journées Annuelles SP2P'22 at École Normale Supérieure Paris-Saclay, France

Zhouyun CHEN, Julien CHRISTMANN, Mohamed SARAKHA

The association between polycarbonate photoaging and oxygen permeability

2022 Jul. 1st

Demi-Journée de l'ICCF at Institut de Chimie de Clermont Ferrand, Clermont Ferrand, France

Zhouyun CHEN, Julien CHRISTMANN, Mohamed SARAKHA

Polycarbonate photoaging and its influence on gas barrier property

2022 Oct. 24th – 28th

Matériaux 2022 at Grand Palais, Lille, France

Zhouyun CHEN, Julien CHRISTMANN, Mohamed SARAKHA

Effect of polycarbonate photoaging on its permeability

2023 Jun. 12th – 15th

34th PDDG Conference at Hilton Hotel, Dubrovnik, Croatia

Julien CHRISTMANN, Zhouyun CHEN, Mohamed SARAKHA

Sequential photooxidation of polycarbonate: consequence on its oxygen permeability

Posters

2021 Oct. 5th – 6th

Journées de remise des prix SCF at Maison de la Culture, Clermont Ferrand, France

Zhouyun CHEN, Julien CHRISTMANN, Mohamed SARAKHA

Effect of photoaging on polycarbonate oxygen permeability

Table of Contents

Table of Contents

Table of Contents	11
General introduction	15
Chapter 1: Literature study	21
1. Introduction	23
2. Permeability	23
2.1. History of permeability	23
2.2. Permeability description and measurement	26
2.3. Factors influencing polymer permeability	36
2.4. Applications of polymers dealing with permeability	41
3. Polymers and aging	45
3.1. Aging of polymers	45
3.2. Photoaging of the selected polymers	51
4. Photoaging of polymer and the correlation with permeability	62
References	66
Chapter 2: Experimental part	81
1. Introduction	83
2. Samples	83
2.1. Polymer samples	83
2.2. Solvents	83
2.3. Permeants for liquid permeability experiments	84
3. Aging devices	84
3.1. Photoaging equipment	84
3.2. Thermal aging equipment	85
4. Characterization of the polymers	86
4.1. Spectroscopic methods	86
4.2. Permeability methods	96
4.3. Other methods	102
References	106

Chapter 3: Oxygen permeability on polycarbonate and polyethylene: effect of photoaging	109
1. Introduction	111
2. Consequences of sequential photooxidation of polycarbonate	113
2.1. Introduction	113
2.2. Results and discussion	117
2.3. Conclusion	129
2.4. Acknowledgments	130
2.5. Supplementary Information	131
3. Photoaging of polyethylene and its O ₂ permeability	137
3.1. Introduction	137
3.2. Results and discussion	138
3.3. Conclusion	146
4. Conclusion	147
References	149
Chapter 4: Permeability of carbazole and naphthalene derivatives solutions on polyethylene: effect of photoaging	157
1. Introduction	159
2. Evaluating the effect of photoaging on polyethylene permeability	162
2.1. Introduction	162
2.2. Results and discussion	165
2.3. Conclusion	176
2.4. Acknowledgments	177
2.5. Supplementary Information	178
References	186
Chapter 5: Permeability in gas phase on polyethylene	191
1. Introduction	193
2. Results and discussion	194
2.1. Transmission rates of polar vapours	194
2.2. Transmission rates of non-polar vapours	198
3. Conclusion	200
References	201
General conclusion & perspectives	203

General conclusions	205
Perspectives	210
Abstract	213
Résumé	213

General introduction

Polymer materials play an essential role and offer numerous applications in our daily lives, including, for example, packaging, agriculture, car industry or construction. Their advantages, such as easy fabrication, relatively low cost, plasticity or lightness, have primarily contributed to their widespread use. However, they also come with disadvantages, such as thermal and photochemical degradation, which reduce their lifetime.

Polycarbonate (PC) and polyethylene (PE) are among the most commonly used polymers. PC is primarily used in car light shields, car windows and some medical materials, while PE finds extensive use in agricultural films, furniture, pipes, etc. In these usage scenarios, PE and PC are exposed to different environmental influences, such as light, heat, humidity, and oxygen. This can lead to changes in their physical and chemical properties, also referred as aging. Such alterations (reversible or not) are more likely to reduce their usability.

Among the numerous properties which can be affected by aging, it would be of great interest to consider the barrier properties of a polymer because these properties are essential in numerous applications such as packaging, protective coatings or membranes. Permeability is a concept used to describe the ease with which gases or vapours can transmit through a material such as a polymer. Several commercially available testing methods exist, such as oxygen and water vapour permeability testers. However, when considering the transport of permeants dissolved into a solvent, no commercial setup is currently available.

This thesis aims to answer the following question: "How does the photoaging of a polymer affect its permeability?". More precisely, we would like to establish a connection between the consequences of photodegradation and the corresponding changes in the permeability of polymers in both gas and liquid phases. The latter case will require the development of a self-designed setup. This study will then be valuable for better understanding the behaviour of polymer materials under aging conditions and expanding methods to measure permeability in the liquid phase.

The present manuscript is structured into five chapters and a conclusive part.

The first chapter builds upon prior research in three key areas: permeability, polymer (photo)aging and the consequences of photoaging on polymer permeability. The permeability section presents the concept, measurement methods, and applications of this phenomenon. The polymer aging section introduces the concept of aging and deals more specifically with the photoaging of PE and PC. The final part explores previous studies on the influence of photodegradation on polymer permeability.

The second chapter presents the experimental part of this study. It covers the materials used and the procedures for sample preparation. It also elaborates on the aging and characterization equipment employed for the polymers. Finally, it introduces the experimental setups dedicated to the measurement of permeability.

The third chapter attempts to demonstrate the relationship between changes in oxygen permeability and the photoaging of PC and PE films. It shows that the physical, chemical, and optical changes resulting from the photoaging of these polymers result in a reduction of their oxygen permeability. Sequential photoaging of PC caused an unexpected result: while oxygen permeability decreased when only one face of the film was exposed to light (that can be associated with polarity increase as well as cross-linking), no further decrease was observed when the second face was photoaged (explained by a so-called “funnel effect”). For PE, the decrease of oxygen permeability might be attributed to the increase of polarity as well as chemicrystallization. In addition, the activation energy of permeation was calculated at several photoaging times from Arrhenius plots and discussed.

The fourth chapter presents results about permeability in the liquid phase for PE upon photoaging. Polar and non-polar permeants derived from naphthalene were dissolved into methanol and their transmission rate across PE films at different stages of photoaging were measured with a self-

designed setup. Different behaviour for polar and non-polar permeants reveals the crucial role of polarity change upon photoaging for the barrier properties of PE.

The fifth chapter presents preliminary results about the permeability of PE to polar (ethanol, methanol) and non-polar (hexane, cyclohexane) vapours determined by a gravimetric method. The properties and changes observed during PE photoaging further supported and validated the conclusions made in the previous chapter about the role of polarity increase upon photoaging on the permeability.

The manuscript ends with a general conclusion and possible perspectives that can be drawn for a better understanding of the relationship between the photoaging of polymer and the permeability.

Chapter 1: Literature study

1. Introduction

The main objective of this thesis is to investigate in depth the correlation between the permeability properties and the photoaging of polymers. These two topics have been extensively studied individually. Since building upon existing knowledge before focusing on the interplay between them is essential, three key aspects will be addressed in this chapter. Firstly, the concept of permeability will be presented along with the corresponding mechanism, influencing factors as well as measurement techniques. Secondly, the focus will shift towards the (photo)aging of polymers, more particularly the corresponding general mechanism and its consequences on the chemical structure, macromolecular architecture, and properties of polymers. A focus will be addressed on the photoaging mechanisms of the selected polymers (*i.e.* polyethylene and polycarbonate). Lastly, existing work about the consequences of photoaging on polymer permeability will be reviewed.

2. Permeability

2.1. History of permeability

Permeability is a property that quantifies the ease of transport of a compound through another. The concept of permeability has a long history, rooted in ancient engineering and agricultural practices. The ancient Romans, for example, used permeable soil layers in their aqueducts to control the water tunnel [1, 2].

2.1.1. Discovery of the permeation

The first scientific studies on permeability can be traced back to the 18th Century, when scientists and engineers began to discover the movement of fluids through materials, including one of the experiments recorded by the French physicist Abbé Jean-Antoine Nollet in 1748. He used a pig bladder to store alcohol into water and discovered the transfer of alcohol through the material [3,4].

2.1.2. Scientific description of permeation

In the 19th Century, advances in science and experimentation led to a better understanding of the factors that influence permeability, such as fluid properties and molar mass of permeants.

In 1829, the Scottish scientist Thomas Graham observed the gas transport through membranes [5]. He measured the rate of diffusion of gases through a small hole and found that it was inversely proportional to the square root of its molecular weight. This is known as Graham's law of diffusion [6]. In 1855, German physicist Adolf Fick attempted to quantify the process of mass diffusion, which was derived by analogy with Fourier's law of heat conduction, Ohm's law for electrical conduction, and Newton's law for momentum transfer [4, 7].

Thomas Graham further proposed in 1866 that the permeation of the gas through rubber was analogous to the solution of a substance dissolving into a solvent. He believed that the first absorption of gas by rubber was due to a chemical affinity between the gas and the rubber and that the liquefied gas would wet the rubber and reappear as a gas on the other side [8]. The basic principles of this solution-diffusion model have been refined and expanded over the years. Still, the core idea of solubilization due to a chemical affinity between the gas and the material remains an important part of the modern understanding of gas permeation. Then, in 1879, the Polish

physicist Szymunt von Wróblewski showed that the gas solubility in rubber obeyed Henry's law (which states that the concentration of a gas dissolved in a liquid is proportional to the gas pressure above the liquid) [9].

These discoveries and understandings form the basis for developing permeability measurement techniques.

2.1.3. Measurement of the gas permeability

Harold Dayne [10], in 1920, demonstrated that the pressure difference between the two sides of a material could be used to measure the diffusion and solubility of a gas and emphasized the importance of measuring at least two coefficients among the permeability (P), solubility (S), and diffusion (D) coefficients (*vide infra*). Moreover, Dayne developed the time-lag method to determine the solubility and diffusion coefficients during permeability experiments.

New Zealand chemist Richard Barrer [11] was inspired by the previous work by Earle Schumacher and Lawrence Ferguson [12] and designed in 1939 a system where he placed a sample of a polymer between two chambers. He used the pressure difference between these two chambers to measure the time for the gases to permeate through the polymer from one chamber to the other [13]. Then, he extended the work from Dayne's time-lag method. This work was used to determine the permeability of a polymer to a gas. The experiment was considered one of the earliest studies in measuring permeability.

Today, permeability is a central concept in geology, civil engineering, and environmental science fields. It continues to play an essential role in designing and optimizing structures and systems that involve flow through polymer media.

2.2. Permeability description and measurement

2.2.1. Description of the permeation process

Based on works of Harold Dayne and Thomas Graham, the main process of a gas or a vapour or a liquid permeating through a polymer can be described as a solution-diffusion model, as shown in Figure 1.1. It has to be emphasized that the term "gas" refers to compounds in the gaseous state at ambient conditions while "vapour" is associated with the molecules in the gas phase in equilibrium with liquid compounds. The main steps of this model are:

- Gas/vapour molecules enter the surface of the polymer from the gas phase and dissolve into the polymer matrix. The amount of the dissolved gas/vapour molecules is proportional to the solubility (S) of the gas/vapour in the polymer.
- Gas/vapour molecules diffuse through the polymer matrix from regions of high concentration to regions of low concentration at a rate proportional to the gas/vapour diffusivity (D) in the polymer.
- Gas/vapour molecules exit the polymer surface and go to the gas phase. The amount of the gas/vapour is proportional to the gas/vapour solubility (S) in the polymer.

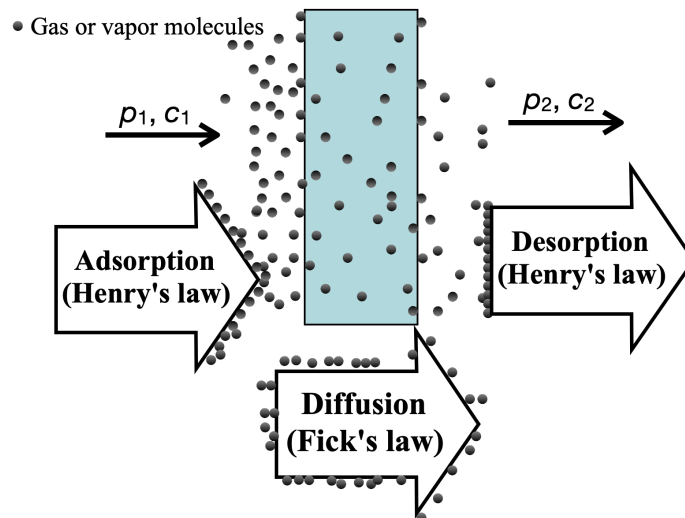


Figure 1.1. Gas/vapour permeation process [14].

To describe permeability mathematically, the permeation flux of a specific gas or vapour (J) depends on the amount of the gas or vapour (Q), the surface area of polymer contact (A), and the duration of passage (t). The following equation can represent it:

$$J = \frac{Q}{At} \quad \text{Eq. 1}$$

According to Fick's first law, the permeation flux (J) has a linear relationship with the concentration gradient between the two sides of the polymer. In the simplest case of 1D permeation (*i.e.* thickness of the polymer by far lower than its other dimensions), it is written as:

$$J = -D \times \frac{\partial C}{\partial z} \quad \text{Eq. 2}$$

where D is the diffusion coefficient of the gas/vapour (expressed in $\text{cm} \cdot \text{s}^{-1}$); C is the concentration of the gas/vapour dissolved in the polymer (expressed in $\text{cm}^3 \cdot \text{cm}^{-3}$ for gases or $\text{kg} \cdot \text{cm}^{-3}$ for vapours), and l is the thickness of the polymer (expressed in cm). This simple 1D permeation case is adequate to describe the gas transport through the thin (from 30 to 150 μm) polymer films tested in this study.

As stated by Henry's law, the concentration of gas/vapour dissolved in the polymer is proportional to the gas/vapour pressure ahead of the polymer. Previous works have demonstrated the validity of applying Henry's law to the sorption of gas/vapour into a polymer [9]:

$$C_1 = S \times p_1 \quad \text{Eq. 3}$$

$$C_2 = S \times p_2 \quad \text{Eq. 4}$$

where 1 and 2 represent the two different sides of the polymer sample, and p is the partial pressure of the gas/vapour (expressed in Pa).

The concentration difference between side 1 and side 2 (ΔC) can be further represented as:

$$\Delta C = S \times \Delta p \quad \text{Eq. 5}$$

where S is the solubility coefficient of the gas/vapour (typically expressed in $\text{kg}\cdot\text{cm}^{-3}\cdot\text{Pa}^{-1}$ for vapours or $\text{cm}^3\cdot\text{cm}^{-3}\cdot\text{Pa}^{-1}$ for gases) and Δp is the pressure gradient between the two sides of the polymer ($\Delta p = p_1 - p_2$, expressed in Pa). During the process of permeation, there is a steady state when the flux passing through the polymer sample becomes constant.

The diffusion coefficient (D) and the solubility coefficient (S) are independent of the permeant concentration at the steady state [9, 15]. As a result, Eq. 2 and Eq. 5 can be combined and the flux of the gas/vapour passing through a polymer can be expressed as:

$$J = -DS \frac{\Delta p}{l} \quad \text{Eq.6}$$

The product DS is ultimately defined as the permeability coefficient (P):

$$P = D \times S \quad \text{Eq.7}$$

In order to describe usual cases, researchers have made great efforts to expand and improve the mathematical description of the permeation mechanism theory [15, 16]. For example, when operating in the normal densified region and intersegmental defects (holes), two sorption models can be applied, which are described by Henry's law and Langmuir's model respectively [17]. Langmuir's law states that a molecule can absorb and reach a steady state of solubility by creating a molecular layer on the surface of the polymer membrane.

The solubility coefficient can be expressed using these models:

$$S' = S + \frac{C_H}{1+b_p} \quad \text{Eq.8}$$

where the C_H and b_p are the hole saturation and the hole affinity constants respectively [17].

Progresses using simulation and different models, especially for the permeation process in glassy polymer membranes [18, 19], are still a topic of study.

2.2.2. Measurement of gas/vapour permeability

This part deals with methods commonly used to measure the permeability of different gases/vapours. Understanding the main principles of measuring permeability is of particular interest within the context of this study, involving the development of an experimental setup for measuring permeability in the liquid phase. Oxygen and water being the permeants most usually studied, permeability methods are more developed and described for them. However, research teams also developed setups to measure the permeability of other gases/vapours, which are described at the end of this section.

Measurement of oxygen permeability

The method for measuring oxygen permeability at temperatures below 60 °C has been well-developed and standardized through ASTM D3985 [20]. A standard method for measuring the oxygen permeability of a polymer is to use a gas permeation cell [21] (Figure 1.2). This cell consists of two chambers separated by the polymer sample. One chamber is filled with pure oxygen at a known pressure and temperature, while the other chamber is either evacuated or filled with an inert gas.

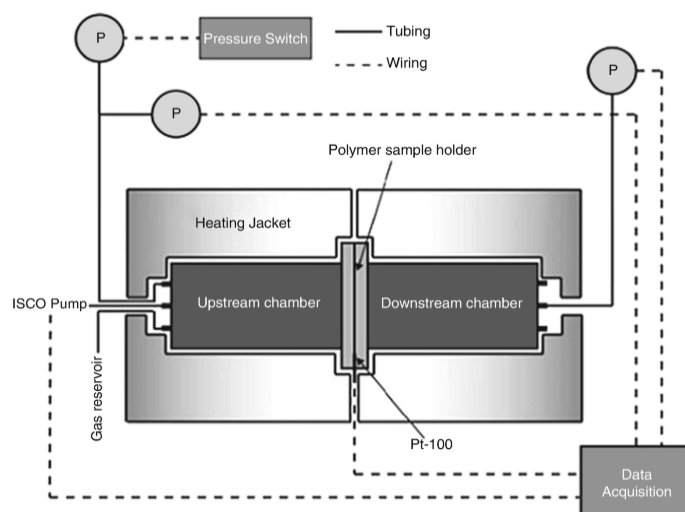


Figure 1.2. Example of a permeability cell for oxygen [21].

The oxygen flow (J) that permeates through the polymer film over time is then measured using an analytical device such as a mass spectrometer or an electrochemical sensor. The flow of oxygen (presented as the Oxygen Transmission Rate or OTR in the apparatus) at the steady state could be converted into permeability coefficient (P):

$$P = OTR \frac{l}{\Delta p} \quad Eq.9$$

Permeability coefficient P is more appropriate than OTR to describe and compare the permeability of different materials since it is independent of the sample thickness l and pressure difference Δp during analysis.

The diffusion coefficient D can be determined experimentally using the time-lag method [10, 22, 23]. Specifically, the tested polymer, initially free from the target gas, is suddenly exposed to it on one side at a constant pressure. The other side of the polymer is maintained free from the target gas. An example of typical result obtained for a time-lag experiment is depicted in Figure 1.3 (amount of the permeation gas Q as a function of the time t). The graph can be decomposed into three regions:

1. The absorption period (Figure 1.3a) is when the gas dissolves into the polymer and diffuses through it, but does not come out.
2. The transition period (Figure 1.3b) is when the gas starts to desorb from the polymer and is detected. However, the steady state is not reached yet.
3. The steady state period (Figure 1.3c) is when the gas flux is constant.

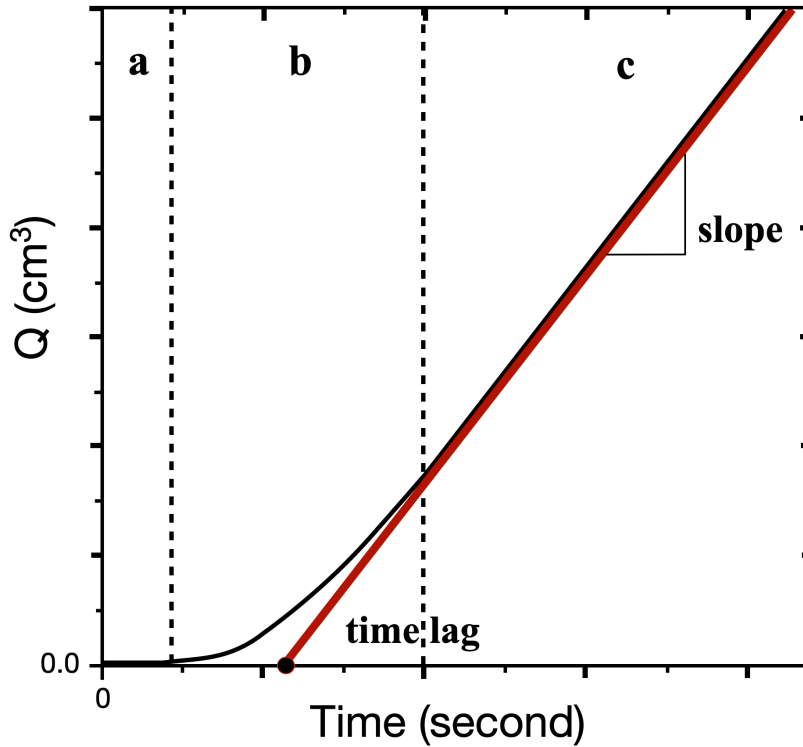


Figure 1.3. Typical curve amount of permeant Q vs. time obtained from a time-lag permeability experiment (with a. The absorption period; b. The transition period; c. The steady state period).

The intersection of the straight line associated with the steady state period with the x-axis (point on the x-axis in Figure 1.3), usually calculated from the steady state linear equation, is called the time-lag t_L . It represents the time at which the first molecule of the target gas desorbs from the testing polymer and is inversely proportional to the gas diffusion coefficient according to [10, 15, 22]:

$$t_L = \frac{l^2}{6D} \quad \text{Eq. 10}$$

From a result similar to that of Figure 1.3, it is possible to extract the OTR value from the slope of the linear part (then converted into permeability coefficient P with Eq. 9), and the diffusion coefficient D from the time-lag value (Eq. 10). The solubility coefficient (S) is ultimately calculated from P and D by using Eq. 7.

Measurement of water vapour permeability

Various methods can be used to measure the permeability to water vapour, including the humidity sensor method as shown in Figure 1.4 (based on ISO 15106-1/ASTM E398 [24]), the gravimetric method (based on ASTM E96/GB 1037), the potassium acetate method (based on ISO 14956), the infrared sensor method (based on ISO 15106-2/ASTM F1249), and the electrolytic sensor method (based on ISO 15106-3). All these methods require a constant temperature, an essential factor influencing relative humidity. The value obtained experimentally is the water vapour transmission rate (WVTR), also called moisture vapour transmission rate (MVTR), which measures the rate at which water vapour passes through a film.

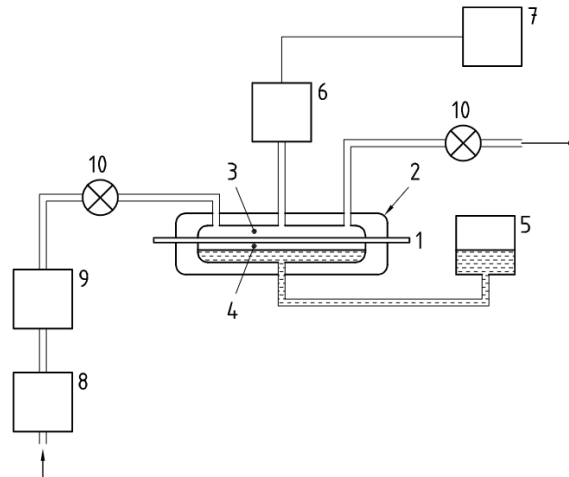


Figure 1.4. Testing method presented in the ISO 15106-1 [24]: 1. sample, 2. transmission cell, 3. upper chamber, 4. lower chamber, 5. water reservoir, 6. humidity sensor, 7. Recorder, 8. pump, 9. drying tube, 10. stop valve.

The humidity sensor method described in ISO 15106-1 process is as follows:

1. Two chambers in the transmission cell (2 in Figure 1.4), one lower (high-humidity) chamber (4) and one upper (low-humidity) chamber (3), with the test specimen (1) installed between them.
2. A humidity sensor (6) is installed in the upper chamber to measure the relative humidity.

3. A pump (8) is used to supply air to the upper chamber.
4. A drying tube (9) and water reservoir (5) are used to control the humidity during experiment.
5. The upper chamber is designed to collect and monitor the relative humidity of the water vapour passing through the specimen, thanks to the humidity sensor (6) and a recorder (7).

The gravimetric method, known as the cup method [25], involves a water cup sealed with the testing polymer sample. A relative humidity difference is created between the inner cup and the outer environment at a constant temperature, causing water vapour to permeate through the polymer sample to the drier side. The WVTR can be calculated by recording the mass loss of the cup as a function of time. The potassium acetate method [26] is a variation of the gravimetric method. A solution of saturated potassium acetate is added to the test cup to a level of about two-thirds of the cup. The sample is then sealed in the test cup; as the potassium acetate is highly dissolving water, the solution could absorb the water vapour from the environment. The increasing mass of the test cup is measured at a constant temperature, and the WVTR can be calculated from this measurement. The potassium acetate could also be replaced by other compounds with similar water-dissolving properties, such as sodium bromide [27], etc. These two methods for WVTR could also be adapted to other liquids.

The infrared sensor method [28] is an excellent alternative to the gravimetric method and is more similar to the humidity sensor method presented earlier. It requires two testing chambers, with the polymer sample in the middle to separate them. One chamber has low relative humidity (stable), while the other has high relative humidity with water vapour at a constant temperature. As the relative humidity difference is created, water vapour permeates through the polymer sample. Transmitted vapour is carried by a dry gas to an infrared sensor which can detect the water vapour and output an electrical signal. This signal is further treated to output the WVTR. The infrared sensor can be replaced by electrolytic sensor, with the basic principle of the method is unchanged.

Measurement of the permeability of other gases

Methods for measuring the permeability of other compounds, such as methanol and ethanol, have also been developed.

Petrusová Z. et al. [29] reported the measure of the hexane vapour permeability through polyethylene. The test requires two chambers with the polyethylene films separating them. One chamber is filled with a hexane vapour flow, while the other is filled with nitrogen. The research team designed a system to monitor the hexane flow and control the pressure in the different chambers. The principle of this measurement is similar to oxygen permeability testing. However, the difficulty with this kind of self-built experimental setup is to achieve a steady flow.

Wootthikanokkhan J. et al. [30] reported a method to measure the permeability of methanol for direct methanol fuel cell membranes based on sulfonated PEEK/PVDF blends. The researchers used two compartments separated by the polymer testing sample: one with methanol dissolved in water solution (A) and the second one with pure water (B), both under magnet stirring. To achieve the methanol transmission rate, the water compartment is measured as a function of time by using a gas chromatography (GC) technique with an FID detector. The following equation was finally used to calculate the permeability of methanol:

$$C_B(t) = \frac{APC_A(t - t_0)}{V_B L} \quad \text{Eq. 11}$$

In Eq.11, the C_A and C_B are the concentration of methanol, and V_B is the volume in compartments B. A and L are the area and thickness of the membrane, and P is the permeability coefficient.

Jansen J.C. et al. [31] presented two methods to measure the permeability of organic vapours through PE and polydimethylsiloxane using barometric and differential flow permeation methods.

The barometric method [32] measures the pressure increase at the steady state flow to determine

not only the permeability coefficient using the permeation curve but also the diffusion coefficient using the time-lag method. The differential flow permeation method [33] requires a home-built instrument, which measures the thermal conductivity changes directly related to the vapours passed on the permeate side as a function of time. It was possible to evaluate D from the amount of the transferred gas as a function of time and P from the steady state.

In the view of designing an experimental setup for measuring permeability in the liquid phase, some basic principles can be extracted from these methods:

- A concentration gradient has to be created between the two sides of the polymer sample.
- The permeant molecule has to be driven to the detector by a "neutral" (*i.e.* to which the detector is not sensitive) compound (gas, solvent...).
- The detector has to be able to detect quantitatively the amount of permeant.

These principles will be applied to design an efficient system in Chapter 4. Alternatively, the gravimetric method can also be used for vapours in Chapter 5.

2.3. Factors influencing polymer permeability

This chapter presents the factors that could affect polymer permeability, related to the environment, the polymer, and the permeant.

2.3.1. Environment

Humidity: Humidity can trigger some hydrophilic polymers to increase their permeability [34]. Engarnevis A. et al. [35] tested the permeability of different types of polymer membranes with different humidity levels. They showed that the water vapour permeability increases with relative humidity in all polymer samples. The researchers' founding agrees with the previous analysis [36-38], reasoning that this effect is caused by the plasticizing effect of water vapour on the polymer matrix at higher humidity that further increased sorption of water vapour. A similar plasticizing effect could be observed in polymers containing polar groups [39]: higher humidity increases the oxygen permeability of these polymers.

Temperature: The permeability changes with temperature. The Arrhenius law for transport parameters (solubility, diffusion, and permeability) can be expressed in the following forms [34, 40]:

$$P = P_0 \exp\left(-\frac{E_P}{RT}\right) \quad \text{Eq. 12}$$

$$D = D_0 \exp\left(-\frac{E_D}{RT}\right) \quad \text{Eq. 13}$$

$$S = S_0 \exp\left(-\frac{\Delta H_s}{RT}\right) \quad \text{Eq. 14}$$

where P_0 , D_0 and S_0 are the pre-exponential factors; R is the perfect gas constant; E_p is the activation energy of permeation, which is the sum of the activation energy of diffusion E_d and the molar enthalpy of solubilization ΔH_S .

$$E_p = E_d + \Delta H_S \quad \text{Eq. 15}$$

Mrkić S. et al. [41] reported different parameters, such as the E_p , E_d and ΔH_S , of oxygen, carbon dioxide, nitrogen, and air of PE, PA, PA/PE, BOPP, and BOPP/PE.

The sign of the activation energy of diffusion E_d and the molar enthalpy of solubilization ΔH_S is the key to understanding the changes of D and S with temperature. The activation energy E_d is always a positive value. Therefore, D always increases with the increase of temperature. In the case of S , the influence of the temperature is more complex. Actually, ΔH_S is expressed as [42, 43]:

$$\Delta H_S = \Delta H_{cond} + \Delta H_1 \quad \text{Eq. 16}$$

ΔH_{cond} is the molar heat of condensation, which is always small and negative [44]; ΔH_1 is the partial molar heat of mixing, a small and positive term [45]. For a gas above its critical temperature at ambient conditions (O_2 , N_2 , and H_2 for example), ΔH_{cond} is very weak and ΔH_S is governed by ΔH_1 . Henceforth, ΔH_S is positive and S increases with the temperature. As both D and S increase, the permeability coefficient P increases; However, for other gases, which are more condensable (CO_2 , SO_2 , NH_3 , and hydrocarbons), ΔH_{cond} is higher, and ΔH_S becomes then negative. Ultimately, S decreases for such systems [46]. In such a case, with D and S showing opposite changes, the impact on the permeability coefficient P is uncertain.

Turan D. et al. [47] analysed the gas permeability of polyurethane films for fresh vegetable product packaging. The study evaluated the oxygen permeability at different temperatures, ranging from 5 °C to 55 °C. The researchers found that at lower temperatures (5 °C to 30 °C), the oxygen permeability follows an Arrhenius-type dependence, increasing with temperature due to enhanced

motion of the polymer chain and increased energy of permeating molecules. However, the Arrhenius-type dependence was weak at higher temperatures (above 38 °C). The researchers explained this phenomenon with the results of differential scanning calorimetry (DSC) of the polyurethane, which show that after reaching the melting temperature of the soft segment (24 °C), the permeability of the film increases significantly due to the transition of the soft segments in the polymer from a crystalline state to an amorphous state.

2.3.2. Polymer

Crystallinity rate: permeating gas or vapour exclusively crosses the polymer only through its amorphous region [48]. This is because the restricted mobility of polymer chains in the crystalline region hinders diffusion. Conversely, in the amorphous region, diffusion and sorption occur more easily. So the increase of the crystallinity rate leads to the decrease of the permeability. Michaels A.S. et al. [49] discovered a linear relationship between the permeability and the amorphous rate of the polyethylene. Kofinas P. et al. [50] reported that the permeability of several gases through semi-crystalline polyethylene/poly(ethylene-propylene) copolymers decreases with the increase of crystallinity.

Density: the amorphous part density has a close relationship with the permeability, as the free volume is the area where the permeant moves across the polymer. Sha H. et al. [51] found a linear decrease of the CO₂ permeability in PE with the increase of the amorphous density, which is caused by the increase of lateral order during the process.

Cross-linking: it is reported that cross-linking decreases the permeability, as the free volume and mobility of the polymer decreases when chains cross-link. Wu S. et al. [52] investigated the influence of cross-linking on oxygen permeability, and the result showed a decrease in oxygen

permeability with the increase of cross-linking. Lin H. et al. [53] prepared poly(ethylene glycol diacrylate) of different cross-link densities. They took extra care during the preparation to other properties such as T_g , and made sure the fractional free volume was in the same range so that the cross-linking results could be compared. The team observed a decrease in gas permeability with higher cross-link density.

Molecular mass: this factor is expected to have an effect on the permeability [34]. Generally speaking, the higher the molecular mass of a polymer, the more entanglements. This reduces the free volume and the mobility within the polymer. Andersson H. et al. [54] presented ethyl cellulose (EC) and water-soluble hydroxypropyl cellulose (HPC) membranes of different molecular mass by modifying the amount of EC. Their results showed that the water permeability decreases in the EC/HPC films with higher molecular mass. The researchers concluded that the molecular weight of EC influences the mass transfer rate through final films, because there are the less and less permeable domains when increasing the amount of EC.

Polarity: the permeation of a gas or vapour through a polymer is analogous to the dissolution of a substance in a solvent. It is known that substances with similar polarities are more likely to dissolve in each other. Therefore, a non-polar polymer could have a higher permeability for a non-polar gas. Houde A.Y. et al. [55] tested the permeability of different substituted polyarylates to different gases (mostly non-polar). The team concluded that the polar nature of the substituents at the polyarylate bridge carbon harms on transport properties of non-polar gases tested.

2.3.3. Permeant

Shape: Berens A.R. et al. [56] studied the diffusion of a wide range of gases and vapours in poly(vinyl chloride), polystyrene, and polymethylmethacrylate. It was found that the n-alkanes, elongated or flattened, present higher diffusivity than the spherical molecular with similar size and mass. A similar study [57] on solubility also found a linear relationship between solubility and the permeant molar volume (represented by the shape of the molecular).

Polarity: Tufani A. et al. [58] tested the permeability of two dyes: Alizarin Yellow (AY) and Phenylazodiphenylamine (PADPA) in poly(2-hydroxyethyl methacrylate), p(HEMA) film. AY and PADPA are similar in size, and only the AY has polar groups (-OH and -NO₂). The AY shows a quicker (4 times higher in 25 hours) permeation of the dyes than PADPA due to its polar similarity with the p(HEMA) film.

Size or mass: it is found that an increase in permeant size provokes an increase in solubility as it requires more energy for solubilization [57]. And permeants with larger sizes have a lower diffusion coefficient because of the need for critical activation permeant volume inside the polymer during the diffusion process [39, 56]. With both the sorption and diffusion processes affected, the permeation process is surely influenced.

In conclusion, the permeability can be influenced by a variety of factors. Permeability changes are rarely a consequence of a single reason; instead, they often result from the contributions of multiple factors.

2.4. Applications of polymers dealing with permeability

Permeability plays an important role in different industries, such as packaging, medical devices, protective coating, and fuel cells. In the following part, these applications will be described.

2.4.1. Packaging

In the food industry, the permeability of packaging materials is carefully controlled as it is a critical evaluation criterion. When preparing a material for the food packaging market, a crucial step is to conduct simulation experiments. Observing the material's permeability under commercial and household food processing methods such as microwaving, freezing, and sterilization can determine whether the permeability meets the required standards. This helps to ensure the safety and quality of the food, and that the packaging material is suitable for use in the food industry.

Cava D. et al. [59] studied different polymers, including PET, PHBV and PCL, to evaluate their resistance to aroma absorption during the stocking process, as well as their solvent resistance to toluene and ethanol, and their oxygen barrier properties. The authors found that biopolymers, such as PHBV, have lower permeability for oxygen, water vapour, and aroma (limonene). However, traditional PET films still outperformed some biopolymers such as PCL. The study did not establish a direct correlation between the nature of the polymer and its barrier properties.

Galić and Ciković [60] investigated the gas permeance characteristics of a triplex film PET/PET-SiO_x/PE. SiO_x is considered an effective oxygen barrier in packaging. The team evaluated the gas barrier properties of the triplex film under various temperature and relative humidity conditions using the manometric method and a permeability testing device. The permeability of different gases (nitrogen, carbon dioxide, and oxygen) was measured with samples treated with various solvents

(ethanol, acetic acid, water, and air). The solvent permeability of the samples was determined by analysing the mass increase (Δm) after immersion in the solutions for an exposed area. The team presented a method for estimating the activation energy by studying the properties of gases without using the Arrhenius law due to an inflection point in the gas permeability measurements. They further found that the gas permeance decreases after treatment with solvents such as water and alcohol due to the formation of extensive hydrogen-bonded networks and strong hydrogen bonding with polar materials. The researchers concluded that the coating material, coating thickness, and surface morphology are key factors affecting the permeability of the triplex film and that the protective coating and gas barrier are effective during processing, handling, and contact with liquid media.

2.4.2. Medical devices

Polymer permeability controls drug delivery in medical devices such as membranes and implantable devices. A multilayer material with polymer and ceramic (SiO_x) was tested by Hogg A. et al. [61]. The team tested the helium gas and water vapour permeability of this material. The gas permeability was measured using a helium leak test system, which consists of a gas injection on the left of the testing membrane to create He flow and a mass spectrometer on the right of the testing membrane chamber to calculate the He amount. The results showed that He permeability hugely depends on the thickness of the membrane; the higher the thickness, the better barrier properties for the film. The water vapour permeability was tested with the calcium mirror test. Calcium is highly reactive with water to form calcium hydroxide, which will transform the silver colour of the sample into transparent, and it will be ready for visual analysis. The teams found that the performance of the multilayer system regarding the water vapour permeability is better than the

conventional single layer. Roohpour N. et al. [62] tested the water resistance of biodegradable chemically modified polyurethane membranes located at the surface of implantable devices. As an implantable material, it should prevent the ingress of body fluids and the migration of ions, which can lead to corrosion or degradation of the device. Two approaches were used to test the water barrier property of polyurethane: the contact angle and water permeability test. The water contact angle was evaluated to assess the changes in hydrophilicity resulting from the chemical modification of the polymer surface. A water-repulsive surface leads to the reduction of water absorption at the surface of the polymer, leading to less water transport. The water permeability was determined by the gravimetric method. The team concluded that the water permeability of polymer membranes is mainly due to two factors. The first is the polymer's inner property: the soft segment mainly affects the mobility and electrostatic repulsion of the polymer while the solid intermolecular forces of the hard segment reduce the water molecules' movement. The second is the surface hydrophobicity: with the chemically modified surface, the polymer increases the separation of two phases, which can reduce the chain mobility.

2.4.3. Protective coatings

Polymer permeability is also studied to assess the protective effect of coatings against environmental exposure in applications such as building and construction materials, or metals. However, different methods were found in the literature to examine the water permeability of protective coating for buildings to have a quantitative result of the water absorption. Zhang P. et al. [63] studied the effect of polymer (polyurethane and chlorinated rubber) coatings on the water permeability. The building material cement was coated with polymer using a wire rod coater. Water permeability was measured using a sealed table method where the coating cement and the water

contact were fixed. The water permeability was evaluated visually when the water trace appeared. The double-layer polyurethane coating shows the best water protection. However, it is fair to point out that the method used in their study, despite its convenience, is not scientifically useful in our study where the permeability should be estimated in a more quantitative way.

2.4.4. Fuel cells

In fuel cells, permeable polymers are used as proton exchange membranes to control the flow of hydrogen and oxygen ions.

Belkhiri Z. et al. [64] studied how the permeability of porous media affects the velocity and pressure fields in proton exchange membrane (PEM) fuel cells. The article proposed numerical simulations to analyse the impact of permeability on gas diffusion and liquid water transport in PEM fuel cells. The researchers concluded that decreasing permeability affects the concentration and distribution of reactants, and therefore, performance may be reduced due to resistance to the transfer of reactant. The model also enables the understanding of many interactions and complex electrochemical and transport phenomena that cannot be studied experimentally.

Permeability is indeed a very important property of polymers in many usual applications. As shown previously, it is especially dependent on the characteristics of the polymer (crystallinity, polarity...). It is then essential to understand how (photo)aging affects these features to understand the possible changes of permeability upon (photo)aging.

3. Polymers and aging

Polymers (*i.e.* groups of macromolecules made up of many repeating units) are used in countless applications taking advantage of their numerous qualities such as lightness, transparency, low cost, etc. However, when exposed to environmental factors (light, heat, humidity, chemicals [65], γ radiations [66]...), polymers age, what is defined as a non-reversible change of one (or more) of their property(ies). This part is dedicated to the degradation of polymers through (photo)aging, with a special focus on the cases of polyethylene and polycarbonate (which are used in this study).

3.1. Aging of polymers

Several mechanisms can describe the aging of a polymer, depending on the changes it causes in the chemical structure and the environmental factor(s) involved. One has then to differentiate between physical aging (no change of the chemical structure of the polymer) and chemical aging (modification of the chemical structure). Photolysis and thermolysis occur under exposure to light or heat, respectively, in the absence of molecular oxygen, while photooxidation and thermooxidation take place in the presence of oxygen (Figure 1.5). For instance, thermolysis can occur during the processing of a polymer (*e.g.* extrusion) or its combustion. Both photo- and thermooxidation are commonly encountered mechanisms in daily life, and they are further described below.

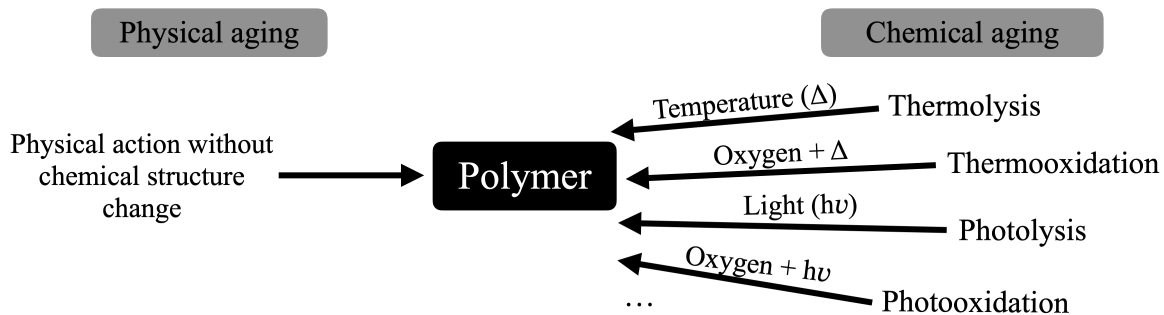


Figure 1.5. Mechanisms of polymer aging.

3.1.1. General mechanism of polymer (photo)oxidation

The oxidation of a polymer involves the chain radical mechanism shown in Figure 1.6 [67, 68].

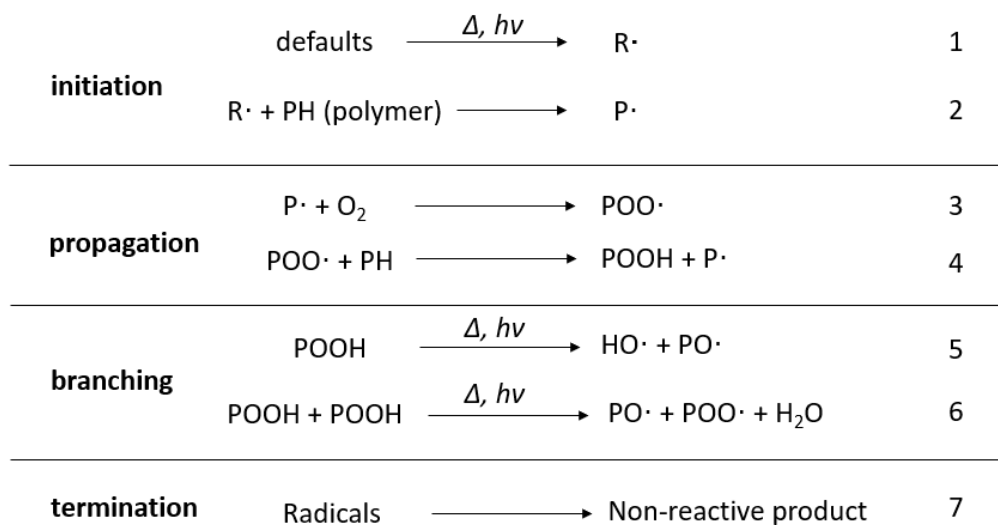


Figure 1.6. Chain radical mechanism of polymer oxidation [67, 68].

This radical chain mechanism involves several steps. The initiation step is linked to the presence of a species sensitive to heat/light (chromophoric group or structural defect, in the polymer chain, impurity such as catalytic residues from the synthesis [69, 70] or side-products from other reactions [71]). Upon an increase of temperature or exposure to light, these defects generate initiating $R\cdot$ radicals (1). These radicals, by tearing off a hydrogen atom from the polymer chain, lead to the formation of a macroradical $P\cdot$ (2). In the presence of oxygen, the reaction could propagate to form macroperoxy radicals $POO\cdot$ (3), and these radicals could continue to abstract hydrogen on the polymer chain PH to form new macroradicals $P\cdot$ as well as hydroperoxides $POOH$ (4). The latter, which are unstable both thermally and photochemically, could decompose into macroalkoxy radicals $PO\cdot$ and hydroxyl radicals $HO\cdot$ (5). Some authors [72, 73] proposed a decomposition mechanism involving two hydroperoxides when their amount is higher than a critical concentration (6). Further decomposition of $PO\cdot$ radicals forms species finally resulting into the formation of

alcohols, carboxylic acids, esters, ketones... In the case of photooxidation, ketones further react through Norrish-I and -II mechanisms (*vide infra*). The chain mechanism terminates (7) by the formation of non-reactive and thermally/photochemically stable products from the radicals.

3.1.2. Thermooxidation

Several researchers investigated the field of thermooxidation of polymers. Celina M.C. et al. [74] introduced the significance of polymer thermooxidation and focused on the complexity of the accelerated thermal aging. They also discussed the importance of thermal aging and lifetime prediction, the relevance of DLO (Diffusion-Limited Oxidation), performance correlation, kinetic models, thermogravimetric analysis) methods, and predictive aging model frameworks. Gardette M. et al. [75] studied the difference between accelerated artificial thermal aging (100 °C) and photoaging of PE. It was found that the number of unsaturated groups affects the rate of thermooxidation, but not that of photooxidation. Moreover, the authors highlighted the dramatic differences between thermal and photoaging, especially in the case of ketones. These species accumulate in the case of thermooxidation while their concentration is very low for photooxidation because of the Norrish-I and -II reactions. Berthumeyrie S et al. [76] investigated the change of thermal and mechanical properties of films made from polylactide (PLA) and PLA/ZnO nanocomposites using Atomic Force Microscopy (AFM), especially nanoindentation and nano-thermal analysis (Vita® mode). The results showed that adding ZnO nanoparticles to PLA films can improve their thermal stability, but also leads to a decrease in their mechanical properties. The study also found that the photodegradation rate of PLA/ZnO nanocomposites is lower than that of pure PLA films under UV irradiation.

3.1.3. Photooxidation

Considering photoaging, polymers can be classified as absorbing ones (*i.e.* able to absorb in the sunlight range – typically $\lambda > 300$ nm, as shown in Figure 1.7 with the black dot line) and non-absorbing ones. For the former, initiation is caused by direct absorption from chromophoric groups in the polymer chains; for the latter, defects and/or impurities trigger the initiation step.

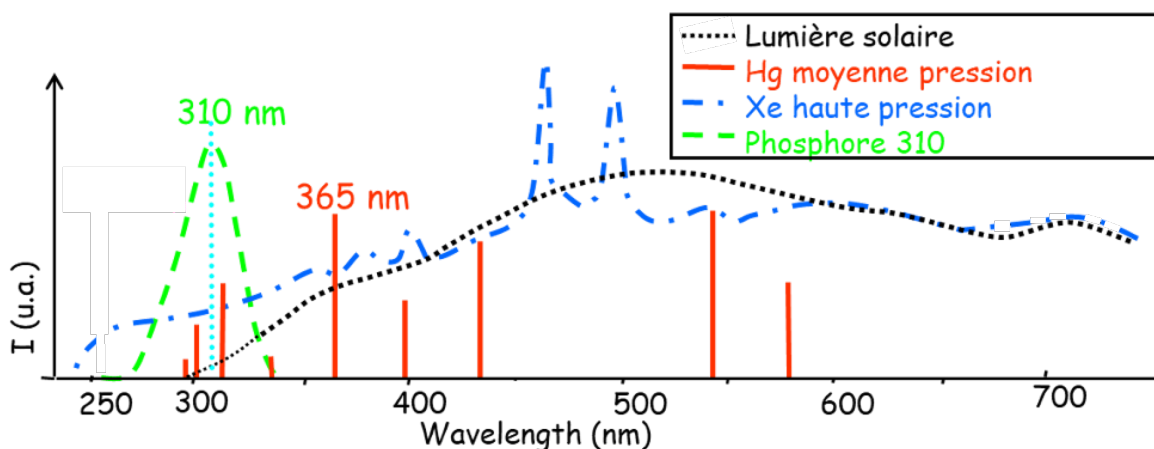


Figure 1.7. Emission spectra of different light sources: Sun (black), medium pressure Hg lamp (red), Xe lamp (blue), and 310 Phosphor lamp (green).

As stated above, one of the main differences between thermal and photochemical aging is the fate of ketones initially present in the polymer or formed upon oxidation. Indeed, the ketones can further react in the presence of light through Norrish-I and Norrish-II reactions [77].

In the Norrish-I mechanism, a bond scission occurs in α position with respect to the carbonyl group upon light exposure (Figure 1.8). This yields an alkyl radical $R_1\cdot$ and an acyl $CH_2-C(O)\cdot$ radical.

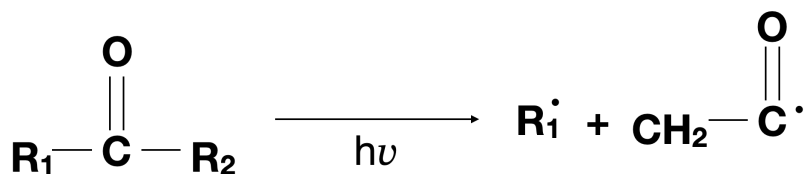


Figure 1.8. Mechanism of Norrish-I reaction.

The Norrish-II mechanism relies on an intramolecular hydrogen abstraction by the carbonyl group (Figure 1.9), followed by a chain scission yielding a vinyl group and an enol. The latter further evolves into a ketone through keto-enol tautomerism, which is able to further react through Norrish reactions.

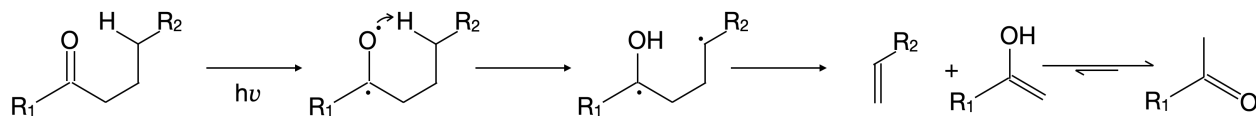


Figure 1.9. Mechanism of Norrish-II reaction.

During this study, the photoaging of polymers was done in an accelerated artificial way thanks to the SEPAP 12/24 system (further described in Chapter 2). Artificial photoaging [78] is a process that simulates the effects of natural aging on materials by exposing them to artificial light sources and other physical factors. The principle of accelerated photoaging assumes that the chemical reactions that cause the degradation of materials are accelerated by increasing the intensity of the stress factors, such as ultraviolet (UV) radiation, temperature, humidity, etc. By applying these stress factors in a controlled manner, it is possible to estimate the lifetime and performance of materials under natural conditions. The acceleration factors between natural and accelerated artificial aging could vary depending on the polymer. Some researchers analysed the acceleration factor for polyacrylate [79]. Four accelerated aging devices including the SEPAP 12/24 system were used to compare with outdoor natural exposure, which was conducted in Clermont Ferrand and 4 other locations in France, Spain, and USA from 2008 to 2010. The samples for outdoor natural exposure were exposed at an angle of 45° facing south. By comparing the changes in properties (micro-hardness, surface morphology...) in SEPAP 12/24 system with the ones under natural outdoor aging, an acceleration factor of 20 – 30 was determined.

3.1.4. Consequences of (photo)oxidation on the macromolecular architecture

The (photo)oxidation of a polymer can be accompanied by some changes of its macromolecular architecture [80]. First, chain scission can occur during the further reaction of $\text{PO}\cdot$ radicals and subsequent reactions. This will lead to a decrease of the macromolecular mass. Chain scission could also be the cause of the chemicrystallization process: mobile chain segments resulting from the scissions can organize themselves as crystallites, thus increasing the rate of crystallinity. Finally, cross-linking can occur from reactions between the radical species formed throughout the oxidation radical chain mechanism. These changes would have different consequences on the permeability of a photoaged polymer (as stated in this Chapter [2.3.2](#)).

In the subsequent sections, the photoaging mechanisms of polyethylene (PE) and polycarbonate (PC), which were studied during this thesis, will be described.

3.2. Photoaging of the selected polymers

3.2.1. Polyethylene (PE)

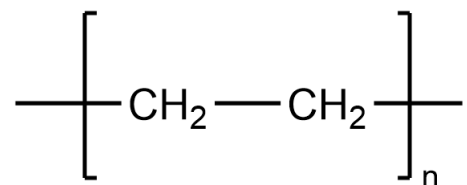
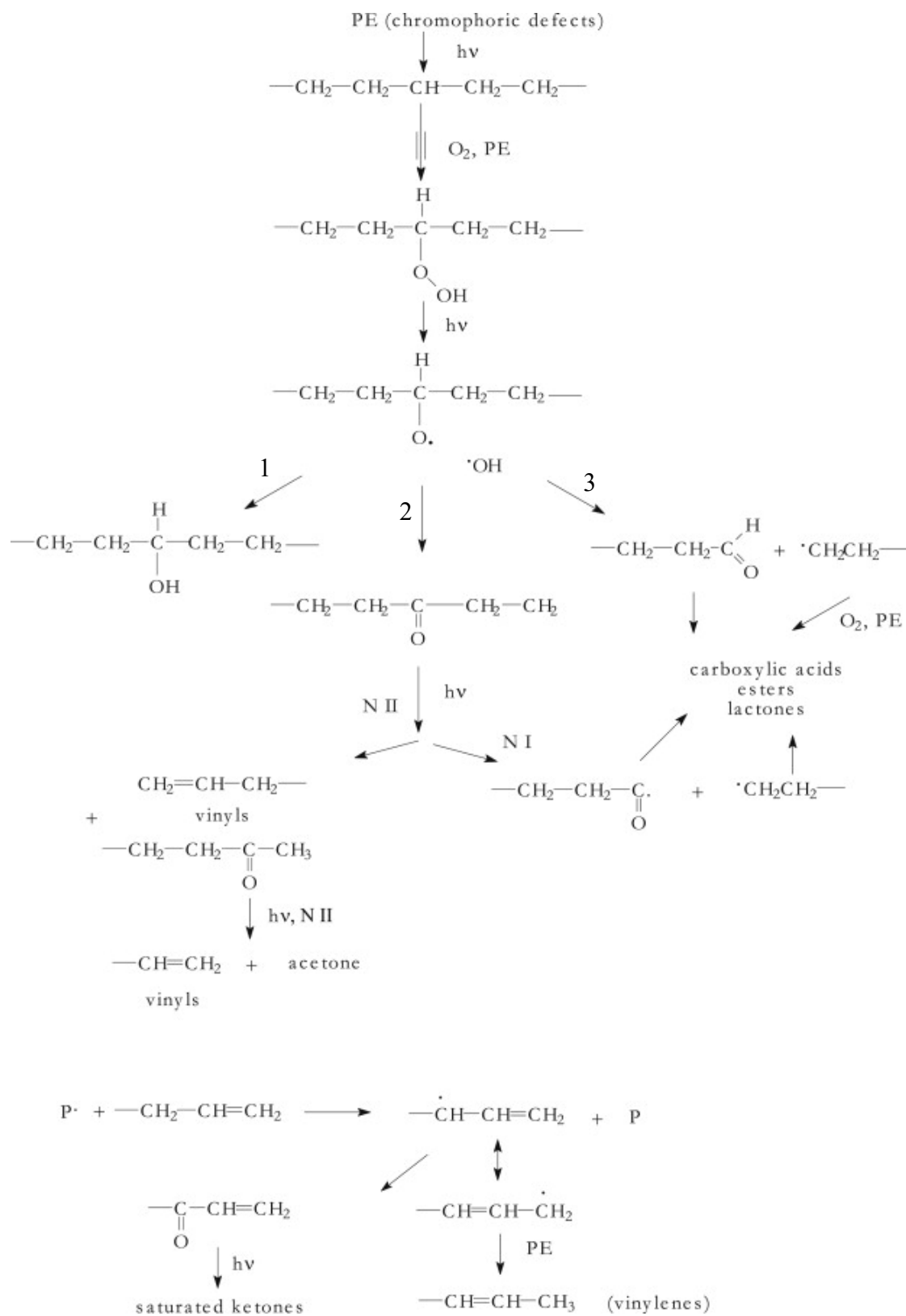


Figure 1.10. Chemical structure of polyethylene (PE).

Polyethylene is one of the most widely used polymers in daily life. With its excellent performances, it is widely used in food packaging, agriculture, medical supplies, pipes, etc. [81, 82] With the development of the Fourier Transform Infrared Spectroscopy (FTIR) measurement, the photodegradation mechanism of polyethylene has been studied thoroughly [75, 83-88] and is now widely recognized.

Figure 1.11. Photooxidation mechanism for PE^[75].

The photooxidation mechanism of PE is represented in Figure 1.11. PE, by itself, cannot absorb ultraviolet energy with a wavelength greater than 300 nm. The initiation step is then kicked off by the presence of chromophoric groups in the form of either external contaminants or catalyst residues from the processing step. As a result, what triggers the initiation step is usually determined by the particular kind of polyethylene that is used and the processing method that is applied [75, 86]. Three reactions (numbered in Figure 1.11) can occur from the macroalkoxy radical $\text{PO}\cdot$ formed upon cleavage of the O-OH bond: 1. hydrogen abstraction to form hydroxyls; 2. cage reactions to obtain ketones (further evolving through Norrish-I and -II reactions); 3. β -scission to produce aldehydes (further oxidized). As a result of the photooxidation of PE, carboxylic acids, esters, lactones, alcohols... are formed.

FTIR analysis can be used to investigate the formation of new functional groups upon photodegradation. Before photoaging, PE exhibits absorption bands at around 719 cm^{-1} and 730 cm^{-1} (CH_2 wagging deformation of single bonds), 1373 cm^{-1} (symmetric deformation of C-H single bonds), and 2849 cm^{-1} and 2914 cm^{-1} (symmetric and asymmetric stretching of CH_2 units in the PE repeat unit). After photoaging, several new bands are seen around $1700 - 1760\text{ cm}^{-1}$ (C=O containing functions), 1260 cm^{-1} and $990 - 1130\text{ cm}^{-1}$ (C-O single bonds), and $1580 - 1680\text{ cm}^{-1}$ and $780 - 900\text{ cm}^{-1}$ (C=C double bonds), and broad band centered at around 3400 cm^{-1} (hydroxyl O-H stretching). The observed stretching vibrations of C=O and C-O bonds are due to the formation of carboxylic acids, aldehydes, or ester compounds. The vibration of unsaturated vinyl (C=C double bonds) may arise from the Norrish-II mechanism [89]. The broad band centered at around 3400 cm^{-1} O-H comes from the formation of monomeric hydroperoxides, hydrogen-bonded alcohols, and hydroperoxides.

Lam S.-M. et al. [89] monitored PE films by assessing changes in morphology, chemical transformation, mechanical strength, and thermal stability. After 200 hours of photoaging of the

PE samples, small cracks appeared on the surface of the PE. The effect of these cracks did not seem significant. The tensile strength of the PE after 200 hours was decreased, indicating that the property was degraded. Thermogravimetric analysis (TGA) showed an earlier decomposition temperature for the photoaged samples, indicating less thermal stability because of the photoaging. Hsueh H.-C. et al. [90] studied the effect of photoaging on high density polyethylene (HDPE). The molar mass and Young's modules were studied upon the UV exposure of HDPE samples. 32 % of the molar mass of HDPE was lost after seven days of UV light exposure, reducing its interlamellar spacing (or the tie-macromolecule concentration). Young's modules were also traced using different intensities of UV radiation. The results showed that the samples expose to the same UV intensity exhibited lower modulus with longer exposure times. This indicates that higher UV intensity leads to increased crystallinity, enhancing their contribution to the fragility of the entire sample. Fairbrother A. et al. [91] reported a mechanical change in HDPE during its photoaging. HDPE initially possessed high ductility, with a fracture elongation exceeding 700 %. However, after photoaging, there was a rapid transition to brittle behaviour with a fracture elongation of less than 20 %. The decrease of a mass molar of HDPE during photoaging is thought to be the main reason. Mazeau E. et al. [92] conducted a study on the photoaging of different stabilized PE with 90 and 300 W.m⁻² irradiances (300 - 420 nm) to describe the influence of this parameter. The researchers found that the higher the irradiance, the higher the photooxidation rate. However, this accelerating effect was not consistent with the ratio of the irradiances (300/90 = 3.3), and was not identical for the different stabilizers used. They concluded that using ultra-acceleration is not a straightforward way of predicting and comparing the lifetime of stabilized polymers. Diepens M. and Tidjani A. et al. [93, 94] investigated the relation between the absorption from the carbonyl groups appearing during the photoaging of LLDPE and the elongation at break. Upon photoaging, more carbonyl groups appeared while the elongation at break decreased. The researchers concluded

that photoaging leads to increased fragility of LLDPE and establishing a clear relationship between the carbonyl groups appeared and the elongation at break is difficult.

3.2.2. Polycarbonate (PC)

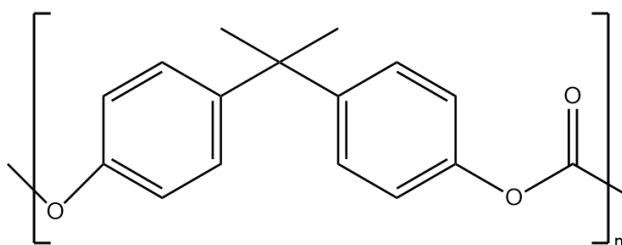


Figure 1.12. Chemical structure of polycarbonate (PC).

Polycarbonate (PC) is a widely used engineering plastic with bisphenol A (BPA) and diphenyl carbonate as its monomers. PC exhibits exceptional performance and properties [34, 95, 96]. Notably, its transparency surpasses that of glass, making it highly valuable in applications where high light transmission is required, such as car headlights. Additionally, PC possesses remarkable impact resistance, indicating its superior strength. This quality has led to its extensive use in producing protective equipment such as helmets, glasses, and precision instrument cases. Moreover, its excellent heat resistance makes it well-suited for everyday applications in automotive components and lighting equipment.

The photoaging of polycarbonate can be traced back at least to 1965 [97]. Over the years, polycarbonate's photodegradation mechanism has been extensively studied and is now widely accepted [34, 69-71, 98-102]. Two main processes are dependent on the irradiation wavelength. For irradiation wavelengths below 330 nm, the main process is the photo-Fries rearrangements. Belluš D. et al. [103] conducted experiments using polycarbonate solutions and irradiated them with light of wavelengths exceeding 254 nm, thus confirming the presence of these rearrangement reactions. Subsequent research was carried out to determine the corresponding mechanism. The

Photo-Fries mechanism of polycarbonate begins with the direct absorption of photons by the carbonate function, which leads to the cleavage of $-(CO)-O-$ bonds. Subsequently, the two formed radicals undergo a cage-like rearrangement reaction to form a phenyl salicylate unit (usually denoted as L_1). Absorption of a second photon results in the same mechanism on the second $-(CO)-O-$ bond in the initial carbonate group, leading to the formation of dihydroxybenzophenone (denoted as L_2). During this process, the formed radicals can also undergo decarbonylation or decarboxylation before recombination. These reactions, which result in a mixture of compounds denoted as L_3 , compete with the reactions yielding L_1 and L_2 (Figure 1.13).

Compounds L_1 and L_2 are characterized by UV and IR absorption bands at 320 nm and 355 nm, and 1690 cm^{-1} and 1630 cm^{-1} , respectively. Compounds L_3 exhibit a broad absorption around 300 nm with a maximum at 284 nm.

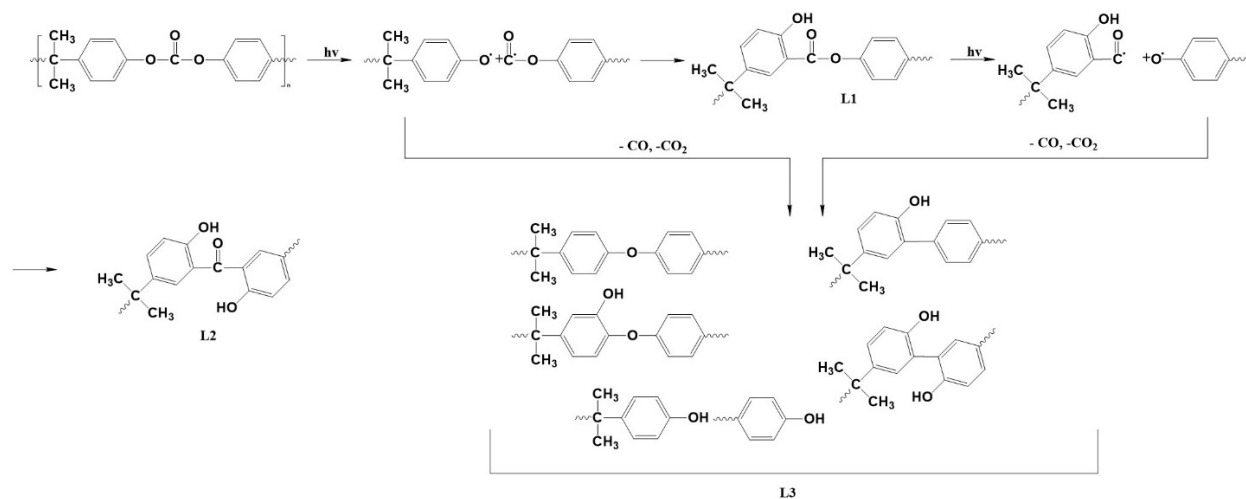


Figure 1.13. Photo-Fries mechanism for polycarbonate.

Another process is photooxidation, happening for irradiation wavelengths higher than 330 nm. The formation of the initiating radical is still under debate between the products of the photo-Fries reaction [34, 104], catalyst residues [69, 70], or charge transfer complex of PC with oxygen [93]. Factor A. et al. and Rivaton A. et al. [98, 99] proposed a photooxidation mechanism involving hydrogen abstraction from the geminal methyl groups of the polymer backbone (Figure 1.14). Subsequent isomerization and reaction with oxygen cause the formation of hydroperoxides, which are unstable and can decompose into alkoxy radicals. The β -scission of these alkoxy radicals leads to the formation of various oxidation products, including aliphatic chain acids at 1713 cm^{-1} (C=O stretching in carboxylic acid), aromatic chain acids at 1840 cm^{-1} , and alcohols at 3480 cm^{-1} (H—O stretching). All of these products can be identified in the FTIR spectra.

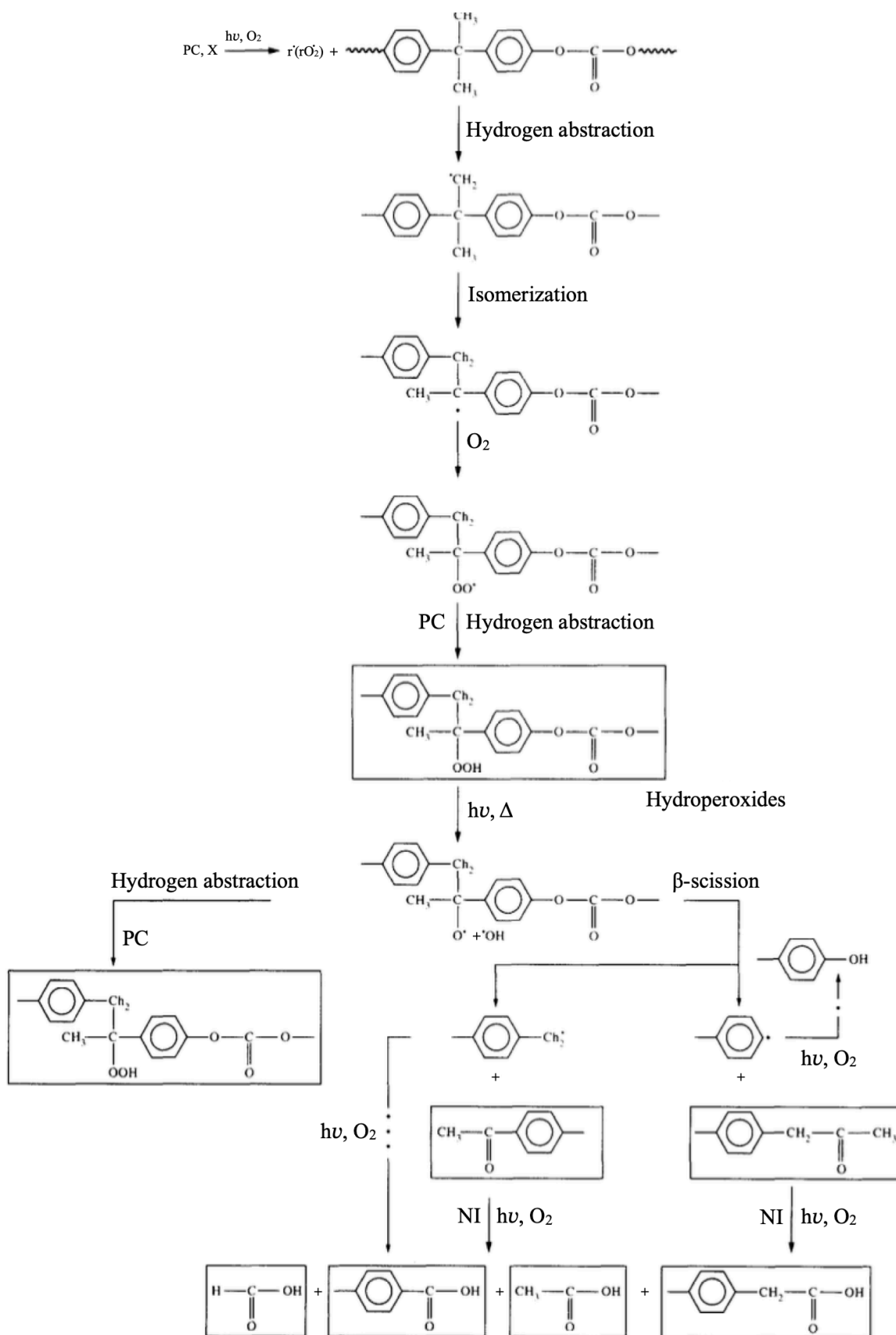


Figure 1.14. Photooxidation mechanism of polycarbonate [70].

Furthermore, an alternative mechanism involving the oxidation of aromatic rings has been proposed, leading to the formation of cyclic anhydrides [70, 105].

Among the many researchers who have thoroughly studied the process of polycarbonate photoaging, some have recognized that it principally occurs at the surface. For example, Nagai N. et al. [106] witnessed a 0.2 μm photodegraded depth of the polycarbonate after 72 hours of photoaging at $75 \text{ mW}\cdot\text{cm}^{-2}$ (295 - 780 nm) at $63 \text{ }^\circ\text{C}$ and 40 % humidity with a weatherometer. They argued that this 0.2 μm photodegraded depth is due to the slightly different characteristics of the surface compared to the inner region, especially in molecular weight and degree of orientation. These differences, higher gradient, between the surface and the inner region are thought to be the cause of this photodegraded depth. Collin S. et al. [107] reported around 10 μm oxidized profile of polycarbonate, which was photoaged 300 hours at $60 \text{ }^\circ\text{C}$ in a SEPAP 12/24. They suggested that the profile is due to either a light absorption profile and/ or a limitation of the oxidation due to limited oxygen diffusion. The UV-visible spectra showed that the light absorption at the surface (first 10 μm) is highly increased upon photoaging (from 27 % to 78 %), which suggests that the photoaging products prevent the light from penetrating deeper inside the samples. This effect demonstrates that, as the photoaging process progresses, less and less light reaches depths beyond 10 μm . Therefore, the photoaging is restricted to the surface, creating an oxidation profile.

Some authors have also reported the occurrence of cross-linking reactions in polycarbonate under photooxidation. Collin S. et al. [107] reported an increase in the nano- and micro-hardness of polycarbonate upon photoaging, observed by nano-indentation and micro-hardness experiments. They observed an increase during the first 200 h, then a plateau. These changes in the mechanical properties were linked to the changes in molecular mobility of the polymer chains during the photoaging, owing to cross-linking. Redjala S. et al. [108] investigated the mechanical properties such as tensile and micro-hardness before and after UV aging and argued the connection with cross-

linking. A decrease of the tensile properties was observed, as the Young's modulus, stress at break and strain at break all decreased after the photoaging. The teams proposed that free radicals from the breakage of the carbonate group in PC can bond with each other or with other chains to form cross-links.

4. Photoaging of polymer and the correlation with permeability

The study of photoaging of various polymers and the consequences on their properties has garnered significant attention within the scientific community [89-94, 107-110]. However, investigations primarily focus on assessing mechanical and optical properties, which play a crucial role in evaluating their suitability for further utilization. Furthermore, the development and commercial availability of testing methodologies have propelled the comprehensive analysis and dissemination of these results.

Investigating the change of permeability upon photoaging has received limited attention, potentially due to the following reasons:

1. Under-appreciation of permeability: The significance of permeability has yet to be fully recognized in certain areas. As previously mentioned in this Chapter [2.4](#), permeability is predominantly relevant to packaging and medical devices. Polymers not commonly employed in these fields may not immediately demonstrate the apparent importance of studying their permeability.
2. Limitations of testing methods: As stated above in this Chapter [2.2.2](#), permeability testing methods still need to be developed. Although oxygen permeability testing may be considered one of the more mature techniques, it still exhibits limitations, such as sample shape and testing conditions. Additionally, the testing methods for other gases or liquids often require research teams to design their own setup [59, 61, 111], further hindering comparison in permeability analysis.

Nevertheless, some researchers worked on the effect of photoaging on the permeability of polymers. Kaplan Z. et al. [111] claimed a potential biodegradable polymer for use in preserving historical building walls. The authors tested the coating performance of PHB and PLA. The water

resistance of the coatings was evaluated using, besides the contact angle, water absorption tests. The water absorption was measured using capillarity and gravimetric methods in controlled temperature and relative humidity conditions. The results showed an increase in the water absorption of samples after weathering (raining), which is attributed to the formation of CO₂ and hydroperoxide, as well as hydrolysis of ester groups and a reduction in molecular weight of the coating polymers during weathering. Furthermore, they tested the coating performance, which showed that the polymers performed better with coating than the non-coated materials. This was proved by a significant reduction in capillary water absorption for coated materials, highlighting the effectiveness of the coating, as water is related to the realistic weathering conditions of building walls. Other without coating materials directly endured ester group decomposition and formation of gamma lactones during the weathering. Despite water absorption is not a permeability measurement, it is actually connected with this property. Greenwood R. et al. [112] reported experiments to assess the changes of O₂ and CO₂ permeability upon the photoaging of poly(p-methyl styrene) at 254 nm under vacuum and in the presence of O₂. Regardless of the photoaging methods (vacuum or O₂), the permeability decreased upon photoaging. However, the permeation coefficient P of the sample photoaged under vacuum decreased more than the one in oxygen. The researchers proposed that, in a vacuum, the radicals from photolysis cross-link, which strongly decreases the permeability. The lower decrease of P for photooxidation is explained by a competitive effect between cross-linking and oxidation (associated with chain scission and then to an increase of P). Philippart J.-L. et al. [113] conducted experiments to study the changes in the CO₂ permeability of poly(ether-block-amide)s due to photoaging. The team observed a decrease of the permeability in PEBA after photoaging due to the decrease of the chain mobility from the cross-linking of the PEBA. Nakatsuka S. et al. [114] investigated the effect of natural and accelerated artificial weathering (Atlas Ci 65 weatherometer) on the water vapour and CO₂ permeability of

polyethylene and (ethylene-carbon monoxide) copolymers. The results showed that the weathering causes a significant increase in the water vapour and CO₂ permeability for the copolymers. The team linked this effect mainly to the plasticization by the low-weight molecules produced during photoaging. Ye X. et al. [115] described a novel route for preparing PVC sheets with high UV irradiation resistance. The oxygen permeability was increased both in the sample with and without coating after a maximum of 15 days of UV irradiation in an accelerating system at 40 ± 5 °C with an average irradiation intensity of 5.5 W/m² at 340 nm. This increase is attributed to the bond breakage in the PVC through the free radical chain reaction mechanism presented earlier in Figure 1.6. The effect of the coating was also proven as the increase is less than for the one without coating. The researchers argued that the coating reduces photochemical reactions, thus reducing the bond breakage and the increase of permeability. Collin S. et al. [116] looked into the accelerated photoaging of organic coatings used as protective layers for Blu-ray Discs. The water permeability was largely decreased after 100 h of irradiation in an accelerating system SEPAP 12/24 at 60 °C due to the cross-linking, which hinders the macromolecular mobility within the degraded part of the sample. Scarfato P. et al. [117] conducted experiments to study the changes in the oxygen permeability of biodegradable nanocomposite films due to 5 days of weathering at 50 °C and 25 % of relative humidity. The team found an increase in oxygen permeability after weathering due to the hydrolysis of the ester linkage and multiple chain scissions in the polymer amorphous part, which increases the mobility of the polymer chains.

In conclusion, it can be seen that the study of the effect of photoaging on the polymer permeability is scarce and often incidental in the scientific literature (in the sense that it is not the core of the articles, but rather complementary information) despite the importance of this property in numerous applications of polymers. This PhD project then endeavours to adopt a comprehensive approach to

answer the question of "How does the photoaging of polymer affect its permeability?". Polymers whose photoaging mechanism is well-known, such as polycarbonate and polyethylene, were selected as model compounds. The changes caused by the photoaging were studied at different scales, from the chemical structure to the use properties by way of the macromolecular architecture. Several permeability test methods (either commercial ones or specially developed) were also chosen to link the results of the multiscale analysis to the changes of permeability observed. It is expected that this study will yield a well-founded and substantiated conclusion regarding this subject, but also open new related topics.

References

1. Frontinus S J, Rolán T G. De aquaeductu urbis Romae. Editorial CSIC-CSIC Press, 1985.
2. Taylor R M. Public needs and private pleasures: water distribution, the Tiber river and the urban development of ancient Rome. L'Erma di Bretschneider, 2000.
3. Suloff E C. Sorption behaviour of an aliphatic series of aldehydes in the presence of poly (ethylene terephthalate) blends containing aldehyde scavenging agents. Virginia Polytechnic Institute and State University, 2002.
4. McKeen L W. Permeability properties of plastics and elastomers. William Andrew, 2016.
5. Graham T. A short account of experimental researches on the diffusion of gases through each other, and their separation by mechanical means. Quarterly Journal of Science, Literature and Art, 1829, 27: 74-83.
6. Mason E A, Kronstadt B. Graham's laws of diffusion and effusion. Journal of Chemical Education, 1967, 44(12): 740.
7. Fick A. Ueber diffusion. Annalen der Physik, 1855, 170(1): 59-86.
8. Graham T. XVIII. On the absorption and dialytic separation of gases by colloid septa. Philosophical transactions of the Royal Society of London, 1866 (156): 399-439.
9. Robertson G L. Food packaging: principles and practice. CRC press, 2005.
10. Daynes H A. The process of diffusion through a rubber membrane. Proceedings of the Royal Society of London. Series A, Containing Papers of a Mathematical and Physical Character, 1920, 97(685): 286-307.
11. Rees L V C. Richard Maling Barrer. 16 June 1910–12 September 1996. Biographical Memoirs of Fellows of the Royal Society, 1998.

12. Schumacher E E, Ferguson L. A convenient apparatus for measuring the diffusion of gases and vapors through membranes. *Journal of the American Chemical Society*, 1927, 49(2): 427-428.
13. Barrer R M, Rideal E K. Activated diffusion in membranes. *Transactions of the Faraday Society*, 1939, 35: 644-656.
14. Siracusa V. Food packaging permeability behaviour: A report. *International Journal of Polymer Science*, 2012, 2012.
15. Crank J. *The mathematics of diffusion*. Oxford university press, 1979.
16. Petropoulos J H. Mechanisms and theories for sorption and diffusion of gases in polymers//*Polymeric gas separation membranes*. CRC Press, 2018: 17-81.
17. Wu H, Thibault J, Kruczek B. The validity of the time-lag method for the characterization of mixed-matrix membranes. *Journal of Membrane Science*, 2021, 618: 118715.
18. Minelli M, De Angelis M G, Sarti G C. Predictive calculations of gas solubility and permeability in glassy polymeric membranes: An overview. *Frontiers of Chemical Science and Engineering*, 2017, 11: 405-413.
19. De Angelis M G, Sarti G C. Solubility of gases and liquids in glassy polymers. *Annual review of chemical and biomolecular engineering*, 2011, 2: 97-120.
20. Fereydoon M, Ebnesajjad S. Development of high-barrier film for food packaging. *Plastic films in food packaging*, 2013: 71-92.
21. Dost K, İdeli C. Determination of polycyclic aromatic hydrocarbons in edible oils and barbecued food by HPLC/UV–Vis detection. *Food Chemistry*, 2012, 133(1): 193-199.
22. Barrer R M, Rideal E K. Permeation, diffusion and solution of gases in organic polymers. *Transactions of the Faraday Society*, 1939, 35: 628-643.

23. Wu H, Kruczek B, Thibault J. Impact of measuring devices and data analysis on the determination of gas membrane properties. *Journal of Membrane Science and Research*, 2018, 4(1): 4-14.
24. ISO 15106-1:2002(E) Packaging - Flexible Barrier Materials - Part 1: Definitions and Test Methods, International Organization for Standardization, 2002.
25. Huang J, Qian X. Comparison of test methods for measuring water vapor permeability of fabrics. *Textile Research Journal*, 2008, 78(4): 342-352.
26. McCullough E A, Kwon M, Shim H. A comparison of standard methods for measuring water vapour permeability of fabrics. *Measurement Science and Technology*, 2003, 14(8): 1402.
27. Othman S H, Edwal S A M, Risyon N P, et al. Water sorption and water permeability properties of edible film made from potato peel waste. *Food Science and Technology*, 2017, 37: 63-70.
28. Chen X, Zhang C, Fang J, et al. A Study on Application of Infrared Sensor Method in Moisture Permeability Test of Food Packaging Materials//*Journal of Physics: Conference Series*. IOP Publishing, 2021, 2044(1): 012182.
29. Petrusová Z, Morávková L, Vejražka J, et al. Comparison of hexane vapour permeation in two different polymeric membranes via an innovative in-line FID detection method. *Chemical and Biochemical Engineering Quarterly*, 2017, 31(2): 145-160.
30. Wootthikanokkhan J, Seeponkai N. Methanol permeability and properties of DMFC membranes based on sulfonated PEEK/PVDF blends. *Journal of applied polymer science*, 2006, 102(6): 5941-5947.
31. Jansen J C, Friess K, Drioli E. Organic vapour transport in glassy perfluoropolymer membranes: A simple semi-quantitative approach to analyse clustering phenomena by time-lag measurements. *Journal of Membrane Science*, 2011, 367(1-2): 141-151.

32. Macchione M, Jansen J C, De Luca G, et al. Experimental analysis and simulation of the gas transport in dense Hyflon® AD60X membranes: influence of residual solvent. *Polymer*, 2007, 48(9): 2619-2635.
33. Friess K, Šípek M, Hynek V, et al. Comparison of permeability coefficients of organic vapors through non-porous polymer membranes by two different experimental techniques. *Journal of membrane science*, 2004, 240(1-2): 179-185.
34. Andrews R J, Grulke E A, Brandrup J, et al. *Polymer handbook*. John Wiley & Sons, New York, 1999.
35. Engarnevis A, Romani S, Sylvester A, et al. The effects of temperature and humidity on the permeation properties of membrane transport media used in energy recovery ventilators. 2017.
36. Metz S J, Van De Ven W J C, Mulder M H V, et al. Mixed gas water vapor/N₂ transport in poly (ethylene oxide) poly (butylene terephthalate) block copolymers. *Journal of membrane science*, 2005, 266(1-2): 51-61.
37. Sijbesma H, Nijmeijer K, van Marwijk R, et al. Flue gas dehydration using polymer membranes. *Journal of Membrane Science*, 2008, 313(1-2): 263-276.
38. Potreck J, Nijmeijer K, Kosinski T, et al. Mixed water vapor/gas transport through the rubbery polymer PEBAX® 1074. *Journal of Membrane Science*, 2009, 338(1-2): 11-16.
39. Jasse B, Seuvre A M, Mathlouthi M. *Permeability and structure in polymeric packaging materials//Food packaging and preservation*. Boston, MA: Springer US, 1994: 1-22.
40. Klopffer M H, Berne P, Espuche É. Development of innovating materials for distributing mixtures of hydrogen and natural gas. Study of the barrier properties and durability of polymer pipes. *Oil & Gas Science and Technology–Revue d'IFP Energies nouvelles*, 2015, 70(2): 305-315.

41. Mrkić S, Galić K, Ivanković M, et al. Gas transport and thermal characterization of mono- and di-polyethylene films used for food packaging. *Journal of applied polymer science*, 2006, 99(4): 1590-1599.
42. Gee G. Some thermodynamic properties of high polymers, and their molecular interpretation. *Quarterly Reviews, Chemical Society*, 1947, 1(3): 265-298.
43. Klopffer M H, Flaconnèche B. Transport properties of gases in polymers: bibliographic review. *Oil & Gas Science and Technology*, 2001, 56(3): 223-244.
44. Crank J. *The mathematics of diffusion*. Oxford university press, 1979.
45. Hildebrand J H, Scott R L. Solutions of nonelectrolytes. *Annual Review of Physical Chemistry*, 1950, 1(1): 75-92.
46. Comyn, John, ed. *Polymer permeability*. Springer Science & Business Media, 1985.
47. Turan D, Sänglerlaub S, Stramm C, et al. Gas permeabilities of polyurethane films for fresh produce packaging: response of O₂ permeability to temperature and relative humidity. *Polymer Testing*, 2017, 59: 237-244.
48. Mokwena K K, Tang J. Ethylene vinyl alcohol: a review of barrier properties for packaging shelf stable foods. *Critical reviews in food science and nutrition*, 2012, 52(7): 640-650.
49. Michaels A S, Parker Jr R B. Sorption and flow of gases in polyethylene. *Journal of Polymer Science*, 1959, 41(138): 53-71.
50. Kofinas P, Cohen R E, Halasa A F. Gas permeability of polyethylene/poly (ethylene-propylene) semicrystalline diblock copolymers. *Polymer*, 1994, 35(6): 1229-1235.
51. Sha H, Harrison I R. CO₂ permeability and amorphous fractional free-volume in uniaxially drawn HDPE. *Journal of Polymer Science Part B: Polymer Physics*, 1992, 30(8): 915-922.

52. Wu S, Zhang X, Sun Y, et al. Study on the influence of crosslinking density and free polysiloxan chain length on oxygen permeability and hydrophilicity of multicomponent silicone hydrogels. *Colloid and Polymer Science*, 2021, 299(8): 1327-1335.
53. Lin H, Kai T, Freeman B D, et al. The effect of cross-linking on gas permeability in cross-linked poly (ethylene glycol diacrylate). *Macromolecules*, 2005, 38(20): 8381-8393.
54. Andersson H, Hjærtstam J, Stading M, et al. Effects of molecular weight on permeability and microstructure of mixed ethyl-hydroxypropyl-cellulose films. *European Journal of Pharmaceutical Sciences*, 2013, 48(1-2): 240-248.
55. Houde A Y, Kulkarni S S, Kharul U K, et al. Gas permeation in polyarylates: effects of polarity and intersegmental mobility. *Journal of membrane science*, 1995, 103(1-2): 167-174.
56. Berens A R, Hopfenberg H B. Diffusion of organic vapors at low concentrations in glassy PVC, polystyrene, and PMMA. *Journal of Membrane Science*, 1982, 10(2-3): 283-303.
57. Rogers C E. *Permeation of gases and vapours in polymers//Polymer permeability*. Dordrecht: Springer Netherlands, 1985: 11-73.
58. Tufani A, Ince G O. Permeability of small molecules through vapor deposited polymer membranes. *Journal of applied polymer science*, 2015, 132(34).
59. Cava D, Giménez E, Gavara R, et al. Comparative performance and barrier properties of biodegradable thermoplastics and nanobiocomposites versus PET for food packaging applications. *Journal of Plastic Film & Sheeting*, 2006, 22(4): 265-274.
60. Ciković N. The effect of liquid absorption on gas barrier properties of triplex film coated with silicon oxide. *Food Technology and Biotechnology*, 2003, 41(3): 247-251.
61. Hogg A, Uhl S, Feuvrier F, et al. Protective multilayer packaging for long-term implantable medical devices. *Surface and Coatings Technology*, 2014, 255: 124-129.

62. Roohpour N, Wasikiewicz J M, Paul D, et al. Synthesis and characterisation of enhanced barrier polyurethane for encapsulation of implantable medical devices. *Journal of Materials Science: Materials in Medicine*, 2009, 20: 1803-1814.
63. Zhang P, Wang W, Lv Y, et al. Effect of polymer coatings on the permeability and chloride ion penetration resistances of nano-particles and fibers-modified cementitious composites. *Polymers*, 2022, 14(16): 3258.
64. Belkhiri Z, Moussa H B, Haddad D, et al. Effect of permeability on the dynamic field in the PEM fuel cell. *International journal of hydrogen energy*, 2015, 40(39): 13789-13798.
65. Schneible J D. *A Material Toolbox for Advanced Therapeutics*. North Carolina State University, 2020.
66. Jaleh B, Shahbazi N. Surface properties of UV irradiated PC–TiO₂ nanocomposite film. *Applied Surface Science*, 2014, 313: 251-258.
67. Bolland J L. Kinetics of olefin oxidation. *Quarterly Reviews, Chemical Society*, 1949, 3(1): 1-21.
68. Gryn'ova G, Hodgson J L, Coote M L. Revising the mechanism of polymer autooxidation. *Organic & biomolecular chemistry*, 2011, 9(2): 480-490.
69. Rivaton A, Sallet D, Lemaire J. The photochemistry of bisphenol-A polycarbonate reconsidered. *Polymer Photochemistry*, 1983, 3(6): 463-481.
70. Rivaton A. Recent advances in bisphenol-A polycarbonate photodegradation. *Polymer Degradation and Stability*, 1995, 49(1): 163-179.
71. Factor A, Chu M L. The role of oxygen in the photo-ageing of bisphenol-A polycarbonate. *Polymer Degradation and Stability*, 1980, 2(3): 203-223.

72. Colin X, Fayolle B, Audouin L, et al. About a quasi-universal character of unstabilised polyethylene thermal oxidation kinetics. *Polymer Degradation and Stability*, 2003, 80(1): 67-74.
73. Richaud E, Colin X, Fayolle B, et al. Induction period in the low-temperature thermal oxidation of saturated hydrocarbons: Example of polyethylene. *International Journal of Chemical Kinetics*, 2008, 40(12): 769-777.
74. Celina M C. Review of polymer oxidation and its relationship with materials performance and lifetime prediction. *Polymer Degradation and Stability*, 2013, 98(12): 2419-2429.
75. Gardette M, Perthue A, Gardette J L, et al. Photo-and thermal-oxidation of polyethylene: comparison of mechanisms and influence of unsaturation content. *Polymer Degradation and Stability*, 2013, 98(11): 2383-2390.
76. Berthumeyrie S, Colin A, Thérias S, et al. Photo And Thermal Degradation Of Polylactide/Zinc Oxide Nanocomposites: Evolution Of Thermal And Mechanical Properties. In: 7th International Conference on Modification, Degradation and Stabilisation of Polymers (MoDeSt); 2012; Prague, Czech Republic
77. Norrish R G W, Bamford C H. Photodecomposition of aldehydes and ketones. *Nature*, 1936, 138(3502): 1016-1016.
78. Lemaire J, Arnaud R, Gardette J L. Vieillissement Des Polymeres. Principes D'etude Du Photovieillissement. *Revue générale du caoutchouc et des plastiques*, 1981, 58: 87-92.
79. Larché J F, Bussière P O, Gardette J L. Characterisation of accelerated ageing devices for prediction of the service life of acrylic-melamine/urethane thermosets. *Polymer degradation and stability*, 2011, 96(8): 1530-1536.
80. Wypych, G. Handbook of UV degradation and stabilization. Elsevier, 2020.

81. Kasirajan S, Ngouajio M. Polyethylene and biodegradable mulches for agricultural applications: a review. *Agronomy for sustainable development*, 2012, 32: 501-529.
82. Paxton N C, Allenby M C, Lewis P M, et al. Biomedical applications of polyethylene. *European Polymer Journal*, 2019, 118: 412-428.
83. Gin hac J M, Gardette J L, Arnaud R, et al. Influence of hydroperoxides on the photothermal oxidation of polyethylene. *Die Makromolekulare Chemie: Macromolecular Chemistry and Physics*, 1981, 182(4): 1017-1025.
84. Lemaire J, Arnaud R, Gardette J L. The role of hydroperoxides in photooxidation of polyolefins, polyamides and polyurethane elastomers. *Pure and Applied Chemistry*, 1983, 55(10): 1603-1614.
85. Guadagno L, Naddeo C, Vittoria V, et al. Chemical and morphological modifications of irradiated linear low density polyethylene (LLDPE). *Polymer degradation and stability*, 2001, 72(1): 175-186.
86. Briassoulis D, Aristopoulou A, Bonora M, et al. Degradation characterisation of agricultural low-density polyethylene films. *Biosystems engineering*, 2004, 88(2): 131-143.
87. Ołdak D, Kaczmarek H, Buffeteau T, et al. Photo-and bio-degradation processes in polyethylene, cellulose and their blends studied by ATR-FTIR and Raman spectroscopies. *Journal of materials science*, 2005, 40: 4189-4198.
88. Rivaton A, Gardette J L, Mailhot B, et al. Basic aspects of polymer degradation//*Macromolecular Symposia*. Weinheim: WILEY-VCH Verlag, 2005, 225(1): 129-146.
89. Lam S M, Chew K C, Sin J C, et al. Ameliorated photodegradation performance of polyethylene and polystyrene films incorporated with ZnO-PVP catalyst. *Journal of Environmental Chemical Engineering*, 2022, 10(3): 107594.

90. Hsueh H C, Kim J H, Orski S, et al. Micro and macroscopic mechanical behaviours of high-density polyethylene under UV irradiation and temperature. *Polymer degradation and stability*, 2020, 174: 109098.
91. Fairbrother A, Hsueh H C, Kim J H, et al. Temperature and light intensity effects on photodegradation of high-density polyethylene. *Polymer Degradation and Stability*, 2019, 165: 153-160.
92. Mazeau E, Pichon G, Bouchut B, et al. Influence of irradiance on the photooxidation of HALS stabilized low-density polyethylene. *Polymer Degradation and Stability*, 2023, 216: 110478.
93. Diepens M, Gijsman P. Photo-oxidative degradation of bisphenol A polycarbonate and its possible initiation processes. *Polymer Degradation and Stability*, 2008, 93(7): 1383-1388.
94. Tidjani A, Arnaud R, Dasilva A. Natural and accelerated photoaging of linear low-density polyethylene: Changes of the elongation at break. *Journal of applied polymer science*, 1993, 47(2): 211-216.
95. Gamal M. Polycarbonate. Higher Technological Institute, 2018.
96. Jadhav V D, Patil A J, Kandasubramanian B. Polycarbonate nanocomposites for high impact applications. *Handbook of consumer nanoproducts*, 2022: 257-281.
97. Gedemer T J. The use of ATR techniques to evaluate UV degradation of plastics. *Applied Spectroscopy*, 1965, 19(5): 141-146.
98. Factor A, Ligon W V, May R J. The role of oxygen in the photoaging of bisphenol A polycarbonate. 2. GC/GC/high-resolution MS analysis of Florida-weathered polycarbonate. *Macromolecules*, 1987, 20(10): 2461-2468.

99. Rivaton A, Mailhot B, Soulestin J, et al. Comparison of the photochemical and thermal degradation of bisphenol-A polycarbonate and trimethylcyclohexane-polycarbonate. *Polymer Degradation and Stability*, 2002, 75(1): 17-33.
100. Diepens M, Gijsman P. Photodegradation of bisphenol A polycarbonate. *Polymer Degradation and Stability*, 2007, 92(3): 397-406.
101. Pickett J E. Influence of photo-Fries reaction products on the photodegradation of bisphenol-A polycarbonate. *Polymer degradation and stability*, 2011, 96(12): 2253-2265.
102. Mehr M Y, Van Driel W D, Jansen K M B, et al. Photodegradation of bisphenol A polycarbonate under blue light radiation and its effect on optical properties. *Optical Materials*, 2013, 35(3): 504-508.
103. Belluš D, Hrdlovič P, Maňásek Z. Photoinitiated rearrangements in poly [2, 2-propanebis (4-phenyl carbonate)]. *Journal of Polymer Science Part B: Polymer Letters*, 1966, 4(1): 1-5.
104. *Polymer durability: degradation, stabilization, and lifetime prediction*. American Chemical Society, 1996.
105. Clark D T, Munro H S. Surface and bulk aspects of the natural and artificial photo-ageing of Bisphenol A polycarbonate as revealed by ESCA and difference UV spectroscopy. *Polymer degradation and stability*, 1984, 8(4): 195-211.
106. Nagai N, Okumura H, Imai T, et al. Depth profile analysis of the photochemical degradation of polycarbonate by infrared spectroscopy. *Polymer degradation and stability*, 2003, 81(3): 491-496.
107. Collin S, Bussière P O, Therias S, et al. Physicochemical and mechanical impacts of photo-ageing on bisphenol a polycarbonate. *Polymer degradation and stability*, 2012, 97(11): 2284-2293.

108. Redjala S, Aït Hocine N, Ferhoum R, et al. UV aging effects on polycarbonate properties. *Journal of Failure Analysis and Prevention*, 2020, 20: 1907-1916.
109. Shi Y, Huang H, Zheng L, et al. Releases of microplastics and chemicals from nonwoven polyester fabric-based polyurethane synthetic leather by photoaging. *Science of The Total Environment*, 2023, 902: 166584.
110. Lourenço E, Felisberti M I. Mechanical properties of photoaged in situ polymerized PS/EPDM blends. *Journal of applied polymer science*, 2007, 106(6): 3617-3623.
111. Kaplan Z, Böke H, Sofuoglu A, et al. Long term stability of biodegradable polymers on building limestone. *Progress in Organic Coatings*, 2019, 131: 378-388.
112. Greenwood R, Weir N. Effects of photo-degradation on the permeability and diffusivity characteristics of poly (p-methylstyrene). *Die Makromolekulare Chemie: Macromolecular Chemistry and Physics*, 1975, 176(7): 2041-2051.
113. Philippart J L, Gardette J L. Analyse du photoviellissement des matériaux polymères par évolution de la perméabilité aux gaz. *Die Makromolekulare Chemie: Macromolecular Chemistry and Physics*, 1986, 187(7): 1639-1650.
114. Nakatsuka S, Andrady A. Studies on enhanced degradable plastics. III. The effect of weathering of polyethylene and (ethylene-carbon monoxide) copolymers on moisture and carbon dioxide permeability. *Journal of environmental polymer degradation*, 1994, 2: 161-167.
115. Ye X, Pi H, Guo S. A novel route for preparation of PVC sheets with high UV irradiation resistance. *Journal of applied polymer science*, 2010, 117(5): 2899-2906.
116. Collin S, Bussiere P O, Gardette J L, et al. Accelerated photo-aging of organic coatings used as protective layers for Blu-ray Discs. *Progress in Organic Coatings*, 2015, 84: 9-17.

117. Scarfato P, Acierno D, Russo P. Photooxidative weathering of biodegradable nanocomposite films containing halloysite. *Polymer Composites*, 2015, 36(6): 1169-1175.

Chapter 2: Experimental part

1. Introduction

This second chapter aims to provide a complete overview of the materials, techniques, and methods used in this thesis.

2. Samples

2.1. Polymer samples

In this study, two polymers in the form of films were mainly used: polyethylene (PE) and polycarbonate (PC). Low-Density Polyethylene (LDPE) films with thicknesses of 30, 60, 90 and 150 μm were produced by the Barbier company from PE-033 (Alcudia®, Repsol). Polycarbonate films with thickness of 125 μm were graciously obtained from Covestro company with the brand name MAKROFOL® DE 1-1 CF 000000. Unless otherwise stated, the PC and PE samples were used as received without any additional treatments.

2.2. Solvents

Methanol with a minimum purity of 99 % was obtained from Honeywell. Hexane with a minimum purity of 99 % was purchased from Sigma Aldrich. Cyclohexane with a minimum purity of 99.8 %, chloroform with a purity of 99.9 % and ethanol with a minimum purity of 99.9 % were supplied by Carlo Erba. They were all used as received.

2.3. Permeants for liquid permeability experiments

Carbazole with a purity range of 98 - 100 % was obtained from Serlabo. 1,4-dimethylnaphthalene (99 %), 2,6-dimethylnaphthalene (99 %), 1,4-naphthoquinone (97 %), 1-naphthol (99 %), and 2-hydroxy-1,4-naphthoquinone (97 %), were all obtained from Sigma Aldrich. Naphthalene (99.6 %) and 1-methyl-naphthalene (97 %) were supplied by Fluka. All of these compounds were used as received.

3. Aging devices

3.1. Photoaging equipment

The photoaging of samples was carried out in a SEPAP 12/24 unit from Atlas [1] in aerated conditions. Such a unit consists of an irradiation chamber, a ventilation system, and a control module. It is equipped with 4 medium-pressure mercury vapour arc lamps (400 W) deployed on the corners of the chamber (Figure 2.1). The lamps are coated with a borosilicate envelope that filters wavelengths lower than 300 nm. SEPAP 12/24 delivers a light irradiance of 90 W.m⁻². A rotating carousel with sample holders is in the middle of the irradiation chamber. The temperature in the chamber was kept constant at around 55 °C throughout the entire photoaging time.

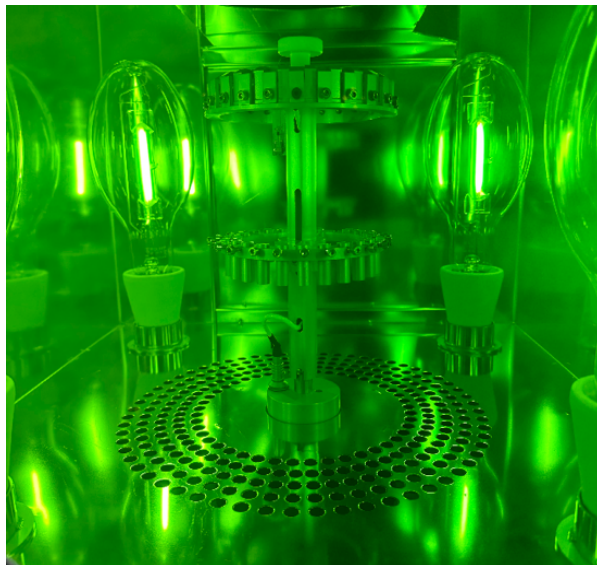


Figure 2.1. Irradiation chamber of a SEPAP 12/24.

3.2. Thermal aging equipment

In order to distinguish between the effect of light and temperature during the photoaging experiments, "dark" (*i.e.* without any light exposure) control experiments were carried out in a forced convection oven from Binder with a temperature of 55°C in aerated conditions.

4. Characterization of the polymers

4.1. Spectroscopic methods

4.1.1. Infrared spectroscopy

Fourier-Transform InfraRed (FTIR) spectroscopy is an analytical technique that identifies chemical functions through the absorption of infrared light that activates the vibration of characteristic bonds at specific wavenumbers. Infrared spectroscopy is classically performed in transmission or attenuated total reflection (ATR) modes. While the transmission mode analyses the whole thickness of the sample, the ATR mode is restricted to its surface, as illustrated in Figure 2.2.

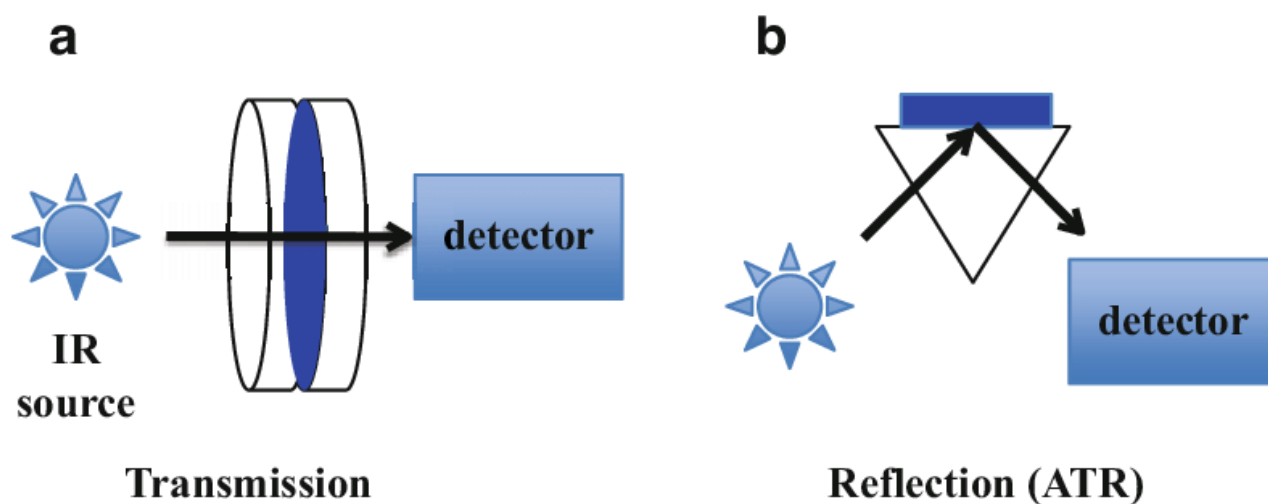


Figure 2.2. FTIR sampling methods: a. transmission, b. Attenuated Total Reflection (ATR) [2].

During this study, FTIR spectroscopy was used either to record spectra on a single position, or on a larger scale (microscopy mode):

- Single spectra:

- Transmission mode

A Nicolet 6700 FTIR spectrometer (ThermoFischer) was used to record transmission spectra for both PE and PC films (32 scans, 4 cm⁻¹ resolution). It is equipped with a DTGS-KBr detector, and the analysis chamber was purged with dry air to remove parasite bands originating from ambient air. When necessary, films were slightly scratched with emery paper to avoid the appearance of interferences on the FTIR spectra.

- Attenuated Total Reflectance (ATR) mode

The IR absorbance at the surface of the PC films was measured with a Nicolet 380 FTIR spectrophotometer equipped with a diamond Golden Gate ATR modulus (Specac). A constant torque of 60 cN.m was applied on the sample to ensure its contact with the diamond. The spectra were normalized with a reference band (C-C-C bending at 1081 cm⁻¹) [3] to compensate for the differences in the contact of the film with the diamond, especially upon the photoaging and the corresponding changes in mechanical properties. 64 scans of resolution 4 cm⁻¹ were recorded within the wavenumber range of 4000 to 630 cm⁻¹. For ATR, the depth of the analysis sample d_p could be calculated from the following equation:

$$d_p = \frac{\lambda}{2\pi \cdot n_1 \cdot \sqrt{\sin^2 \theta - \left(\frac{n_2}{n_1}\right)^2}} \quad \text{Eq. 1}$$

where λ is the wavelength of the IR radiation, θ is the incidence angle (45°), n_1 and n_2 are the refractive index of the crystal (2.4 for diamond) and the sample (1.6 for PC [4]), respectively.

For both transmission and ATR modes, data treatment and analysis were performed using OMNIC software. The measurement was triplicated for each aging time, and the results were presented in the form of the average value of the reproducible measurements.

- Microscopy mode:
 - FTIR microspectroscopy mapping

A Hyperion 3000 FTIR imaging microscope was used to obtain transmission IR mappings of PE films. One mapping typically corresponds to a $360 \times 360 \mu\text{m}$ area composed of 128×128 spectra (32 scans, 4 cm^{-1} resolution). The extent of photoaging was evaluated by integrating the carbonyl band (typically between 1850 and 1650 cm^{-1}) and normalization with the area of the $1490 - 1420 \text{ cm}^{-1}$ region.

- FTIR microspectroscopy mapping on cross-sectional samples

Cross-sectional samples were first cut with a LEICA RM2165 microtome. Because the mechanical properties of PC and PE are different, the cutting procedure is different for them.

In the case of PC, the original samples were cooled down with liquid nitrogen to stiffen them. They were then fixed in a sample holder which was securely positioned on the microtome with its surface facing the cutting blade (Figure 2.3, 1, the sample holder of the microtome is not drawn). The microtome ensured the precise adjustment of the blade's movement, to obtain a $50 \mu\text{m}$ thickness of the cross-sectional samples (Figure 2.3, 4). During the cutting, tape was needed to fix the sample on one side (Figure 2.3, 2) as the samples could curve themselves. The cut sample was finally firmly secured onto a sample holder with both sides taped (Figure 2.3, 3) for spectroscopic analysis.

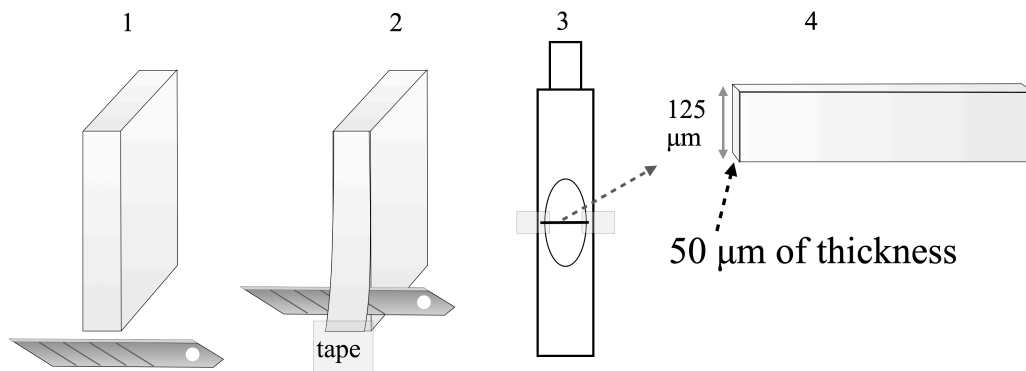


Figure 2.3. Preparation of PC samples for transmission infrared microspectroscopy: 1. sample after cooling with liquid nitrogen, 2. sample cutting using microtome, 3. sample final state, 4. sample scale.

Oxidation profiles were obtained from the FTIR microspectroscopy mappings of the cross-sectional samples according to the following procedure:

1. Export spectra from a line of the mapping (as shown in Figure 2.4), with a few points out of the edge of the sample
2. Measure the absorbance values at 1713 and 1081 cm^{-1} (reference band for normalization) for each point of the line.
3. Calculate the ratio of these values.
4. Plot the ratio as a function of the position of the corresponding point on the cross-sectional sample (*i.e.* its position in the film thickness).

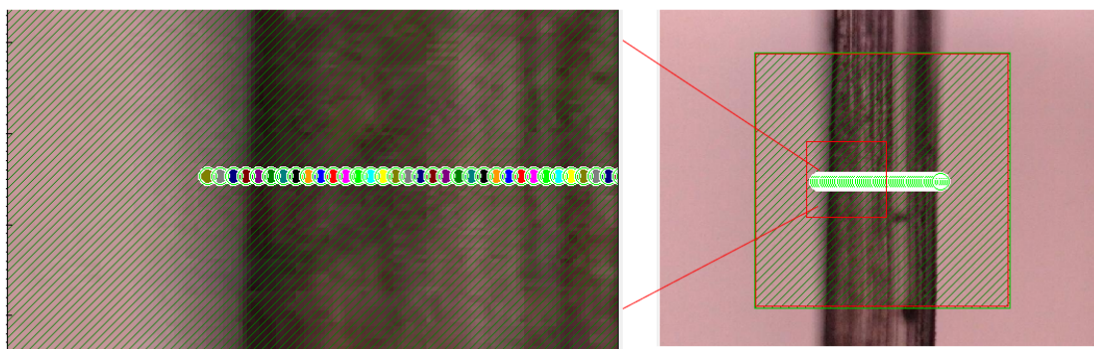


Figure 2.4. Data point selection in the case of PC.

Exportation of spectra from the original mappings was done using OPUS software, and further treatments were performed using OMNIC software. The reproducible results of the profiles were presented as the averages of 3 lines from different samples.

In the case of the less rigid PE, it was necessary to sandwich the films between layers of epoxy resin to stiffen them in view of microtoming. The preparation of the cross-sectional samples involved the following steps:

1. Sandwich the PE film between the epoxy layers and cool down the obtained structure in liquid nitrogen before fixing it on the microtome (Figure 2.5, 1, the sample holder of the microtome is not drawn).
2. Cut a 50 μm -thick slice of the sandwich structure with the microtome blade (Figure 2.5, 2).
3. Place the cut sample (Figure 2.5, 3) in the sample holder for further analysis.

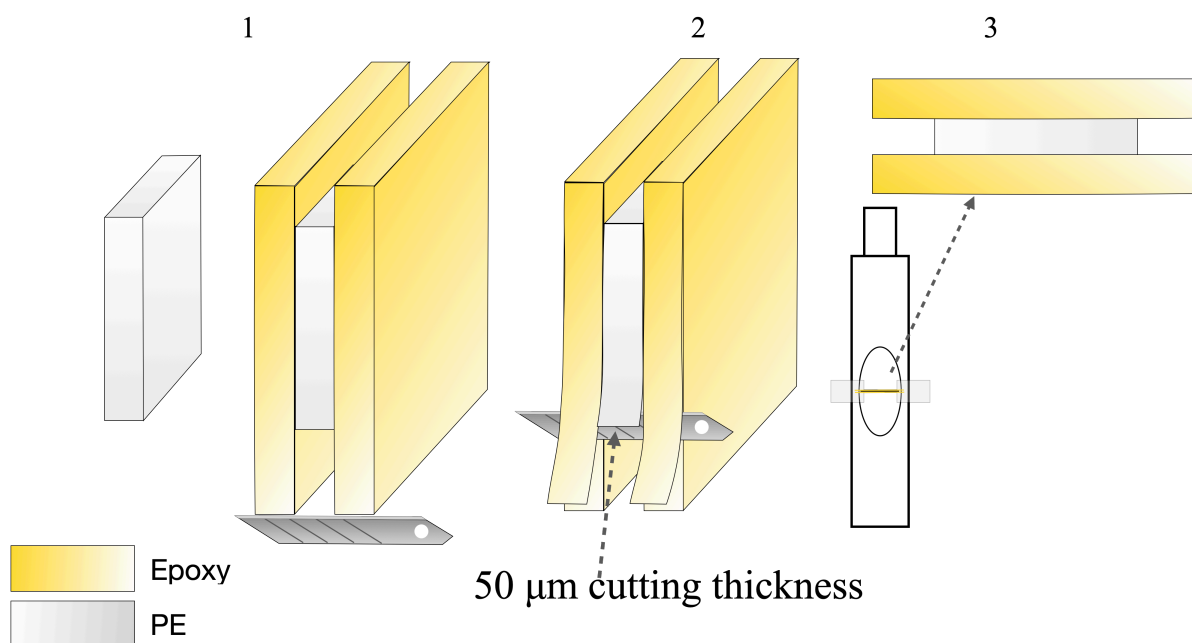


Figure 2.5. Preparation of PE sample for infrared transmission microspectroscopy: 1. PE sample and the sample sandwiched between epoxy layers, 2. sample cutting using microtome, 3. final sample.

As it was impossible to apply this procedure to a 30 μm film (as mostly used in Chapter 4), it was decided to work with a more rigid film of 90 μm : if no oxidation profile is observed with a thicker sample, the same can be assumed for a thinner one. The obtained results were then treated as presented above for PE: integration of the carbonyl band (1650 - 1850 cm^{-1}) and normalization with the area of the 1490 - 1420 cm^{-1} region to consider any thickness variation.

4.1.2. UV-visible spectroscopy

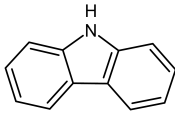
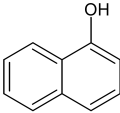
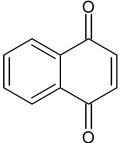
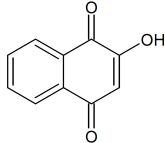
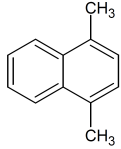
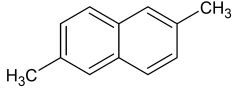
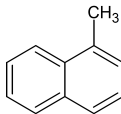
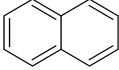
UV-visible spectroscopy [2] is a quantitative and analytical technique employed to measure the absorption of visible or ultraviolet (UV) light (typically within the wavelength range of 200 nm to 800 nm).

During this study, UV-visible spectroscopy was used to characterize the photoaging of polymer films in stationary mode, and to detect the transmission of non-fluorescent permeants for liquid permeability in kinetic mode (Chapter 4).

For photoaging, the absorption spectra in the UV-visible range (200 nm to 800 nm), with parameters of slow mode, 2 nm data interval, and 5 nm slit width, were obtained using a Shimadzu UV-2600 spectrophotometer equipped with an ISR-2600 Plus integrating sphere.

For liquid permeability experiments (detailed in this Chapter [4.2.2](#)), the results were collected using an Agilent Cary 60 UV-vis spectrophotometer in kinetic mode (1 point collected every 1.2 seconds) Calibration curves were determined and systematically verified to ensure the validity of the Beer-Lambert law within the obtained concentration (1.0×10^{-5} - 2.5×10^{-4}) for each probe at the detection wavelength, in order to calculate concentration values from absorbance. For 2 permeants using UV-visible spectroscopy, the associated characteristic wavelengths for them are listed in Table 2.1 with their structures and dipole moments.

Table 2.1. Structure, dipole moment and spectroscopic detection method (with characteristic wavelengths) for the various permeants used for permeability measurements in the liquid phase.

Permeant	Carbazole C ₁₂ H ₉ N	1-naphthol C ₁₀ H ₈ O	1,4-naphthoquinone C ₁₀ H ₆ O ₂	2-hydroxy-1,4-naphthoquinone C ₁₀ H ₆ O ₃
Structure				
Dipole moment (D)	1.77	1.29-1.49	1.36	2.99
Detection method (wavelengths)	Fluorescence ($\lambda_{exc} = 320$ nm, $\lambda_{em} = 360$ nm)	Fluorescence ($\lambda_{exc} = 300$ nm, $\lambda_{em} = 360$ nm)	UV-visible ($\lambda_{abs} = 330$ nm)	UV-visible ($\lambda_{abs} = 330$ nm)
Permeant	1,4-dimethylnaphthalene C ₁₂ H ₁₂	2,6-dimethylnaphthalene C ₁₂ H ₁₂	1-methylnaphthalene C ₁₁ H ₁₀	Naphthalene C ₁₀ H ₈
Structure				
Dipole moment (D)	0.06	0.00	0.37	0.00
Detection method (wavelengths)	Fluorescence ($\lambda_{exc} = 290$ nm, $\lambda_{em} = 340$ nm)	Fluorescence ($\lambda_{exc} = 270$ nm, $\lambda_{em} = 340$ nm)	Fluorescence ($\lambda_{exc} = 290$ nm, $\lambda_{em} = 336$ nm)	Fluorescence ($\lambda_{exc} = 290$ nm, $\lambda_{em} = 336$ nm)

4.1.3. Fluorescence spectroscopy

Fluorescence spectroscopy is a technique used to analyse the emitted photons from a sample following excitation by light absorption. When a sample absorbs photons with sufficient energy, it transitions from its ground state (S_0) to an excited singlet state ($S_1, S_2 \dots$). Initially, the electrons of the sample undergo non-radiative decay to reach the first excited singlet level, S_1 . Then the electrons decay radiatively to the ground singlet state, causing fluorescence emission. Fluorescence spectroscopy enables qualitative and quantitative analysis of fluorescent compounds in a sample by measuring the emitted photons. Alternatively, the electrons transiting from a singlet excited state to a triplet state may return radiatively to the ground singlet state, resulting in phosphorescence emission. However, in our experimental conditions, observing phosphorescence emission for the samples chosen is rare and not a priority.

The processes presented above are shown in the Perrin–Jablonski diagram in Figure 2.6.

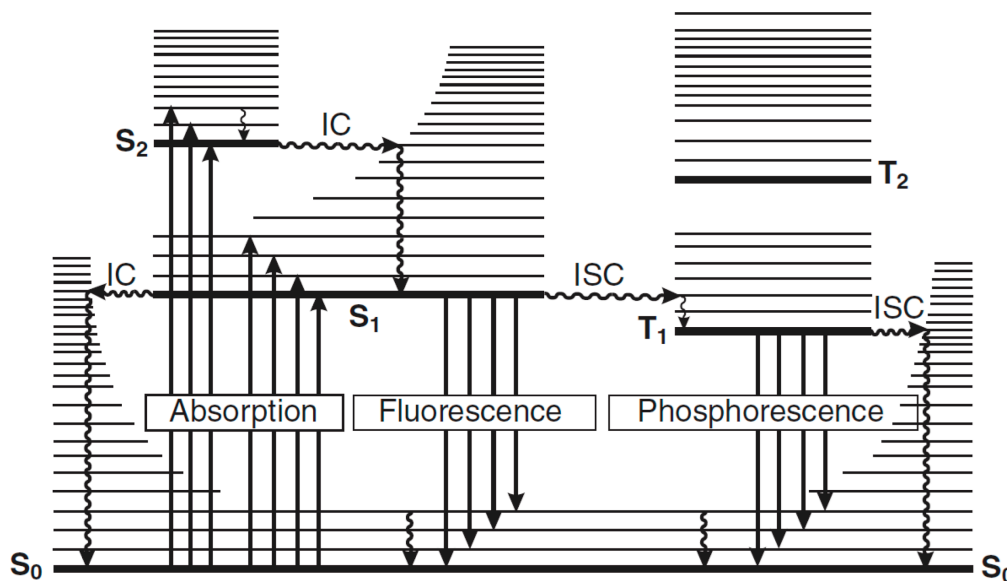


Figure 2.6. Perrin–Jablonski diagram with the possible radiative transitions (straight arrows) of absorption, fluorescence and phosphorescence; and the non-radiative transitions (wavy arrows) of vibrational relaxation, internal conversion (IC) and intersystem crossing (ISC), occurring among ground state (S_0), excited energy singlet level (S_1 and S_2), and triplet state (T_1)[5].

In this study, fluorescence was employed to detect permeants crossing PE films during the liquid permeability experiments (detailed in this Chapter 4.2.2). A Varian Cary Eclipse fluorescence spectrophotometer was used in kinetic mode (1 point per 1.2 seconds). Excitation and emission slit widths were set at a relatively high value (10 nm) to maximize the fluorescence intensity from the permeants in trace amounts. The experiments were performed at room temperature. For 6 permeants using fluorescence spectroscopy, the associated characteristic wavelengths for them are also listed in Table 2.1 with their structures and dipole moments.

Calibration curves were determined for each permeant at its detection wavelength in order to calculate the concentration values from fluorescence intensity with the following equations:

$$I_F = \Phi_F \times I_a = \Phi_F \times (I_0 - I_t) = \Phi_F \times I_0 \times \left(1 - \frac{I_t}{I_0}\right) \quad \text{Eq. 2}$$

where I_F is the fluorescence intensity and Φ_F the fluorescence quantum yield. I_0 , I_a and I_t represent, respectively, the incident, absorbed and transmitted light intensities.

$$\frac{I_t}{I_0} = 10^{-A} = e^{-2.3A} \quad \text{Eq. 3}$$

with A the absorbance.

$$I_F = \Phi_F \times I_0 \times (1 - 10^{-A}) = \Phi_F \times I_0 \times (1 - e^{-2.3A}) \quad \text{Eq. 4}$$

in the case with carbazole (concentration between 2.5×10^{-6} - 1.5×10^{-5} mol.L⁻¹), A is below 0.1, the following approximation could be made:

$$(1 - e^{-2.3A}) \approx 2.3A \quad \text{Eq. 5}$$

Eq. 4 results finally in:

$$I_F \approx \Phi_F \times I_0 \times 2.3A \approx (\Phi_F I_0 2.3 \epsilon l) \times c \quad \text{Eq. 6}$$

with ϵ the molar absorption coefficient, l the light pathlength and c the concentration of absorbing species. The fluorescence intensity appears then to be proportional to the concentration in that specific case.

For all other permeants (concentration within the range 1.0×10^{-5} - 5.0×10^{-4} mol.L⁻¹), the approximation of Eq. 6 could not be made since the absorbance was above 0.1. Thus, Eq. 4 was used directly with the fitting tool of Origin software to establish the more general relation between the concentration and the fluorescence intensity. Take the permeant naphthalene as an example, where the original data is a curve, as shown in Figure 2.7. The data were fitted by using the function $I_F = A(1-10^{-B \times C})$, in order to obtain the independent parameters $A = 496.7$ and $B = 1790.0$. These parameters were used to determine the concentration of naphthalene in the solution.

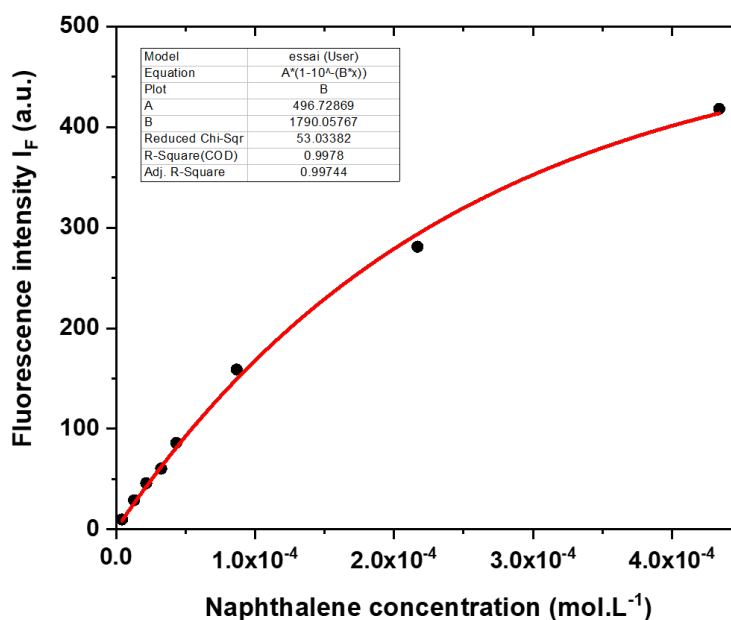


Figure 2.7. Fluorescence calibration plot for naphthalene The data were fitted to obtain the independent parameters.

4.2. Permeability methods

4.2.1. Oxygen permeability

The measurement of oxygen permeability was performed using a Systech Illinois 8003 oxygen permeation analyser equipped with a coulometric detector. Unless otherwise stated, the temperature was maintained at 23 °C.

An oxygen permeability sample consists of a polymer film sandwiched between two adhesive aluminium plates (Figure 2.8a) with a central hole of 5 cm² (Figure 2.8b). The thickness of the samples was determined using an MTS Micrometer mi20 device. Five measurements (black measurement points in Figure 2.8b) were taken at different positions of the samples, and the average value was considered as the sample thickness.

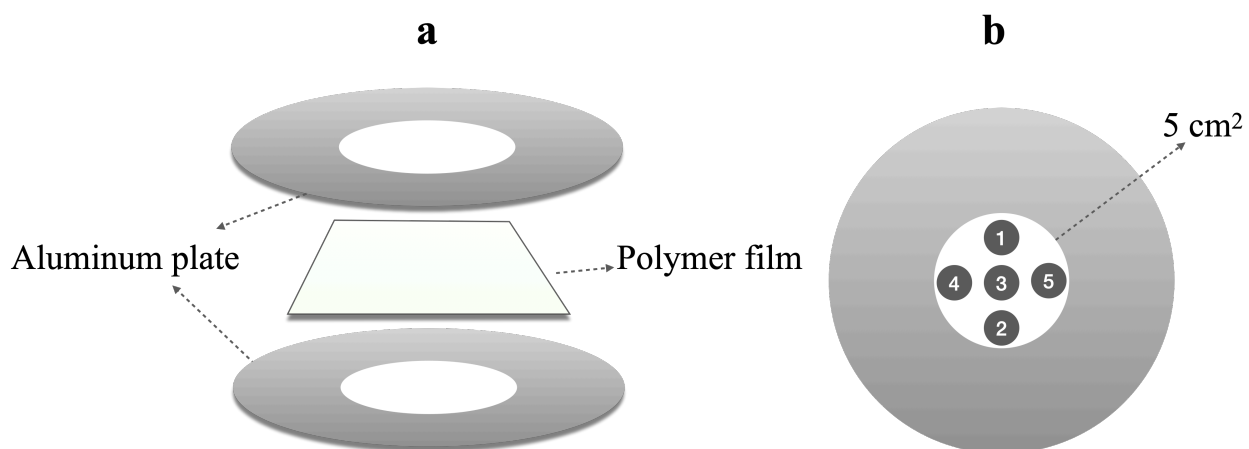


Figure 2.8. Oxygen permeability sample: a. sample structure, b. sample scale and measurement points.

The sample prepared was securely placed between two chambers, as shown in Figure 2.9:

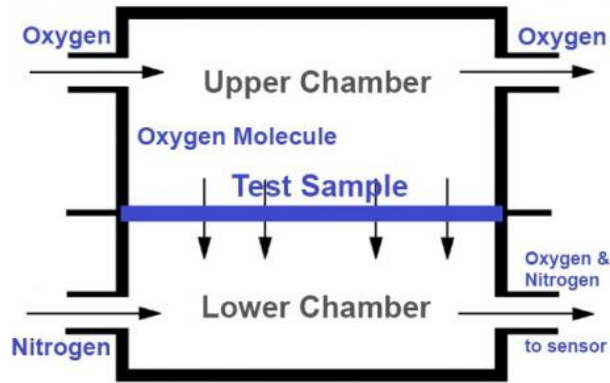


Figure 2.9. Oxygen permeability testing chamber.

The whole system was first purged from any residual oxygen with pure nitrogen. Then, the upper chamber was subjected to a flow of pure oxygen at 1 atmosphere pressure. The lower chamber, on the other hand, was exposed to a flow of pure nitrogen whose role is to carry the transmitted oxygen molecules towards the sensor, which could output the oxygen transmission rate (OTR) during the experiments. The permeability coefficient P was finally calculated from the steady state OTR value with:

$$P = OTR \times \frac{l}{\Delta p} \quad \text{Eq. 7}$$

where l represents the thickness of the sample, and Δp denotes the oxygen pressure difference between the two chambers, which is set at 1 atmosphere pressure here. The permeability coefficient is typically expressed in units of $\text{cm}^3(\text{STP}) \cdot \text{cm} \cdot \text{cm}^{-2} \cdot \text{s}^{-1} \cdot \text{Pa}^{-1}$.

Diffusion coefficient can also be calculated from time-lag experiments (as presented in [Chapter 1 2.2.2](#)). In that case, the purging step was reinforced to ensure that all oxygen molecules initially dissolved into the polymer were removed prior to the introduction of oxygen gas on top of the sample. Three samples were considered for each aging time, and the average value of the reproducible measurements of the P (and D if considered) was presented.

4.2.2. Self-designed permeability experiment for permeants in liquid phase preparation

This part represents a crucial step of this study. Indeed, no system is commercially available to evaluate the transmission rate (permeability) in the liquid phase, so we took some time to design an appropriate system for these experiments. The main principle to estimate the permeability of different permeants in the liquid phase was to create a two-chamber-like closed system similar to the oxygen permeability analyser. The main difficulties were to:

1. seal appropriately the system,
2. find suitable analytical methods for detecting transmitted permeant in the bottom part of the system without interrupting the progress of the experiment,
3. enhance the sensitivity of detection.

The design of the final experimental system was continually refined and improved according to the feedback and results from several previous experimental setups. The final system is shown in Figure 2.10:

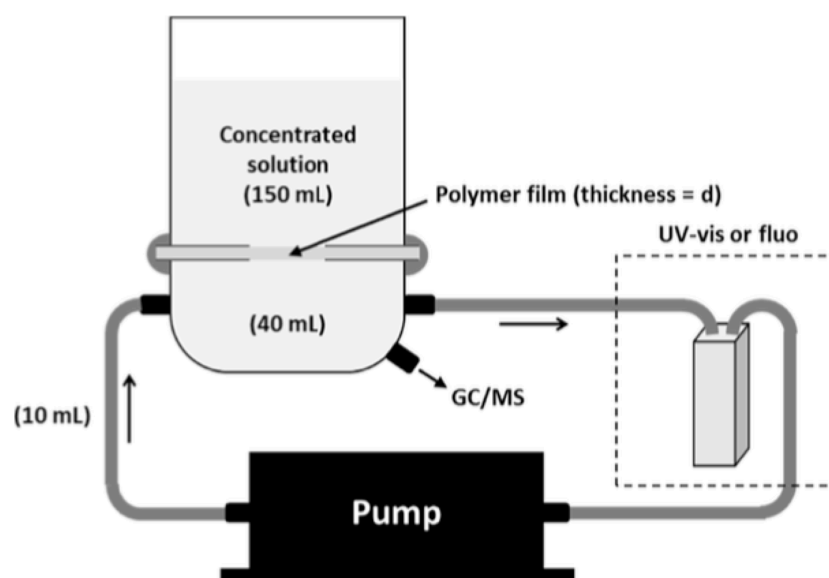


Figure 2.10. Self-Designed System for TR Measurements in the Liquid Phase .

The sealing was done from outside the system with hot-melt glue, while UV-visible or fluorescence spectroscopy (depending on the permeant used, see Table 2.1) was selected as the online detection method.

The lower part of the system (Figure 2.11) was specially designed with a glass manufacturer and deserves some explanations as it greatly improved the performances of the system. In fact, it consists of a small volume (40 mL) that enables to enhance the sensitivity (higher concentration). Additionally, it offers multiple ports for connection with a flow cell and a pump for online detection by fluorescence or UV-visible spectroscopy, or possible extraction of a small volume (1 μL) for GC analysis.



Figure 2.11. Custom-designed lower part.

Methanol (MeOH) was selected as the solvent used for these experiments for several reasons: it has a sufficiently low viscosity for pumping with small diameter pipes; it does not react with PE or PC; it has a high ability to dissolve organic compounds. This last point offers the possibility to have a high concentration gradient between the two chambers, and then fasten the experiments. The concentration of permeants in the lower part being far lower than that in the upper part (10^{-5} - 10^{-6} vs. 4.0×10^{-2} mol.L⁻¹ respectively), this concentration gradient was considered constant throughout the experiments.

The following procedure was used to launch a liquid permeability experiment:

1. Equilibrate the system with MeOH only, by filling the lower part and introducing 10 mL in the upper part for at least 10 minutes.
2. Add 140 mL of the MeOH solution containing the permeant in the upper part (concentration of $4.0 \times 10^{-2} \text{ mol.L}^{-1}$ in the total 150 mL in the upper part).

Thanks to the pump, the transmitted permeant is transferred to the UV-visible or fluorescence spectrometer for detection, and the permeability of the permeant through the polymer is estimated by the corresponding transmission rate (slope of the linear part of the concentration vs. time curve recorded).

Results from the spectroscopic methods were double-checked by GC experiments (see details below) for two substances: carbazole and naphthol. This confirmed the results obtained with UV-visible and fluorescence. Experiments with other permeants were then done with a spectroscopic method.

A permeant calibration procedure was conducted to optimize the GC method and select an appropriate column to analyse the different permeants comprehensively. 1 μL was regularly extracted from the experimental setup in Figure 2.9 and injected into a GC-MS from Thermo Fischer Scientific (Trace GC Ultra DSQ). It was equipped with a column from Agilent J&W GC column with the following features: HP-5MS UI; 30 m; 0.250 mm diameter and 0.25 μm . The temperature program was set as: time 0 - 9 min temperature 60 $^{\circ}\text{C}$ – 325 $^{\circ}\text{C}$ followed by a holding time of 5 minutes. Method edition and results collection were performed using Xcalibur software. Data treatment and calibration fitting were done using Origin® 2019.

All liquid permeability experiments were done, at least, two times to ensure reproducibility.

4.2.3. Gas transmission rate

For gases different from oxygen, a gravimetric method was used to determine the corresponding Gas Transmission Rate (GTR) [6] for PE. The polymer sample was fixed at the top of a 40 mL cylindrical-like bottle (inner diameter of 3.5 cm and height of 5.0 cm, as shown in Figure 2.12a). The contact surface between the polymer and the vapour was of 3.14 cm². Experiments were started with an initial given volume of solvent (33 mL) at a temperature of 40 °C. The weight change of the bottle content, which should be due to the permeation through the PE of the vapour in equilibrium with the liquid present in the bottle, was monitored regularly. The slope of the weight loss Δm as a function of time, which can be converted into GTR, was determined with a linear fitting (Chapter 5).

At least five samples were prepared for each aging time, and the average value of the reproducible gas transmission rate was calculated.

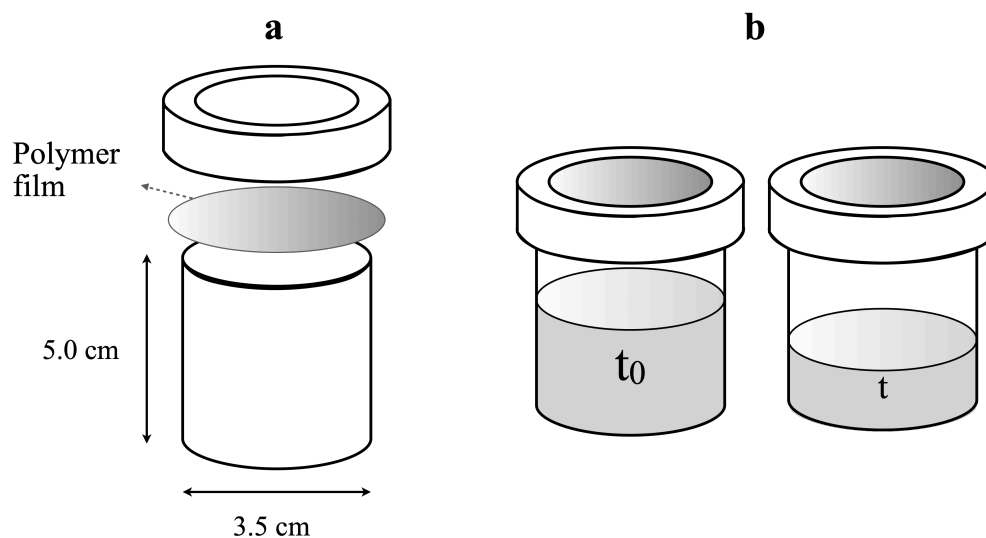


Figure 2.12. Gas transmission rate testing system: a. bottle characteristics, b. change in the liquid content between initial time (t_0) and a certain time (t) during the experiments.

4.3. Other methods

4.3.1. Differential Scanning Calorimetry

The measurement of thermal transitions in polymers was achieved with Differential Scanning Calorimetry (DSC) [7, 8]. This technique involves monitoring the heat flow of a sample compared to an empty crucible while subjecting them to a temperature scan. Through DSC analysis, valuable information such as the glass transition temperature (T_g), melting temperature (T_m), crystallization temperature (T_c), and corresponding enthalpies of transition (ΔH_f , ΔH_c) can be obtained. The degree of crystallinity (χ_c) of a polymer can be determined based on its melting enthalpy (ΔH_f) using the following equation:

$$\chi_c = \frac{\Delta H_f}{\Delta H_{f0}} \quad \text{Eq. 8}$$

where ΔH_{f0} is the melting enthalpy of a 100 % crystalline polymer, which is 293 J.g⁻¹ for PE [9, 10].

The analyses were performed using a Mettler Toledo DSC 3+ instrument equipped with an Intracooler cooling system. 5 to 15 mg of polymer were placed in a closed 40 μ L aluminium crucible. The thermograms were recorded under a dry air flow, with a heating rate of 10 °C.min⁻¹. For each aging time, three films were analysed, and the average crystallinity value was calculated. The DSC curve data were treated using the STARe® software.

4.3.2. Gel fraction measurement

In order to quantify the cross-linked fraction within PC, a gel fraction [11-13] test was conducted. When a polymer is introduced into a solvent, two distinct fractions could emerge. The gel fraction represents the insoluble cross-linked portion, while the soluble fraction corresponds to the non-

cross-linked component. By assessing the gel fraction at a specific aging time, it becomes possible to estimate the amount of cross-linked material, providing valuable evidence of its occurrence upon aging.

100 mg of PC was introduced inside 60 mL of chloroform for 2 days at room temperature. The insoluble part was then filtered and dried in a vacuum oven at room temperature overnight to remove as much solvent as possible. The gel fraction was calculated as follows:

$$gel\ fraction = \frac{m_{insoluble}}{m_{total}} \quad Eq. 9$$

where the $m_{insoluble}$ is the mass of the insoluble fraction, and m_{total} is the initial mass of the polymer introduced. Three gel fraction experiments were carried out for each aging time to ensure reproducibility, and the average value of the gel fraction was calculated.

4.3.3. Atomic force microscopy

Atomic Force Microscopy (AFM) is a surface analysis relying on the interactions between a scanning tip and the atoms at the surface of a sample [14, 15]. Tapping mode in AFM involves the oscillation of the probe at a frequency close to its resonance frequency during scanning. This allows for higher-resolution imaging by minimizing the interaction forces between the tip and the sample while maintaining intermittent contact.

For this study, PE samples were analysed in this mode. The measurements were performed using an Innova® atomic force microscope (Bruker). Topography and phase images were recorded using RTESPA 300 probes (Bruker) with a nominal tip radius of 8 nm. The surface images of the polymer were captured on three films for each aging time to ensure reproducibility using the Nano Drive Innova Tapping software. Photo treatment was performed using NanoScope Analysis 3.00.

4.3.4. Micro-hardness tester

Micro-hardness is one way to characterize the mechanical properties of a polymer. More specifically, it evaluates the resistance to the deformation caused by an indenter. Depending on the shape and the material of the indenter, one can distinguish between several methods (Vickers, Brinell...).

In this study, Vickers micro-hardness was measured for PC with a Shimadzu HMV hardness tester. In that case, a pyramidal diamond indenter was applied on the polymer surface with a constant force to make an indentation. The results of the indentation scale were then used to calculate the micro-hardness H_v using the following equation [16]:

$$H_v = 1.8544 \frac{F}{d^2} \quad \text{Eq. 10}$$

where F is the applied load (100 gf in our case, which equals the force of 0.1 kg), and d is the average of the diagonal lengths as presented in Figure 2.13. According to the standard of Vickers indenter, the depth of the indenter that penetrated the sample is estimated to be $d/7$ [17].

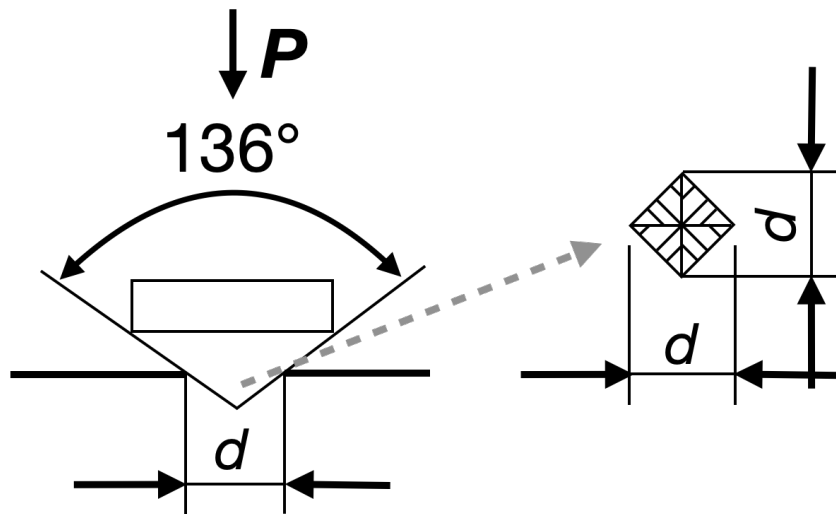


Figure 2.13. Principle of Vickers micro-hardness measurement.

Five independent measurements were done on three films for each aging time to ensure reproducibility, and the average value of the micro-hardness was calculated.

References

1. Lemaire J, Arnaud R, Gardette J L. Vieillissement Des Polymeres. Principes D'etude Du Photovieillissement. Revue générale du caoutchouc et des plastiques, 1981, 58: 87-92.
2. Gardette J L. Caractérisation des polymères par spectrométrie optique. Ed. Techniques Ingénieur, 1997.
3. Kraus R G, Emmons E D, Thompson J S, et al. Infrared absorption spectroscopy of polycarbonate at high pressure. Journal of Polymer Science Part B: Polymer Physics, 2008, 46(7): 734-742.
4. Matar Z S, Al-Dossari M, Awasthi S K, et al. Theoretical Study on Polycarbonate-Based One-Dimensional Ternary Photonic Structures from Far-Ultraviolet to Near-Infrared Regions of Electromagnetic Spectrum. Crystals, 2022, 12(5): 642.
5. Valeur B, Berberan-Santos M N. Molecular fluorescence: principles and applications. John Wiley & Sons, 2012.
6. Baschetti M G, Minelli M. Test methods for the characterization of gas and vapor permeability in polymers for food packaging application: A review. Polymer Testing, 2020, 89: 10660
7. Höhne G W H, Hemminger W F, Flammersheim H J, et al. Applications of Differential Scanning Calorimetry. Springer Berlin Heidelberg, 2003.
8. Wunderlich B. Thermal analysis of polymeric materials. Springer Science & Business Media, 2005.
9. Kodre K V, Attarde S R, Yendhe P R, et al. Differential scanning calorimetry: A review. Research and Reviews: Journal of Pharmaceutical Analysis, 2014, 3(3): 11-22.

10. Wunderlich B, Cormier C M. Heat of fusion of polyethylene. *Journal of Polymer Science B Polymer Physics*, 1967, 5(5): 987-988.
11. Lopérgolo L C, Lugão A B, Catalani L H. Direct UV photocrosslinking of poly (N-vinyl-2-pyrrolidone)(PVP) to produce hydrogels. *Polymer*, 2003, 44(20): 6217-6222.
12. Rivaton A, Mailhot B, Derderian G, et al. Investigation of the photophysical processes and photochemical reactions involved in PVK films irradiated at $\lambda > 300$ nm. *Macromolecules*, 2003, 36(15): 5815-5824.
13. Alcântara M T S, Brant A J C, Giannini D R, et al. Influence of dissolution processing of PVA blends on the characteristics of their hydrogels synthesized by radiation—Part I: Gel fraction, swelling, and mechanical properties. *Radiation Physics and Chemistry*, 2012, 81(9): 1465-1470.
14. Kumar B, Bonvallet J C, Crittenden S R. Dielectric constants by multifrequency non-contact atomic force microscopy. *Nanotechnology*, 2011, 23(2): 025707.
15. Khan M K, Wang Q Y, Fitzpatrick M E. Atomic force microscopy (AFM) for materials characterization//Materials characterization using nondestructive evaluation (NDE) methods. Woodhead Publishing, 2016: 1-16.
16. Wu J. Pantograph and contact line system. Academic Press, 2017.
17. Chandler, H., Hardness testing. ASM international, 1999.

Chapter 3: Oxygen permeability on polycarbonate and polyethylene: effect of photoaging

1. Introduction

The third chapter of this thesis is dedicated to the connexion between oxygen permeability and the photoaging of two different polymers, polycarbonate (PC) and polyethylene (PE). Nowadays, PC and PE are two of the most commonly used polymers in the industry. During their usage and due to the environmental conditions, they could undergo severe aging either thermally or photochemically, leading to an important change in their permeability. For example, in agricultural film for PE and car headlights for PC, these two polymers are highly exposed to solar light throughout their lifetime. Thus, it is necessary to evaluate the extent of the permeability change, and understand it. Our choice of the two polymers PC and PE was made by considering some crucial factors:

1. PC is a polar polymer, while PE is non-polar.
2. PC is amorphous, while PE is semi-crystalline.
3. PC can absorb solar light that initiates its photoaging, while PE does not.

Thus, studying these polymers will permit us to understand and compare the changes in oxygen permeability upon their photoaging. It will lead us to a general comprehension and insight into the effect of photoaging on permeability. Oxygen permeability is used to evaluate the polymer performance as a critical industry property. Since the oxygen permeation analyser is commercially available, reliable and efficient results for the evaluation of permeability and diffusion coefficients will represent a perfect entry point for this part of the study.

The study is then organized as follows:

- PC and PE samples were photoaged in a SEPAP 12/24 within the wavelength 300 - 420 nm wavelength range, leading to crucial changes from physical, chemical, and also optical points of view.

- The consequences of this photoaging on their oxygen permeability were intensely evaluated.
- The various properties of PC, such as micro-hardness, gel fraction, etc., were also explored.
- For PE, the Arrhenius equation of permeation was examined within the range of temperature 10 °C - 50 °C. It was used to determine the activation energy of permeation and its possible change after photoaging.

The first part of this chapter, which concerns PC, is presented in the form of an article that was published in Journal of Applied Polymer Science (<https://doi.org/10.1002/app.54397>):

Chen Z, Sarakha M, Christmann J. Consequences of sequential photooxidation of polycarbonate: Relating microscopic modifications to the change of oxygen permeability. Journal of Applied Polymer Science, 2023, 140(37): e54397.

The experimental part of the published article has been described in Chapter 2; it is removed in the following part for the smooth reading of the manuscript.

The second part of the chapter is dedicated to the effect of photoaging on the oxygen permeability of PE, with a special attention to the role of the temperature on the latter process.

2. Consequences of sequential photooxidation of polycarbonate



RESEARCH ARTICLE

2.1. Introduction

Polycarbonate is a common amorphous thermoplastic polymer whose excellent properties (high transparency, toughness, heat and flame resistance...) open up a wide range of applications [1], from automotive (car headlights) to digital recording (protective layers of optical discs [2]). The permeability of polycarbonate to gases (especially oxygen and water vapour) is of great and fundamental importance for applications in the medical field (*e.g.* blood reservoirs and filters, connection components, packaging...) and for food packaging.

Such as all polymers, polycarbonate is sensitive to environmental stress factors such as heat or UV light that lead to its degradation, resulting in a negative effect on its mechanical and optical properties. The photoaging mechanism of polycarbonate has been studied in details for many years [3] and is now widely accepted [1, 4-8]. It consists in two main reaction pathways whose relative importance is irradiation wavelength dependent (dual photochemistry): photo-Fries rearrangements and fragmentation/coupling reactions are the main processes at $\lambda < 320\text{-}330$ nm while photooxidation of the geminal methyl groups is dominant at $\lambda > 320\text{-}330$ nm [5, 6, 9-11]. Ring oxidation have been also reported [8, 12].

Upon excitation at short wavelengths, direct light absorption by the aromatic rings moiety of PC permits the scission of CO-O bonds of the carbonate groups. The generated radicals may react,

either by two successive photo-Fries rearrangements leading to the formation of species L1 (phenyl salicylate) that further gives rise to L2 (dihydroxy benzophenone) [13], or by decarbonylation/decarboxylation followed by a recombination process (L3 compounds) [7, 12]. At longer wavelengths, radicals whose origin is still under debate [14, 15] (chromophoric defects or impurities [6, 7], photo-Fries photoproducts [1, 8], charge transfer complex of PC with oxygen [16]) initiate an oxidative chain radical process by hydrogen atom abstraction from the geminal methyl groups of PC. Successive isomerization, reaction with oxygen and H-abstraction by this radical lead to the formation of hydroperoxides, which can further evolve into various species such as carboxylic acids or alcohols that are easily detected by infrared spectroscopy [2, 6].

From a general point of view, photodegradation of polymers can lead to chain scission and/or cross-linking reactions [17], with the former possibly causing an increase of the crystallinity rate through the organization of the more mobile chain fragments obtained into crystalline areas (chemicrystallization) [18]. This results in the modification of the polymer structure, ultimately affecting its use properties (mechanical, optical etc.). In the case of PC, chain scissions are mainly β scissions that are consecutive to the decomposition of the hydroperoxides, as well as Norrish reactions of the resulting ketones [6]. Cross-linking results from reactions between radical species formed at different steps of the photooxidation mechanism [2]. Both chain scissions [19] and cross-linking [2, 4, 6, 20, 21] have been reported for PC upon photoaging. On the contrary, chemicrystallization has never been observed for such amorphous polymer.

Compared to the changes of mechanical and optical properties upon photoaging which have been extensively studied, the corresponding modification of permeability has been scarcely considered [22-30], and has never been studied for polycarbonate. Permeation of gases at ambient pressure for polymers is generally described by the solution-diffusion model [31-34], whose mechanism involves three consecutive steps: 1. solubilization of the penetrant at the polymer surface, 2.

diffusion from the entrance to the exit surface, 3. desorption at the latter. The first and third steps are purely thermodynamics and depend on the intensity of the penetrant-polymer interactions compared to penetrant-penetrant and polymer-polymer ones. In the simplest case, the concentration C of the penetrant at the surface of the polymer can be related to its partial pressure p by Henry's law:

$$C = Sp \quad \text{Eq. 1}$$

where S represents the solubility coefficient of the penetrant into the polymer. It should be noted that more complex cases of sorption can be described by other models (Langmuir, dual-mode...). Diffusion is a kinetic step which is controlled by a difference in chemical potential between the two sides of the polymer film. The penetrant molecules diffuse through successive random "jumps" from free volume areas within the polymer structure. The diffusion coefficient D is related to the penetrant flux J by Fick's first law (in one dimension here):

$$J = -D \frac{dC}{dx} \quad \text{Eq. 2}$$

The easiness of the whole permeation process is finally described by the permeability coefficient P whose value is specific to a polymer-penetrant couple:

$$P = D \times S \quad \text{Eq. 3}$$

The permeability of a polymer to a penetrant can be affected by several factors related to the environmental conditions (temperature, pressure), the nature of the penetrant (size, shape, molar mass, polarity) and the nature of the polymer (density, crystallinity rate, orientation, cross-linking rate, presence of fillers or plasticizers) [31, 32].

Upon photoaging, several of the characteristics of the polymer could be modified, especially its cohesive energy, crystallinity, and cross-linking rate. This would have ultimately an effect on its permeability. Indeed, the appearance of polar groups during the oxidation process would reinforce

the polymer-polymer interactions through various intermolecular interactions. In addition, it will also modify the polymer-penetrant interactions, in a way depending on the polarity. Since crystallites are considered impermeable to penetrant owing to their high density [35], it is clear that an increase of the crystallinity rate caused by chemicrystallization would reduce the polymer permeability. Moreover, the appearance of small crystallites and/or the growth of existing ones would also modify the tortuosity of the crystalline phase as well as its influence on the mobility of the neighbouring amorphous phase (respectively described by the tortuosity factor τ and the immobilization factor β in Reference [35]) and thus affect the permeation process. Finally, the increase of cross-linking rate upon photoaging could reduce the polymer permeability by limiting the available sorption/desorption sites at the surfaces as well as hinder the diffusion process within the polymer.

In the present work, we aim to relate the consequences of the photoaging on the polycarbonate structure to the change of its permeability to oxygen. To get a better control of the photooxidation process, each side of PC films was sequentially exposed to light in an accelerated photoaging setup. The progress of the photoaging process was tracked by FTIR and UV-visible spectroscopies, through the appearance and growth of polar oxidation groups. FTIR microspectroscopy was also used to evaluate the extent of the oxidation within the film thickness, *i.e.* its oxidation profile. The change in the oxygen permeability coefficient was then studied upon sequential photoaging and discussed in relation with the changes in the polycarbonate polarity, caused by oxidation, and structure, owing to cross-linking. The latter was evidenced by the increase of micro-hardness and gel fraction.

2.2. Results and discussion

2.2.1 Sequential photooxidation of PC films

It has been shown that photooxidation of PC is restricted to distances of roughly 20 μm from the surface because of the progressive yellowing of the polymer [2], which is caused by the appearance of coloured species generated by further oxidation of compounds resulting from photo-Fries rearrangements, fragmentation/coupling reactions as well as photooxidation and ring oxidation [1, 6, 8, 11, 12]. These species act as light absorbers which hinder light penetration into the polymer. Photooxidation and its consequences on the polymer structure (*vide supra*) are then limited to the sample surface according to a light absorption profile [2]. Because the entrance and exit surfaces are particularly important for the sorption and desorption steps of permeation, respectively, it was decided to sequentially expose the two sides of the PC samples to light (one of the two sides was covered with protective black paper in order to avoid any light exposure).

Upon irradiation, the FTIR transmission spectra of the samples progressively evolves, as can be seen in Figure 3.1a upon exposure of the first side (side #1). The appearance and growth of new bands is better observed on differential spectra, which were calculated by subtracting the spectrum obtained after a certain photoaging time by the spectrum recorded prior to light exposure (Figure 3.1b). Bands located at 1713 ($\text{C}=\text{O}$ stretching in carboxylic acids), 1840 ($\text{C}=\text{O}$ stretching in anhydrides) and 3480 cm^{-1} ($\text{H}-\text{O}$ stretching, not shown) clearly increase as a function of irradiation time [6]. These observed changes can be associated with the formation of oxidation groups such as carboxylic acids, anhydrides and alcohols/hydroperoxides, respectively. In addition, it can be observed the appearance and growth of two bands located at 1690 and 1630 cm^{-1} , which can be associated with compounds L_1 (phenyl salicylate) and L_2 (dihydroxy benzophenone) respectively,

resulting from the photo-Fries rearrangements [6, 13, 14, 36]. It has to be pointed out that similar observations were made when the second side (side #2) was exposed in its turn to light.

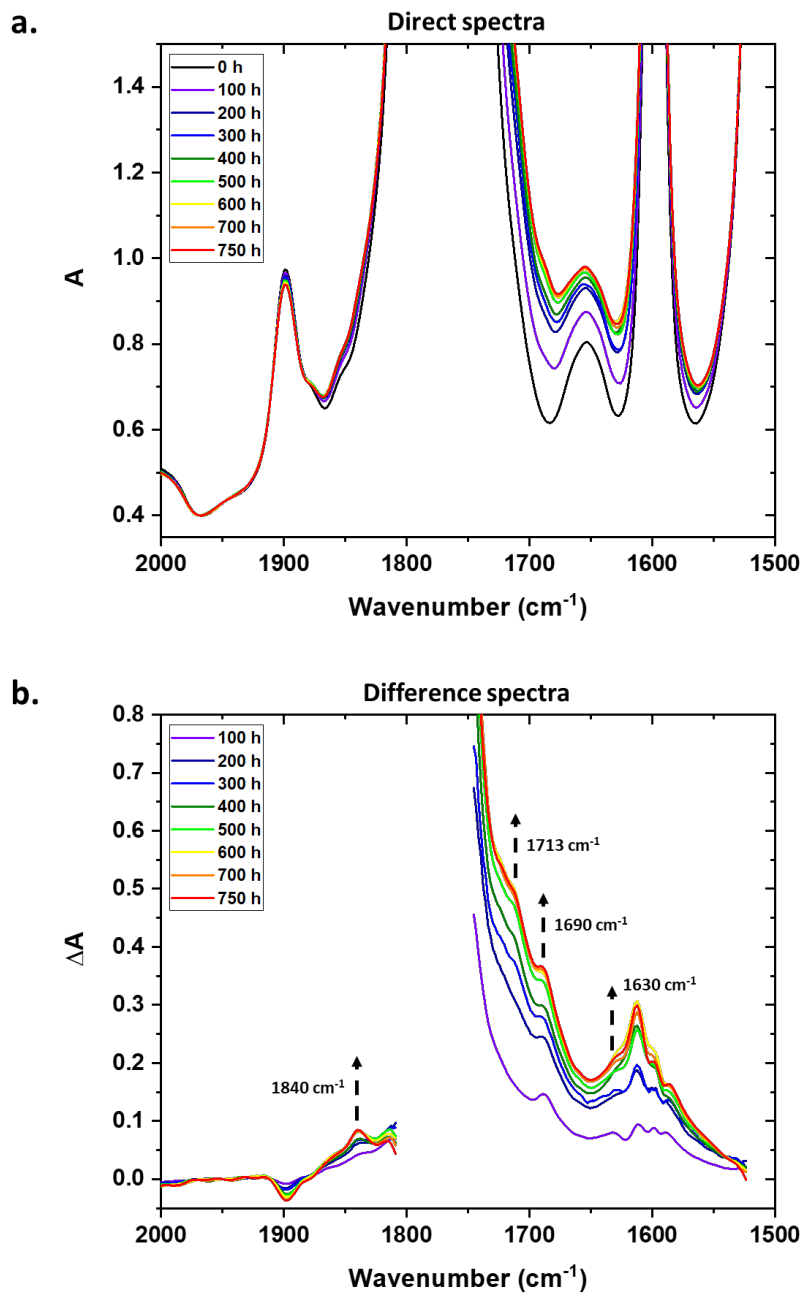


Figure 3.1. a. Direct and b. difference transmission FTIR spectra in the 2000 - 1500 cm⁻¹ region upon photooxidation of side #1 - $I = 90 \text{ W.m}^{-2}$, $CT = 55 \text{ }^\circ\text{C}$.

Figure 3.2 shows the change of absorbance ΔA at 1713 cm^{-1} as a function of the photoaging time in transmission IR for a sequential photoaging sample. ΔA value was calculated by subtracting the spectrum recorded prior to irradiation from the spectra obtained after a given exposure time.

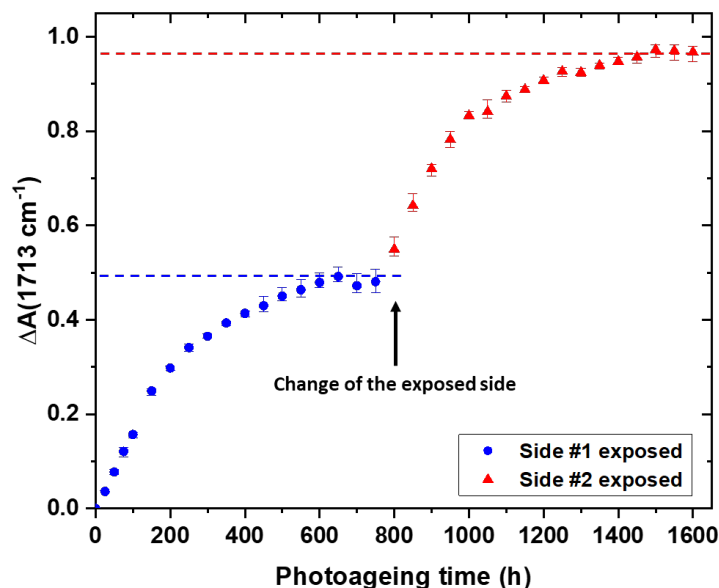


Figure 3.2. Difference of absorbance at 1713 cm^{-1} with respect to unexposed film upon sequential photooxidation (blue points = side #1 exposed, red triangles = side #2 exposed) – $I = 90\text{ W.m}^{-2}$, $CT = 55\text{ }^{\circ}\text{C}$. Results are an average from 3 samples, minimum and maximum values are also indicated to show the reproducibility.

As expected, an identical behaviour is observed for both sides, namely a progressive increase up to a limit value (plateau) at roughly 500 h. A similar behaviour was obtained when considering ΔA values at 1840 and 3480 cm^{-1} . The appearance of the limit value results from the progressive yellowing of the sample which hinders further light penetration and the subsequent photooxidation process (vide supra). The extent of yellowing can be assessed by UV-visible spectroscopy (Figure 3.3 for side #1 exposed). In addition, the limit value after sequential irradiation of each side (0,96) is twice that obtained for side #1 alone (0,49). This indicates that the oxidation process which is achieved on side #1 after around 500 h (first plateau) then develops on side #2 when it is exposed to light, *i.e.* the sequential nature of the photoaging process on the two sides.

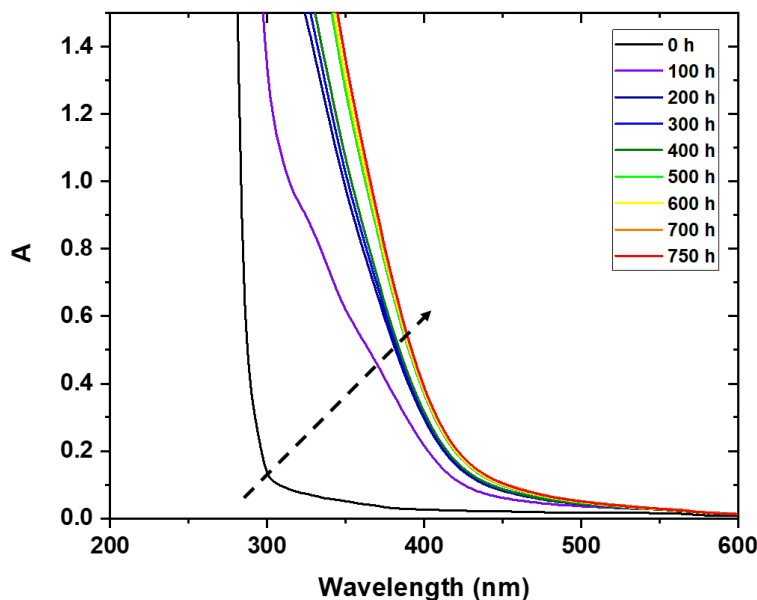


Figure 3.3. UV-visible spectra upon photooxidation of side #1 – $I = 90 \text{ W.m}^{-2}$, $CT = 55 \text{ }^\circ\text{C}$.

In parallel, PC samples were placed for 1600 h in an oven at $55 \text{ }^\circ\text{C}$ (corresponding to the temperature measured in the SEPAP 12/24) in the absence of light for a "dark" control experiment. In order to reproduce the sequential photoaging procedure, side #2 only was covered with a black paper for the first 800 h and side #1 only for the last 800 h. No change in the transmission FTIR and UV-visible spectra was observed upon the total photoaging time, which clearly indicates that the initiation of oxidation is purely caused by light.

To further assess this sequential character, ATR FTIR spectra were also recorded on the exposed and non-exposed sides of the samples upon photoaging (see Figure S3.8). It clearly shows the appearance and growth of oxidation products only on the exposed side, up to a plateau. FTIR microscopy was finally performed on a cross-sectional sample sequentially exposed 800 h on each face. The extent of oxidation was then assessed by calculating the oxidation profile within the sample according to the method detailed in [Chapter 2 4.1.1](#) (Figure 3.4).

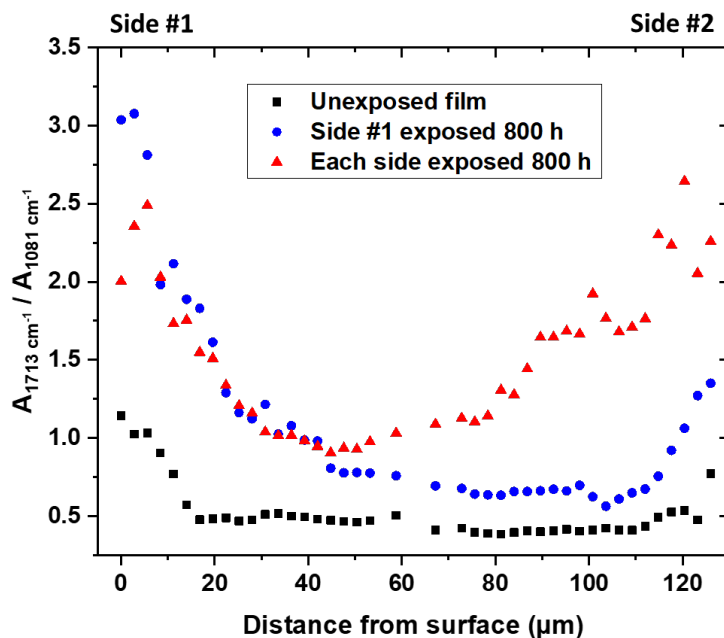


Figure 3.4. Photooxidation profile of a 125 μm unexposed film (black squares), a film exposed 800 h on side #1 (blue circles) and a film sequentially exposed on each side (red triangles) – $I = 90 \text{ W}\cdot\text{m}^{-2}$, $CT = 55 \text{ }^\circ\text{C}$. Each profile is an average from 6 lines.

Upon exposure of side #1 only, a non-symmetrical oxidation profile is obtained (blue circles). This indicates that oxidation compounds are mostly produced at the surface of side #1. ΔA values rapidly decrease within the thickness of the sample because of the light penetration profile as a consequence of PC yellowing (*vide supra*): photooxidation is then restricted to the surface of side #1 and ends when all its reactive sites are degraded. When side #2 in its turn is exposed to light, an almost symmetrical oxidation profile is obtained (red triangles), resulting from the formation of photoproducts on side #2. This clearly confirms the sequential nature of the photooxidation process. Such data also permit to estimate the oxidation depth in the PC film. This was found to be roughly $30 \pm 5 \mu\text{m}$, in good agreement with the value reported in literature [2].

2.2.2 Change in oxygen permeability upon photoaging

The change in oxygen permeability in the course of the photoaging is given in Figure 3.5 upon sequential exposure to light. An initial value of $1.92 \times 10^{-13} \text{ cm}^3(\text{STP}).\text{cm}.\text{cm}^{-2}.\text{s}^{-1}.\text{Pa}^{-1}$ was obtained and is consistent with published values for PC [38]. As can be observed, the changes in permeability coefficient P are different after sequential photooxidation of side #1 and both sides, and will be then discussed separately.

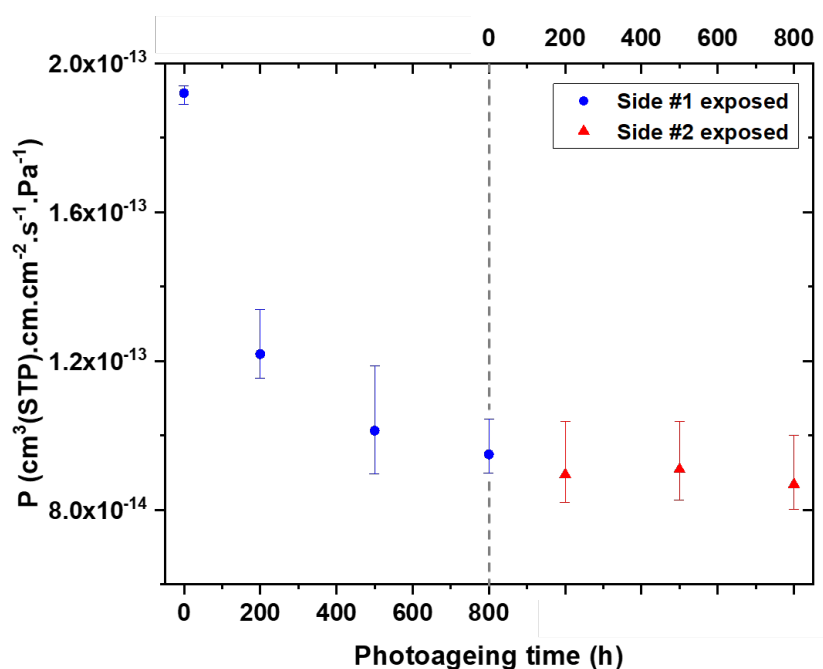


Figure 3.5. Permeability coefficient P upon sequential photooxidation of films (blue points = side #1 exposed, red triangles = side #2 exposed) – $I = 90 \text{ W.m}^{-2}$, $CT = 55 \text{ }^\circ\text{C}$. Results are an average from 3 samples, minimum and maximum values are also indicated to show the reproducibility.

Photooxidation of side #1

Upon photooxidation of side #1 only, a progressive decrease of P up to a limit value (plateau) between 500 and 800 h is observed. After 800 h of light exposure, the permeability coefficient P is almost half its initial value (0.95×10^{-13} vs. $1.92 \times 10^{-13} \text{ cm}^3(\text{STP}).\text{cm}.\text{cm}^{-2}.\text{s}^{-1}.\text{Pa}^{-1}$ respectively). The

observation of a plateau at 500 h for both $\Delta A(1713 \text{ cm}^{-1})$ (Figure 3.2) and P (left part of Figure 3.5) changes upon photoaging clearly reveals that the decrease of P is correlated to the photooxidation process. This is confirmed by the absence of any change of the P values for samples from the "dark" control experiments at 55 °C (for which no appearance of any oxidation products after 800 h was observed, *vide supra*).

In addition, the diffusion coefficient D of samples prior to photoaging and after 800 h of light exposure was determined from time-lag measurements. After intense purging of the permeameter with nitrogen, oxygen was delivered, whose total transmitted quantity Q_{oxygen} was plotted as a function of time (Figure S3.10, Figure S3.11 and Figure S3.12 in the supplementary information). The time-lag t_L was obtained by extrapolating the linear part of the curve, which corresponds to the steady state of permeation, and D was then calculated with equation (presented in [Chapter 1 2.2.2](#)) [37]. The solubility coefficient S was finally deduced from P and D values with Eq. 3. D and S values are reported in Table 3.1.

Table 3.1. Values of the diffusion coefficient D and the solubility coefficient S for a non-exposed sample, a sample exposed 800 h on side #1 only and a sample exposed 800 h on each side. Each result is an average from 3 samples, minimum and maximum values are also indicated in parenthesis to show the reproducibility.

Photooxidation time (h)	Diffusion coefficient D ($\text{cm}^2 \cdot \text{s}^{-1}$)	Solubility coefficient S ($\text{cm}^3(\text{STP}) \cdot \text{cm}^{-3} \cdot \text{Pa}^{-1}$)
0	1.67×10^{-8} ($1.57-1.76 \times 10^{-8}$)	1.15×10^{-5} ($1.09-1.21 \times 10^{-5}$)
800 (side #1 only)	1.53×10^{-8} ($1.39-1.62 \times 10^{-8}$)	0.62×10^{-5} ($0.62-0.63 \times 10^{-5}$)
800 (side #1 and side #2)	1.47×10^{-8} ($1.38-1.52 \times 10^{-8}$)	0.59×10^{-5} ($0.53-0.62 \times 10^{-5}$)

D and S values determined prior to photooxidation are also consistent with reported values [38]. As can be observed, both values decrease upon photoaging, which clearly explains the decrease of P (*vide infra*). However, the extent of their change is quite different: -8 % for D and -47 % for S. This indicates that the decrease of P is mainly due to the decrease of S. As S represents the ability of oxygen to dissolve/desorb at the surface, this seems consistent with the fact that photooxidation is mainly occurring at the PC surface.

In addition, it should be pointed out that there was no difference in the P, D and S values determined when the oxidized side faced or not the oxygen flow (see Table S3.2 in the supplementary information). This may be explained by what can be called a "funnel effect": when several funnels are placed one after the other, the flow exiting the last funnel only depends on the diameter of the smallest one, no matter its position within the series. When the oxidized side faces the oxygen flow, the sorption ability of the polymer is reduced. On the contrary, its desorption capacity is decreased when the oxidized face is opposite to the oxygen flow. As the permeation analyser is only able to determine the amount of gas crossing the polymer (*i.e.* determine the whole permeation capacity, which results from sorption, diffusion, and desorption steps), no difference could be observed between these two cases.

Thus, by considering the photoaged sample as a multilayer sample constituted by an oxidized layer A ($l_A = 30 \pm 5 \mu\text{m}$) and a non-affected layer B ($l_B = 95 \pm 5 \mu\text{m}$) whose permeability coefficient is equal to that prior to photoaging ($P_B = 1.92 \times 10^{-13} \text{ cm}^3(\text{STP}).\text{cm}.\text{cm}^{-2}.\text{s}^{-1}.\text{Pa}^{-1}$), it is possible to estimate the permeability coefficient of the photogenerated oxidized layer according to [32]:

$$\frac{l_{tot}}{P_{tot}} = \frac{l_A}{P_A} + \frac{l_B}{P_B} \quad \text{Eq. 4}$$

where P_{tot} and l_{tot} stand for the permeability coefficient and the total thickness of the whole sample after 800 h of photooxidation, respectively. A value of $P_A = (0.37 \pm 0.05) \times 10^{-13} \text{ cm}^3(\text{STP}).\text{cm}.\text{cm}^{-2}.\text{s}^{-1}.\text{Pa}^{-1}$ is obtained, which reveals that the permeability coefficient in the oxidized layer is reduced by a factor of 5 when compared to the non-photoaged sample.

As stated earlier, the reduction of oxygen permeability upon photoaging can be due to three main factors (*vide supra*): 1. increase in crystallinity through chemicrystallization, 2. increase of polymer polarity owing to the formation of polar groups, 3. cross-linking. DSC experiments were performed upon photoaging (see Figure S3.13 and Figure S3.14) but do not show the appearance of any crystallites within the initially amorphous PC, which rules out any chemicrystallization. The increase in PC polarity due to the formation of polar groups (especially carbonyl and hydroxyl groups) upon photooxidation was clearly evidenced from the evolution of the FITR spectra (see Figure 3.1a) and might be one of the reasons of the decrease of P. Indeed, the formation of extra polar groups may decrease the possible interactions between the polymer and the non-polar oxygen molecules, as well as reinforce the polymer-polymer interactions. This would result in a decrease of solubility. In addition, extra polymer-polymer interactions may also hinder the movement of the chains, then the diffusion process. Finally, the occurrence of cross-linking can be assessed through the increase of micro-hardness (Figure 3.6) [2, 39] and the determination of the gel polymer fraction (Figure 3.7) [40, 41] upon photooxidation.

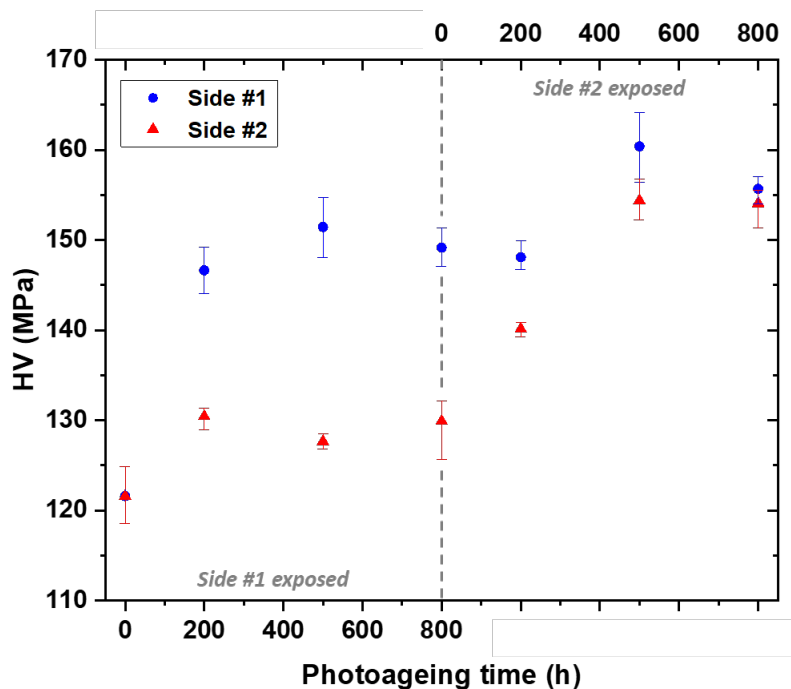


Figure 3.6. Vickers micro-hardness HV upon sequential photooxidation (blue points = side #1, red triangles = side #2) – $I = 90 \text{ W.m}^{-2}$, $CT = 55 \text{ }^\circ\text{C}$. Results are an average from 3 samples; minimum and maximum values are also indicated to show the reproducibility.

As can be seen in Figure 3.6 (left part), the Vickers micro-hardness (HV) of side #1, when it is exposed, strongly increases up to a plateau, while that of side #2 (non-exposed) is only slightly modified. The penetration depth of the indent crystal was estimated between 20 and 25 μm , meaning that only the surface was actually permeated with this technique. In addition, the amount of cross-linked material can be estimated through the measurement of the gel fraction. Sequentially photoaged samples were then dissolved into chloroform before drying and weighing the non-soluble residues.

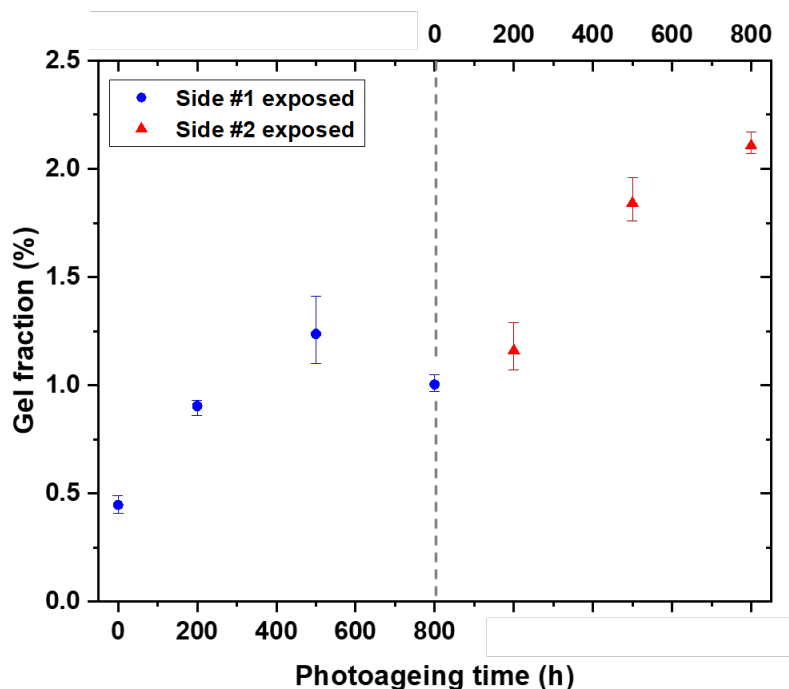


Figure 3.7. Insoluble gel fraction upon sequential photooxidation (blue points = side #1 exposed, red triangles = side #2 exposed) – $I = 90 \text{ W.m}^{-2}$, $CT = 55 \text{ }^{\circ}\text{C}$. Results are an average from 3 samples; minimum and maximum values are also indicated to show the reproducibility.

After light exposure of side #1 only (left part of Figure 3.7), the gel fraction increases up to a plateau (from 0.5 % prior to photoaging to 1.1 % at 800 h, *i.e.* +0.6 %), in agreement with the micro-hardness results. It has to be reminded that the gel fraction is determined from the mass of the whole sample, but it was shown that the oxidized part only concerns the first 30 μm over the total 125 μm of the PC films (Figure 3.4), so the actual increase of insoluble fraction should be rather estimated to approximately 2.5 % in the modified layer.

Simultaneous increases in micro-hardness and gel fraction clearly demonstrate the occurrence of cross-linking reactions during the photooxidation of PC, as proposed in previous works [2, 4, 6, 20, 21], with the corresponding mechanism proposed in Reference [2]. Although the amount of cross-linked material is rather low, the formation of cross-links between polymer chains could

strongly hinder the diffusion process, as well as reduce the number of sorption sites at the surface, owing to the reduction in chain mobility it causes. This would also contribute to the observed decrease in permeability upon photooxidation.

The decrease of the permeability coefficient upon photooxidation of side #1 would thus be a consequence of both the appearance of polar oxidation products and/or the occurrence of a cross-linking reaction. Although it is not possible to estimate the relative importance of these two phenomena, it could be expected that the decrease of solubility is mainly caused by the increase of polarity, while the reduction in diffusion is due to cross-linking.

Photooxidation of side #2

Photoaging of side #2 consecutive to that of side #1 (which was now protected from light) leads to a further increase of the concentration of oxidation products (Figure 3.2, red triangles), but only on the second surface (Figure 3.4). Cross-linking reactions (right parts of Figure 3.6 and Figure 3.7) also occur on this side, again up to a plateau. The increase of $\Delta A(1713\text{ cm}^{-1})$ and gel fraction is almost twice that upon exposure of side #1, which confirms the sequential nature of the photooxidation process. It was then expected that the permeability coefficient P would decrease again to the same extent as that obtained for side #1. However, it can be observed that P remains constant during the whole photooxidation process of side #2 (Figure 3.5, right part). No change in D and S was also observed (Table 3.1).

This unexpected result could also be discussed on the basis of the "funnel effect" previously invoked (*vide supra*). Indeed, the permeation process is already limited by the complete photooxidation of side #1 (which acts as a first "funnel"), so a modification of side #2 to the same extent as side #1 (second "funnel" of identical diameter to the first one) will not further reduce the whole oxygen permeability. In other words, it could be concluded that the permeation process is

limited by the most photoaged surface of the PC. This explains the absence of a second decrease of P during the photooxidation of the second side despite the consequent chemical and structural modifications observed in the latter.

2.3. Conclusion

Upon sequential UV light excitation of a 125 μm PC film, each side is oxidized up to a limit value within roughly 500 h. This is owing to the important formation of coloured species and/or moieties during the oxidation process, which acts as an inner filter preventing any further photodegradation. The thickness of the oxidized layer was estimated to be $30 \pm 5 \mu\text{m}$ for each side.

Upon photooxidation of the first side (side #1), the permeation coefficient P decreases to a plateau value within 500 h. Such decrease was estimated to -49 % and is rather due to the decrease of the solubility coefficient S (-47 %) than that of the diffusion coefficient D (-8 %). This is consistent with the localization of the oxidation process at the film surface, which affects the solubilization phenomenon. The decrease of P can be explained by two effects resulting from the photooxidation process: the appearance of extra polar groups and cross-linking, which would impact both solubility and diffusion. Indeed, the appearance and growth of carboxylic acids, esters, or hydroxyls was evidenced by FTIR spectroscopy and might modify polymer-polymer as well as polymer-oxygen interactions, which mainly result in a decrease of oxygen solubility in photoaged PC. The occurrence of cross-linking was proved by the increase of both Vickers micro-hardness and gel fraction during photoaging. This would reduce the number of available sorption sites at the surface of the polymer, as well as restrict oxygen diffusion. From the point of view of the applications of polycarbonate (packaging, medical components...), the decrease of oxygen permeability upon photoaging is then a positive feature.

The photoaging of side #2 leads to the same consequences as that observed for side #1 (*i.e.*, the appearance of extra polar groups, cross-linking, and yellowing...). However, it is not accompanied by a further decrease of the permeability coefficient P . This can be explained by the so-called "funnel effect": as the oxidation of side #1 already limits the whole permeation process, mainly through a reduction of solubility at its surface, the degradation of side #2 to the same extent would not further modify the measured value of P .

2.4. Acknowledgments

The authors wish to thank the *Université Clermont Auvergne* for financial support (Zhouyun Chen's PhD scholarship). In addition, Covestro® is warmly acknowledged for graciously providing Makrofol® DE 1-1 CG 000000 PC films and Prof. Jean-Luc Gardette and Dr. Sandrine Therias for the fruitful discussions.

2.5. Supplementary Information

ATR spectra of side #1 and side #2 upon sequential photooxidation

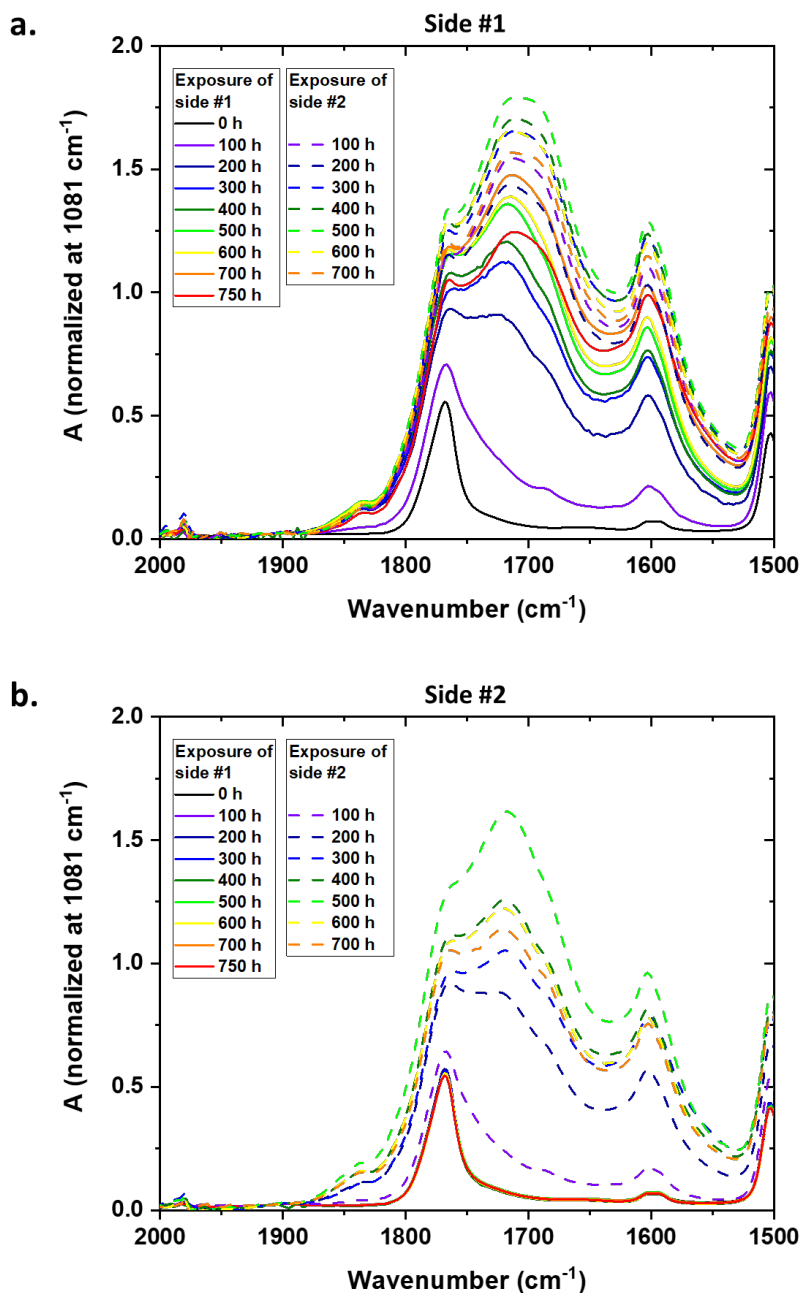


Figure S3.8. ATR FTIR spectra of a. side #1, b. side #2 in the 2000-1500 cm^{-1} region upon sequential photooxidation – $I = 90 \text{ W.m}^{-2}$, $CT = 55 \text{ }^\circ\text{C}$.

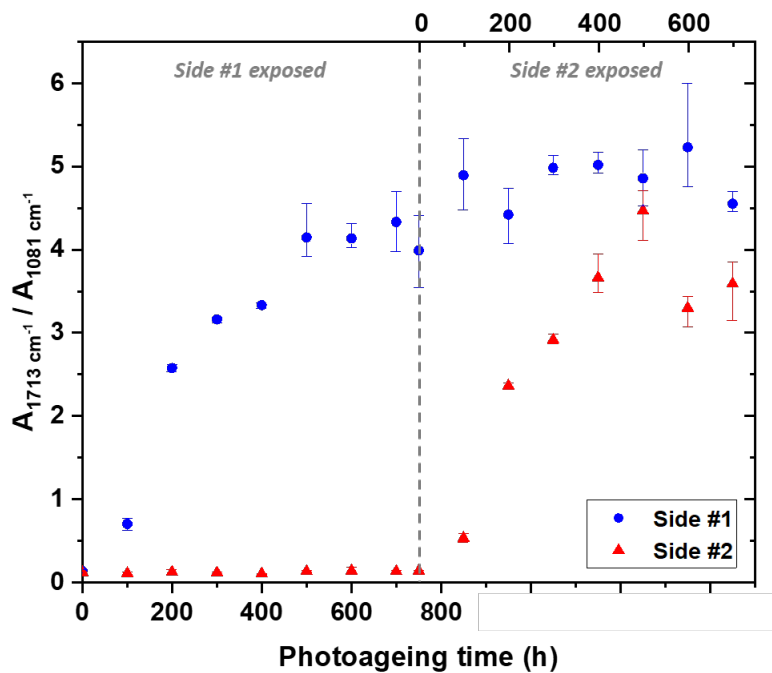
ATR photooxidation kinetics at 1713 cm⁻¹

Figure S3.9. 1713/1081 cm⁻¹ absorbance ratio of side #1 (blue points) and side #2 (red triangles) upon sequential photooxidation – $I = 90 \text{ W.m}^{-2}$, $CT = 55 \text{ }^\circ\text{C}$. Results are an average from 3 samples; minimum and maximum values are also indicated to show the reproducibility.

Time-lag experiments

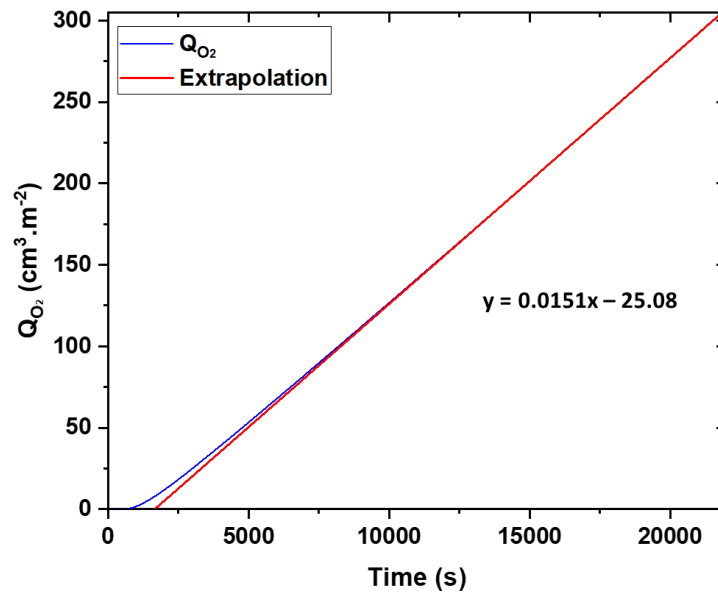


Figure S3.10. Quantity of oxygen (per m^2) transmitted as a function of time (blue) and extrapolation deduced from the steady state (red) for a non-photoaged sample.

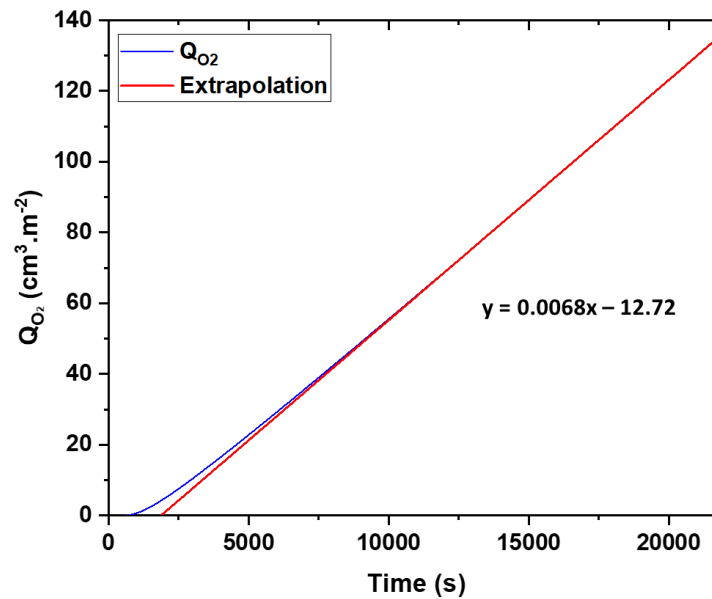


Figure S3.11. Quantity of oxygen (per m^2) transmitted as a function of time (blue) and extrapolation deduced from the steady state (red) for a sample photoaged 800 h on side #1 only – $I = 90 \text{ W} \cdot \text{m}^{-2}$, $CT = 55 \text{ }^\circ\text{C}$.

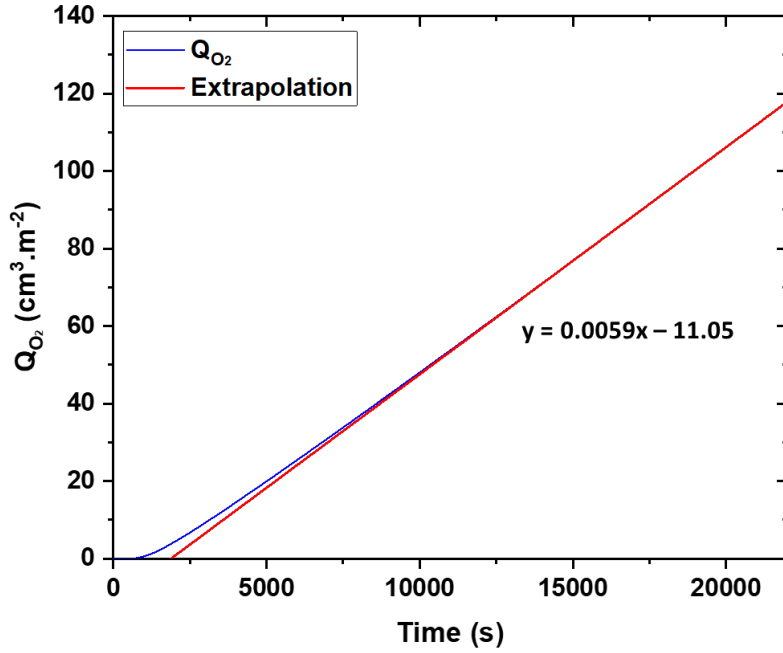


Figure S3.12. Quantity of oxygen (per m^2) transmitted as a function of time (blue) and extrapolation deduced from the steady state (red) for a sample photoaged 800 h on each side – $I = 90 \text{ W} \cdot \text{m}^{-2}$, $CT = 55 \text{ }^\circ\text{C}$.

Effect of the side exposed to O₂ on P, D, and S values

Results reported in the article for samples photoaged 800 h on side #1 only were obtained with this side facing the incoming oxygen flux into the permeameter ("up"). To assess that there is no effect from the position of the photoaged side on the P, D, and S values, three experiments were done with the photoaged side opposite to the oxygen flux ("down"). As can be seen in Table S3.2, there is no difference between results with side #1 "up" or "down".

Table S3.2. Values of the permeability coefficient P, the diffusion coefficient D, and the solubility coefficient S for a sample exposed 800 h on side #1 only, facing ("up") or not ("down") the incoming oxygen flux. Each result is an average from 3 samples, minimum and maximum values are also indicated in parenthesis to show the reproducibility.

Photooxidation time (h)	Permeability coefficient P (cm³(STP).cm.cm⁻².s⁻¹.Pa⁻¹)	Diffusion coefficient D (cm².s⁻¹)	Solubility coefficient S (cm³(STP).cm⁻³.Pa⁻¹)
800 (side #1 "up")	0.95×10 ⁻¹³ (0.85-1.00×10 ⁻¹³)	1.53×10 ⁻⁸ (1.39-1.62×10 ⁻⁸)	0.62×10 ⁻⁵ (0.62-0.63×10 ⁻⁵)
800 (side #1 "down")	0.95×10 ⁻¹³ (0.85-1.01×10 ⁻¹³)	1.53×10 ⁻⁸ (1.40-1.62×10 ⁻⁸)	0.62×10 ⁻⁵ (0.61-0.64×10 ⁻⁵)

DSC thermograms

A 3+ Differential Scanning Calorimetry (DSC) apparatus (Mettler Toledo) was used to record thermograms of PC films (10 to 20 mg) prior to photoaging (Figure S3.13) and after 800 h of photooxidation on each side (Figure S3.14). Thermal cycle was: heating (25 → 260 °C), cooling (260 → 25 °C) and heating (25 → 260 °C) at 10 °C/min under a dry air atmosphere.

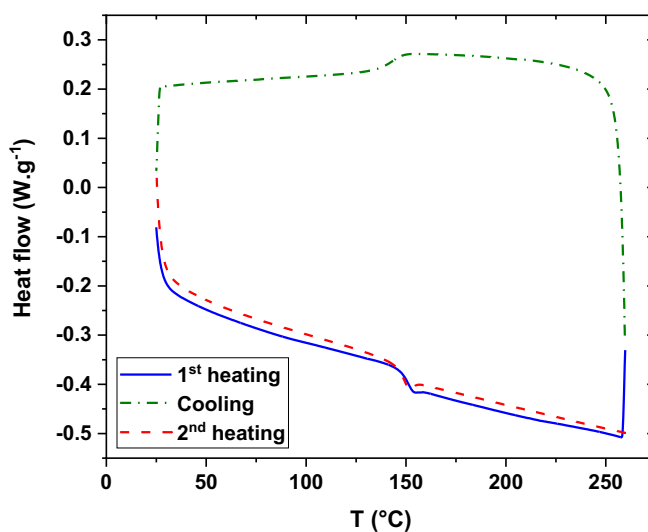


Figure S3.13. DSC thermogram of PC prior to photoaging.

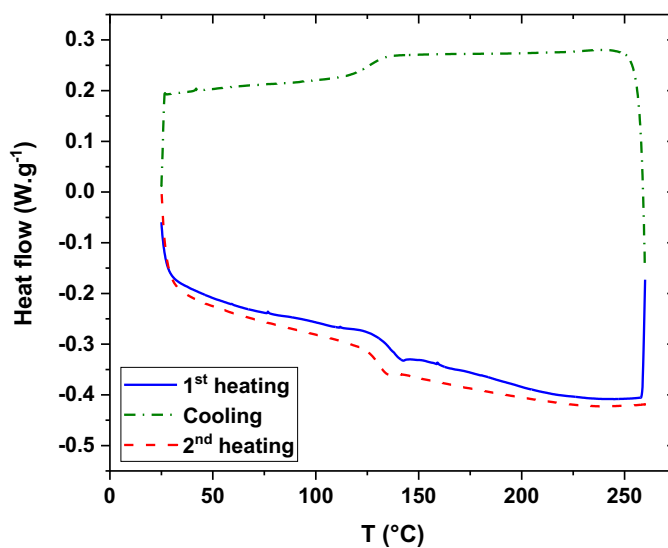


Figure S3.14. DSC thermogram of PC after 800 h of photoaging on each side – $I = 90 \text{ W.m}^{-2}$, $CT = 55 \text{ }^\circ\text{C}$.

3. Photoaging of polyethylene and its O₂ permeability

3.1 Introduction

This part presents the correlation between the photoaging and the oxygen permeability of 30 μm films of polyethylene (PE). Polyethylene was photoaged in a SEPAP 12/24 unit in the presence of air and at a light intensity of $I = 90 \text{ W.m}^{-2}$ within the wavelength range of 300 - 420 nm at 55 °C. Firstly, PE photoaging was monitored by several techniques, such as FTIR and UV-visible (appearance of oxidation products), DSC (crystallinity changes), and AFM (surface morphology changes), in order to have an insight into the consequences of the light exposure. Furthermore, the oxygen permeability on photoaged PE was also tested with an oxygen permeation analyser within the temperature range of 10 °C to 50 °C. Thus, the activation energy of oxygen permeability can be calculated according to the following Arrhenius equation:

$$P = P_0 \exp\left(-\frac{E_p}{RT}\right) \quad \text{Eq.5}$$

Diffusion coefficient D was also calculated at 10 °C using the time-lag method presented in [Chapter 1.2.2.2](#).

3.2 Results and discussion

3.2.1 Photooxidation of PE

This point is further developed in [Chapter 4 2.2.1](#). However, we decided to summarize the main key points necessary for discussion.

- Chemical changes upon photooxidation

Photooxidation of PE leads to the generation of new polar chemical groups, particularly carbonyl (C=O) and hydroxyl groups (O-H). They are observed by the net changes in the infrared spectra that demonstrate the formation of carboxylic acids, esters, lactones, and vinyls. This leads more likely to the increase of the polarity of the initially non-polar PE. Such increase in the polarity owing to the photooxidation can potentially modify the permeability of PE by altering the interactions with the permeants and the cohesion energy density of the polymer (interactions between polymer chains).

The photooxidation of the samples continued for up to 300 hours, and it was confirmed to be a photochemical process since no changes were observed in the reference experiments performed in the absence of light at the same temperature (55 °C). As the samples subjected to photoaging for more than 200 hours have a high risk of rupture, the study was then limited to 200 hours of photoaging time.

- Homogeneity of the photooxidation process in the sample

Cross-sectional transmission FTIR mappings showed no in-depth oxidation profile for 90 µm PE films, suggesting homogeneity of the oxidation throughout the sample thickness. The same conclusion can be assumed for thinner films of 30 µm studied here. Such homogeneity of

photooxidation was confirmed by FTIR transmission microspectroscopy across various positions on 30 μm films.

- Change in crystallinity rate upon photooxidation

Photoaging may increase the crystallinity rate of PE through chemicrystallization. It has been reported that shorter chains that result from chain scissions, are able to organize, either as new crystallites or by addition to existing ones [18]. This could, of course, affect the permeability which is excluded from the crystalline regions. DSC was used to examine the crystallinity variation of the PE upon photoaging. The crystallinity rate is given as a function of the irradiation time in Figure 3.15. This clearly shows an increase in the crystallinity rate of PE (+8 %) after 200 hours of photoaging.

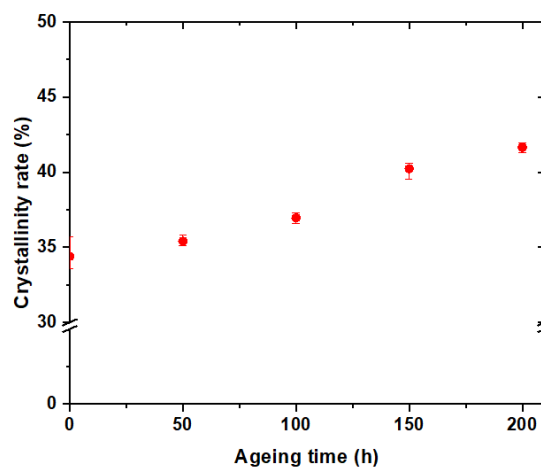


Figure 3.15. Crystallinity rate of PE films (30 μm) upon photooxidation – $I = 90 \text{ W.m}^{-2}$, $T = 55 \text{ }^\circ\text{C}$.

Results are an average from 3 samples, minimum and maximum values are also indicated to show the reproducibility.

- AFM imaging

AFM images, detailed and illustrated in [Chapter 4 2.5](#), were recorded at several positions of the PE films before and after photooxidation. They permit us to account for the absence of cracks during the photoaging process, which could strongly affect the permeability of the polymer film.

3.2.2 Oxygen permeability at different temperatures

Table 3.3 presents the oxygen permeability coefficient of PE at different temperatures from 10 to 50 °C and at different photoaging times (0, 100 and 200 hours). At a temperature of 20 °C, the observed value of $3.54 \times 10^{-13} \text{ cm}^3(\text{STP}).\text{cm}.\text{cm}^{-2}.\text{s}^{-1}.\text{Pa}^{-1}$ is consistent with previously reported findings [42].

Table 3.3. Oxygen permeability coefficient of PE at different temperatures and photoaging times, minimum and maximum values are also indicated in parenthesis to show the reproducibility.

Temperature °C	0 h Photoaging time	100 h Photoaging time	200 h Photoaging time
	P ($\text{cm}^3.\text{cm}.\text{cm}^{-2}.\text{s}^{-1}.\text{Pa}^{-1}$)		
10	2.19×10^{-13}	1.78×10^{-13}	1.55×10^{-13}
	($1.84-2.71 \times 10^{-13}$)	($1.68-1.95 \times 10^{-13}$)	($1.49-1.68 \times 10^{-13}$)
20	3.54×10^{-13}	3.21×10^{-13}	2.74×10^{-13}
	($3.33-3.92 \times 10^{-13}$)	($3.03-3.54 \times 10^{-13}$)	($2.59-3.03 \times 10^{-13}$)
30	5.83×10^{-13}	5.42×10^{-13}	4.83×10^{-13}
	($5.39-6.03 \times 10^{-13}$)	($5.12-6.01 \times 10^{-13}$)	($4.52-5.12 \times 10^{-13}$)
40	1.02×10^{-12}	9.16×10^{-13}	7.45×10^{-13}
	($0.95-1.13 \times 10^{-12}$)	($8.40-9.90 \times 10^{-13}$)	($7.03-8.12 \times 10^{-13}$)
50	1.60×10^{-12}	1.40×10^{-12}	1.17×10^{-12}
	($1.47-1.79 \times 10^{-12}$)	($1.32-1.57 \times 10^{-12}$)	($1.11-1.28 \times 10^{-12}$)

As expected from the literature [43], the oxygen permeability increases with increasing temperature for a given photoaging time. The Arrhenius law for transport parameters (solubility, diffusion, and permeability) can be expressed in the following forms [1, 44]:

$$D = D_0 \exp\left(-\frac{E_d}{RT}\right) \quad \text{Eq.6}$$

$$S = S_0 \exp\left(-\frac{\Delta H_s}{RT}\right) \quad \text{Eq.7}$$

where P_0 , D_0 , and S_0 are the pre-exponential factors; R is the perfect gas constant; E_p is the activation energy of permeation, which is the sum of the activation energy of diffusion E_d and the molar enthalpy of solubilization ΔH_s .

$$E_p = E_d + \Delta H_s \quad \text{Eq.8}$$

And the ΔH_s can be expressed as [45]:

$$\Delta H_s = \Delta H_{cond} + \Delta H_1 \quad \text{Eq.9}$$

ΔH_{cond} is the molar heat of condensation, which is small and negative [46]; ΔH_1 is the partial molar heat of mixing. This is a small and positive term [47]. For oxygen, a gas above the critical temperature, ΔH_{cond} is weak, and ΔH_s is governed by ΔH_1 . As a result, the ΔH_s is positive, and S increases with the temperature. S could decrease with temperature in other condensable gases as the negative ΔH_s is governed by the ΔH_{cond} [48]. The activation energy E_d represents the minimum energy required for a molecule to move from one position to another, and it is consistently a positive value. Therefore, the D is always increasing when the temperature increases. As a result, the increase of the oxygen permeability coefficient for PE with temperature is the consequence of the increase of both S and D .

Figure 3.16 illustrates the evolution of oxygen permeability during photoaging of PE at the tested temperatures. It demonstrates that the oxygen permeability coefficient decreased during photoaging in all the cases.

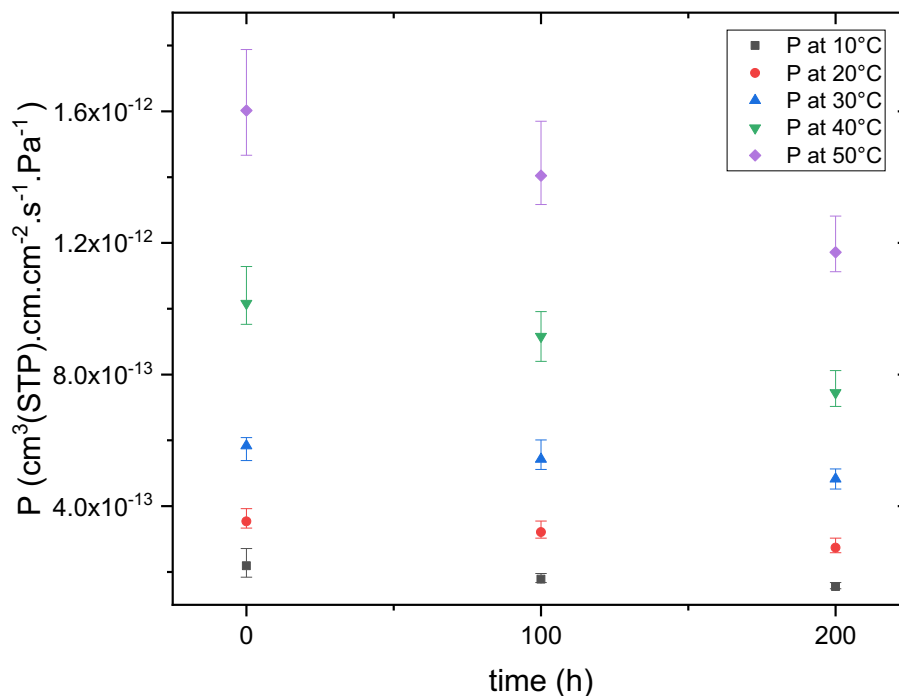


Figure 3.16. Oxygen permeability coefficients P upon photoaging – $I = 90 \text{ W.m}^{-2}$, $CT = 55 \text{ }^\circ\text{C}$. at different temperature, minimum and maximum values are also indicated to show the reproducibility.

Several factors may potentially account for this reduction in oxygen permeability: 1) increase in crystallinity via chemicrystallization. 2) enhancement of polymer polarity due to the formation of polar groups. 3) appearance of cross-linking.

DSC experiments revealed an 8 % increase in PE crystallinity within the initial 200 hours of photoaging, which could potentially contribute to this decrease. FTIR results demonstrated an increase in PE polarity owing to the form of polar groups such as carbonyl and hydroxy groups during photooxidation (*vide supra*). Such higher polarity may lead to a decrease in diffusion and sorption processes. In the case of sorption, the polar groups reduce the potential interactions between the polymer and non-polar oxygen while strengthening the interactions between polymer molecules [33]. For diffusion, these additional interactions could reduce the mobility of the polymer chains, which is not in favour of oxygen diffusion. It should be pointed out that cross-linking was not obvious in our experimental conditions, and the AFM ensured the absence of

cracks, as stated before. Thus, the decrease of P during photoaging is likely attributed to the combined influence of the appearance of polar oxidation products and the increase in crystallinity. The Arrhenius plot of the oxygen permeability coefficient of PE upon photoaging is presented in Figure 3.17. The corresponding activation energy of permeation E_p is estimated to be 38.3 kJ/mol for the sample before photoaging, 39.4 kJ/mol for 100 h of photoaging, and 38.4 kJ/mol for 200 h of photoaging, as calculated based on the slope of the Arrhenius plot. The activation energy of permeation for non-photoaged PE appears to be consistent with reported values [49].

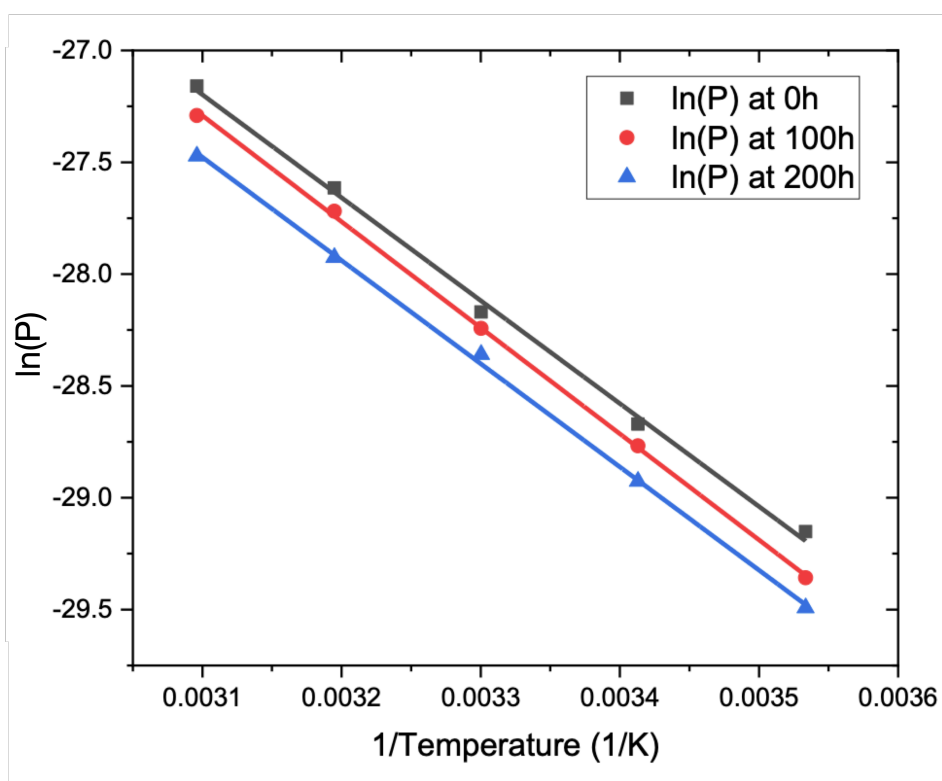


Figure 3.17. Arrhenius plot for the permeation of PE at 0, 100, and 200 h of photoaging.

From these results, the activation energy of permeation seems unchanged under our experimental conditions. However, based on the observed change upon photoaging (change of the polymer chemical structure and decrease of the oxygen permeability coefficient), it is hard to convince that the activation energy of permeation is constant upon photoaging. This could be owing to an

opposite change in the activation energy of diffusion E_D and molar enthalpy of solubilization ΔH_s , which results in a constant value of E_p , as Eq. 8 shows. This interesting point should be studied more deeply to have a better insight into the process. Such an assumption could be assessed by measuring D at different temperatures and calculating the activation energy of diffusion. However, at higher temperatures, the time-lag is so short that it is beyond the detection range of our experimental instrument.

Another possibility is that the activation energy of permeation is slightly modified, but this change is not observable under our experimental conditions. To verify this assumption, a PE sample that can endure a higher time of photoaging could be used to analyse and calculate the activation energy of permeation at a larger photoaging time.

3.2.3 Measurement of the diffusion coefficient D at 10 °C

Diffusion coefficient D was measured at 10 °C upon photooxidation with the time-lag method [37, 50, 51] (Figure 3.18, as presented in [Chapter 1 2.2.2](#)). As stated earlier, measuring it at a higher temperature was impossible as the time-lag was too short.

$$t_L = \frac{l^2}{6D} \quad \text{Eq. 10}$$

Values of D and S (calculated from the values of P at the same temperature, see equation below [37, 50, 51]) are reported in Table 3.4.

$$P = D \times S \quad \text{Eq. 11}$$

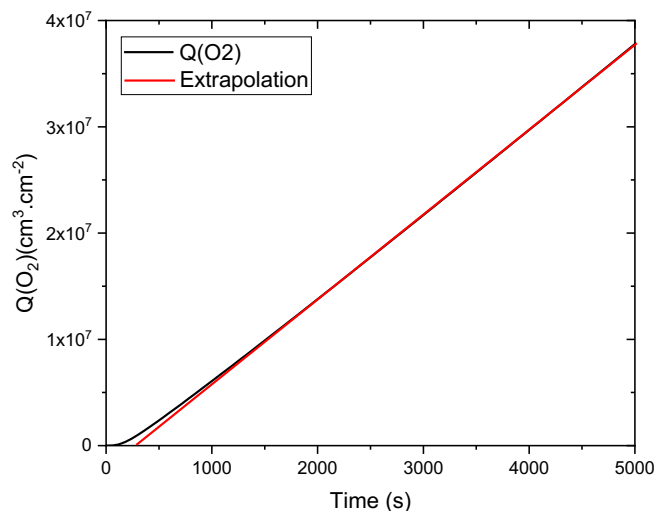


Figure 3.18. Quantity of oxygen (per m^2) transmitted Q as a function of time (black) and extrapolation deduced from the steady state (red) for a non-photoaged PE sample.

Table 3.4. Values of the time-lag, diffusion coefficient D and solubility coefficient S for PE samples at different photoaging times, minimum and maximum values are also indicated in parenthesis to show the reproducibility.

Photo aging time (h)	Time-lag (s)	Diffusion coefficient D ($cm^2.s^{-1}$)	Solubility coefficient S ($cm^3.cm^{-3}.Pa^{-1}$)
0	390 (388-414)	4.16×10^{-9} ($3.16-4.63 \times 10^{-9}$)	5.33×10^{-5} ($4.29-5.86 \times 10^{-5}$)
100	435 (417-455)	3.66×10^{-9} ($3.06-3.94 \times 10^{-9}$)	4.90×10^{-5} ($4.27-5.49 \times 10^{-5}$)
200	455 (426-476)	3.55×10^{-9} ($2.82-3.81 \times 10^{-9}$)	4.46×10^{-5} ($3.92-5.28 \times 10^{-5}$)

Table 3.4 shows an increase in the time-lag and a consequent decrease of D (-15 %). S reveals a similar drop. This indicates that the photooxidation process affects both the diffusion and the solubilization processes to the same extent.

3.3 Conclusion

Upon 200 h of photoaging, it is observed a decrease of the oxygen permeability. This phenomenon is attributed to the increase in polarity and crystallinity of the polymer during the photooxidation. The activation energy of permeation E_p appears constant upon photoaging (between 38 and 40 kJ/mol). This could be explained by the absence of any change, a possible opposite effect on diffusion and solubilization activation energy, or a change too small to be observable. This part has to be more deeply studied. Finally, the measurement of the time-lag at 10 °C upon photooxidation shows a decrease of D and S to the same extent.

4 Conclusion

In this chapter, the photooxidation processes of two different polymers, PC and PE, were studied in detail after exposure to UV light, and the effects on oxygen permeability were explored.

For PC, a sequential photooxidation led to a limit value on each side. This is attributed to the formation of coloured species and/or moieties which play the role of internal filters preventing further photodegradation.

The estimated thickness of the oxidized layer on each side is approximately $30 \pm 5 \mu\text{m}$. The oxygen permeation coefficient P decrease to a plateau value within 500 hours, with an estimated decrease of 49 %, primarily owing to the reduction in the solubility coefficient S (-47 %) rather than the diffusion coefficient D (-8 %). This is consistent with the localized oxidation process at the film surface, mostly affecting the dissolution phenomenon. The decrease in P can be explained by two effects resulting from the photooxidation process: the emergence of additional polar groups and cross-linking, impacting both solubility and diffusion. A "funnel effect" can be used to explain the unchanged oxygen permeation coefficient upon photooxidation of side #2, as the oxidation of side #1 already restricts the entire permeation process, mainly by reducing solubility at its surface.

For PE, it is found that oxygen permeability decreased during the photooxidation process over 200 hours. This phenomenon can also be attributed to the increase in polarity and crystallinity during photooxidation. The activation energy of permeation, E_p , remains roughly constant during photoaging, ranging between 38 and 40 kJ/mol. Lastly, measurements of time-lag at 10 °C after photooxidation reveal that the diffusion coefficient, D , and the solubility coefficient, S , decrease similarly.

In summary, our results demonstrate that the photooxidation process decreases the oxygen permeability of PC and PE. Changes in crystallinity and polarity, as well as the occurrence of cross-

linking could explain this decrease. In addition, diffusion and solubility should be considered separately to get a better understanding of the changes in permeability. These findings provide important background information for the upcoming chapter, which will focus on studying the permeability in solution and the ability of permeants of different polarities to pass through the PE.

References

1. Andrews R J, Grulke E A, Brandrup J, et al. Polymer handbook. John Wiley & Sons, New York, 1999.
2. Collin S, Bussière P O, Therias S, et al. Physicochemical and mechanical impacts of photo-ageing on bisphenol a polycarbonate. *Polymer degradation and stability*, 2012, 97(11): 2284-2293.
3. Gedemer T J. The use of ATR techniques to evaluate UV degradation of plastics. *Applied Spectroscopy*, 1965, 19(5): 141-146.
4. Factor A, Chu M L. The role of oxygen in the photo-ageing of bisphenol-A polycarbonate. *Polymer Degradation and Stability*, 1980, 2(3): 203-223.
5. Rivaton A. The bisphenol-A polycarbonate dual photochemistry. *Die Angewandte Makromolekulare Chemie: Applied Macromolecular Chemistry and Physics*, 1994, 216(1): 147-153.
6. Rivaton A. Recent advances in bisphenol-A polycarbonate photodegradation. *Polymer Degradation and Stability*, 1995, 49(1): 163-179.
7. Rivaton A, Sallet D, Lemaire J. The photochemistry of bisphenol-A polycarbonate reconsidered. *Polymer Photochemistry*, 1983, 3(6): 463-481.
8. *Polymer durability: degradation, stabilization, and lifetime prediction*. American Chemical Society, 1996.
9. Torikai A, Mitsuoka T, Fueki K. Wavelength sensitivity of the photoinduced reaction in polycarbonate. *Journal of Polymer Science Part A: Polymer Chemistry*, 1993, 31(11): 2785-2788.

10. Mullen P A, Searle N Z. The ultraviolet activation spectrum of polycarbonate. *Journal of applied polymer science*, 1970, 14(3): 765-776.
11. Andradý A L, Searle N D, Crewdson L F E. Wavelength sensitivity of unstabilized and UV stabilized polycarbonate to solar simulated radiation. *Polymer Degradation and Stability*, 1992, 35(3): 235-247.
12. Factor A, Ligon W V, May R J. The role of oxygen in the photoaging of bisphenol A polycarbonate. 2. GC/GC/high-resolution MS analysis of Florida-weathered polycarbonate. *Macromolecules*, 1987, 20(10): 2461-2468.
13. Belluš D, Hrdlovič P, Maňásek Z. Photoinitiated rearrangements in poly [2, 2-propanebis (4-phenyl carbonate)]. *Journal of Polymer Science Part B: Polymer Letters*, 1966, 4(1): 1-5.
14. Diepens M, Gijsman P. Photodegradation of bisphenol A polycarbonate. *Polymer Degradation and Stability*, 2007, 92(3): 397-406.
15. Pickett J E. Influence of photo-Fries reaction products on the photodegradation of bisphenol-A polycarbonate. *Polymer degradation and stability*, 2011, 96(12): 2253-2265.
16. Diepens M, Gijsman P. Photo-oxidative degradation of bisphenol A polycarbonate and its possible initiation processes. *Polymer Degradation and Stability*, 2008, 93(7): 1383-1388.
17. Rabek J F. *Photodegradation of polymers: physical characteristics and applications*. Springer Science & Business Media, 2012.
18. Fayolle B, Richaud E, Colin X, et al. Degradation-induced embrittlement in semi-crystalline polymers having their amorphous phase in rubbery state. *Journal of materials science*, 2008, 43: 6999-7012.
19. Gesner B D, Kelleher P G. Oxidation of bisphenol a polymers. *Journal of applied polymer science*, 1969, 13(10): 2183-2191.

20. Davis A, Golden J H. Stability of polycarbonate. *Journal of Macromolecular Science, Part C*, 1969, 3(1): 49-68.
21. Claude B, Gonon L, Duchet J, et al. Surface cross-linking of polycarbonate under irradiation at long wavelengths. *Polymer Degradation and Stability*, 2004, 83(2): 237-240.
22. Greenwood R, Weir N. Effects of photo-degradation on the permeability and diffusivity characteristics of poly (p-methylstyrene). *Die Makromolekulare Chemie: Macromolecular Chemistry and Physics*, 1975, 176(7): 2041-2051.
23. Philippart J L, Gardette J L. Analyse du photoviellissement des matériaux polymères par évolution de la perméabilité aux gaz. *Die Makromolekulare Chemie: Macromolecular Chemistry and Physics*, 1986, 187(7): 1639-1650.
24. Nakatsuka S, Andrady A. Studies on enhanced degradable plastics. III. The effect of weathering of polyethylene and (ethylene-carbon monoxide) copolymers on moisture and carbon dioxide permeability. *Journal of environmental polymer degradation*, 1994, 2: 161-167.
25. Gardette J L, Colin A, Trivis S, et al. Impact of photooxidative degradation on the oxygen permeability of poly (ethyleneterephthalate). *Polymer degradation and stability*, 2014, 103: 35-41.
26. Collin S, Bussiere P O, Gardette J L, et al. Accelerated photo-aging of organic coatings used as protective layers for Blu-ray Discs. *Progress in Organic Coatings*, 2015, 84: 9-17.
27. Scarfato P, Acierno D, Russo P. Photooxidative weathering of biodegradable nanocomposite films containing halloysite. *Polymer Composites*, 2015, 36(6): 1169-1175.
28. Siracusa V, Lotti N, Munari A, et al. Poly (butylene succinate) and poly (butylene succinate-co-adipate) for food packaging applications: Gas barrier properties after stressed treatments. *Polymer Degradation and Stability*, 2015, 119: 35-45.

29. Gigli M, Genovese L, Lotti N, et al. Gas barrier and thermal behaviour of long chain aliphatic polyesters after stressed treatments. *Polymer-Plastics Technology and Engineering*, 2017, 56(1): 71-82.
30. Ye X, Pi H, Guo S. A novel route for preparation of PVC sheets with high UV irradiation resistance. *Journal of applied polymer science*, 2010, 117(5): 2899-2906.
31. Klopffer M H, Flaconnèche B. Transport properties of gases in polymers: bibliographic review. *Oil & Gas Science and Technology*, 2001, 56(3): 223-244.
32. SUSlick K S. *Kirk-Othmer encyclopedia of chemical technology*. 1998., Wiley & Sons: New York, NY, USA.
33. George S C, Thomas S. Transport phenomena through polymeric systems. *Progress in Polymer science*, 2001, 26(6): 985-1017.
34. Naylor T. *Comprehensive Polymer Science*. Pergamon, Oxford, 1989, 643.
35. Michaels A S, Parker Jr R B. Sorption and flow of gases in polyethylene. *Journal of Polymer Science*, 1959, 41(138): 53-71.
36. Webb J D, Czanderna A W. End-group effects on the wavelength dependence of laser-induced photodegradation in bisphenol-A polycarbonate. *Macromolecules*, 1986, 19(11): 2810-2825.
37. Crank J. *The mathematics of diffusion*. Oxford university press, 1979.
38. Moon S I, Monson L, Extrand C W. Outgassing of oxygen from polycarbonate. *ACS Applied Materials & Interfaces*, 2009, 1(7): 1539-1543.
39. Bajpai R, Keller J M, Datt S C. On the microhardness of irradiated polycarbonate // *Makromolekulare Chemie. Macromolecular Symposia*. Basel: Hüthig & Wepf Verlag, 1988, 20(1): 461-464.

40. Rivaton A, Mailhot B, Soulestin J, et al. Comparison of the photochemical and thermal degradation of bisphenol-A polycarbonate and trimethylcyclohexane-polycarbonate. *Polymer Degradation and Stability*, 2002, 75(1): 17-33.
41. Berthumeyrie S, Colin A, Esparcieux C, et al. Photodegradation of tetramethylpolycarbonate (TMPC): Correlation of properties with chemical modifications. *Polymer degradation and stability*, 2013, 98(10): 2081-2088.
42. Michiels Y, Van Puyvelde P, Sels B. Barriers and chemistry in a bottle: mechanisms in today's oxygen barriers for tomorrow's materials. *Applied Sciences*, 2017, 7(7): 665.
43. Villaluenga J P G, Seoane B. Experimental estimation of gas-transport properties of linear low-density polyethylene membranes by an integral permeation method. *Journal of applied polymer science*, 2001, 82(12): 3013-3021.
44. Klopffer M H, Berne P, Espuche É. Development of innovating materials for distributing mixtures of hydrogen and natural gas. Study of the barrier properties and durability of polymer pipes. *Oil & Gas Science and Technology—Revue d'IFP Energies nouvelles*, 2015, 70(2): 305-315.
45. Gee G. Some thermodynamic properties of high polymers, and their molecular interpretation. *Quarterly Reviews, Chemical Society*, 1947, 1(3): 265-298.
46. Crank J. *The mathematics of diffusion*. Oxford university press, 1979.
47. Hildebrand J H, Scott R L. Solutions of nonelectrolytes. *Annual Review of Physical Chemistry*, 1950, 1(1): 75-92.
48. Comyn, John, ed. *Polymer permeability*. Springer Science & Business Media, 1985.
49. Shi L, Chew M Y L. A review of fire processes modeling of combustible materials under external heat flux. *Fuel*, 2013, 106: 30-50.

50. Daynes H A. The process of diffusion through a rubber membrane. Proceedings of the Royal Society of London. Series A, Containing Papers of a Mathematical and Physical Character, 1920, 97(685): 286-307.
51. Barrer R M, Rideal E K. Permeation, diffusion and solution of gases in organic polymers. Transactions of the Faraday Society, 1939, 35: 628-643.

Chapter 4: Permeability of carbazole and naphthalene derivatives solutions on polyethylene: effect of photoaging

1. Introduction

In this fourth chapter of the thesis, we deeply explored the vast and not-studied world of permeability in solution. The main objective was to test the solubility-diffusion process through a polymer for various permeants of a rather similar raw structure but different polarity. Such permeability refers then to the ability of a solute to pass through the polymer when dissolved in a solvent. The study was carried out with polyethylene, a non-polar polymer whose consequences of photoaging on the oxygen permeability were considered in the previous chapter.

When dealing with the permeability of solutions, the most fundamental factor influencing this permeability is the permeant (solute) concentration gradient. The movement of permeant molecules from the higher to the lower concentration side is considered the driving force. Such force depends then on the concentration of the permeant, the temperature, and the physical and chemical properties of both the solvent and the permeant. It is essential, first, to control these parameters for reproducible and coherent results. With this objective, methanol was chosen as the solvent. Our study found it the most convenient solvent of all the studied permeants, because one of the most important reasons is that methanol allows us to work at a relatively high constant concentration. These concentration conditions associated with other advantages (as thoroughly presented in [Chapter 2 4.2.2](#)) of MeOH permitted the control of experiment duration (maximum of 24 hours).

The most challenging part of studying a permeant's transmission rate (permeability) in solution involves using specialized equipment associated with a sensitive detection method. Because such equipment is not commercialized, it was necessary to develop our own setup. After multiple, not always successful, attempts, an experimental system was designed. It comprises two compartments separated by a given surface of the studied polymer. The upper compartment was filled with the

solution, while the lower compartment contained only the solvent. The setup can be performed continuously through fluorescence or UV-visible (for non-fluorescent permeants) spectroscopy when equipped with a pump or/and not continuously through GC-MS detections. These techniques with their high sensitivity are well adapted for the permeability experiments.

Concerning the permeants, the transmission rate of non-photoaged PE and photoaged PE for several solutes was studied by roughly maintaining the main chemical structure. Our choice was made on the naphthalene derivatives that show high solubility in methanol, relatively significant fluorescence quantum yield and/or high absorption coefficient (ϵ) making them excellent candidates for the planned experiments.

The study is organized then as follows:

- Exploring the changes in PE's chemical and physical changes upon light excitation using various techniques such as FTIR spectroscopy microscopy, DSC, etc.
- Evaluating the transmission rate. First, this was performed with carbazole (highly fluorescent compound) with non-photoaged PE to validate the self-designed equipment. The effect of various parameters was tested, such as polymer thickness, by evaluating the lag period and the transmission rate.
- Analysing the effect of photoaging on carbazole's transmission rate and discuss the various changes observed, mainly in terms of polarity change.
- Studying the effect of the photoaging with various permeants (naphthalene derivatives with different dipole moments) on the transmission rate.

This chapter is presented in the form of an article published in ACS Applied Polymer Materials under the title "*Evaluating the Effect of Photoaging on Polyethylene Permeability: Measurement of the Transport Properties in the Liquid Phase*", (<https://doi.org/10.1021/acsapm.3c02178>).

Zhouyun Chen, Julien Christmann, Mohamed Sarakha

The experimental part of the article has been described in Chapter 2; it is removed in the following part for the smooth reading of the manuscript.

2. Evaluating the effect of photoaging on polyethylene permeability



2.1. Introduction

Polyethylene, PE, is the most widely used polymer present in our daily life [1]. Owing to its excellent performance, it is employed in multiple applications such as food packaging, agriculture, medical supplies, pipes, etc. [2, 3]. As with all polymer materials, PE undergoes photodegradation processes upon ultraviolet irradiation from solar light that causes irreversible changes in its functional properties. The corresponding oxidative chain radical mechanism has been widely reported and is now well admitted [4-10]. PE, by itself, cannot absorb ultraviolet light with $\lambda > 290$ nm. Thus, the initiation step is kicked off by chromophoric groups in the form of catalyst residues or external contaminants resulting from the synthesis and/or processing steps. Upon light exposure, primary radicals are generated from these compounds, which can abstract a hydrogen atom from the polymer chain PH to generate a macroradical P[•]. In the presence of oxygen, macromolecular hydroperoxides POOH are then formed, whose O-O bond can further dissociate under light exposure to form macroalkoxy radicals PO[•] and hydroxyl radicals [•]OH [11]. The former radicals may undergo further reactions: 1. β -scission to produce aldehydes (further evolving into carboxylic acids, esters...), 2. hydrogen abstraction to form hydroxyl functions, 3. in-cage reaction leading to chain ketones. Unlike thermal oxidation, ketones do not accumulate during photooxidation as they are involved in Norrish-I and -II mechanisms, with the formation of carbonylated functions and

vinyls, respectively [9]. The extent of PE photooxidation can then be easily permeated by FTIR spectroscopy through the formation of carbonyl functions (carboxylic at 1713 cm⁻¹, esters at 1740 cm⁻¹, lactones at 1780 cm⁻¹), hydroxyl (broad band centered at around 3400 cm⁻¹) and vinyl functions (909 cm⁻¹) [9, 11].

Changes in the mechanical and optical properties of polymers upon photoaging have also been studied carefully over the years [12, 13]. In comparison, the modifications of their barrier properties, especially in the liquid phase, are largely understudied despite the wide use of polymers as membranes for separation techniques, packaging films for food and drinks, and coatings for medical devices [14, 15]. The permeation of molecules through a polymer membrane is usually described in terms of a solution-diffusion mechanism that involves sorption of the molecules at the entrance surface, diffusion through the membrane, and desorption from the exit surface [13, 14, 16, 17]. At steady state, the flux F of permeant molecules across a polymer membrane of thickness d is given by Eq. 1, which derives from Fick's laws of diffusion [14]:

$$F = \frac{DH}{d}(C_d - C_0) \quad \text{Eq. 1}$$

D stands for the diffusion coefficient, and H for the partition coefficient. The latter gives the equilibrium between the concentration outside the membrane (C) to that inside (c) at the two interfaces (entrance $z = 0$, exit $z = d$):

$$C_0 = HC_0 \quad \text{Eq. 2}$$

$$C_d = HC_d \quad \text{Eq. 3}$$

The value $D \times H$ is generally called the membrane permeability [14]. Many factors can affect the permeability of a compound through a polymer [13, 16]: 1. environmental conditions (temperature, pressure), 2. permeant's characteristics (size, shape, mass, and polarity), 3. polymer's features (chemical structure, polarity, density, crystallinity rate, cross-linking, orientation, etc.). It could be

easily anticipated that the photooxidation of a polymer would affect its permeability owing to the associated modifications of its structure (appearance of polar groups, *vide supra*, and chain scissions), its crystallinity (through chemicrystallization [18]) and the occurrence of cross-linking [10].

In the present work, the photoaging of polyethylene and its effect on the transmission rate of various permeants in the liquid phase were explored. Polyethylene was photoaged in an accelerated photoaging setup to control the photooxidation process, whose extent was tracked by FTIR and UV-visible spectroscopies. Permeants of various polarities were selected and dissolved into methanol to measure their transmission rate through polyethylene with a self-designed setup before and after photoaging, with real time detection of transferred permeant by fluorescence or UV spectroscopy, double-checked by GC-MS measurements. The changes in the transmission rate upon photoaging for the different permeants were finally discussed in the light of the photooxidation mechanism and its consequences on the structure and morphology of polyethylene.

2.2. Results and discussion

2.2.1. Photooxidation of PE

Formation of new functions resulting from the photooxidation of polyethylene, PE, is easily monitored by infrared spectroscopy [9]. The major changes caused by the photoaging are actually observed in the carbonyl ($1900 - 1500 \text{ cm}^{-1}$, Figure 4.1), hydroxyl ($3600-3000 \text{ cm}^{-1}$, Figure S4.7 and Figure S4.8) and fingerprint regions ($1300-800 \text{ cm}^{-1}$, Figure S4.9 and Figure S4.10).

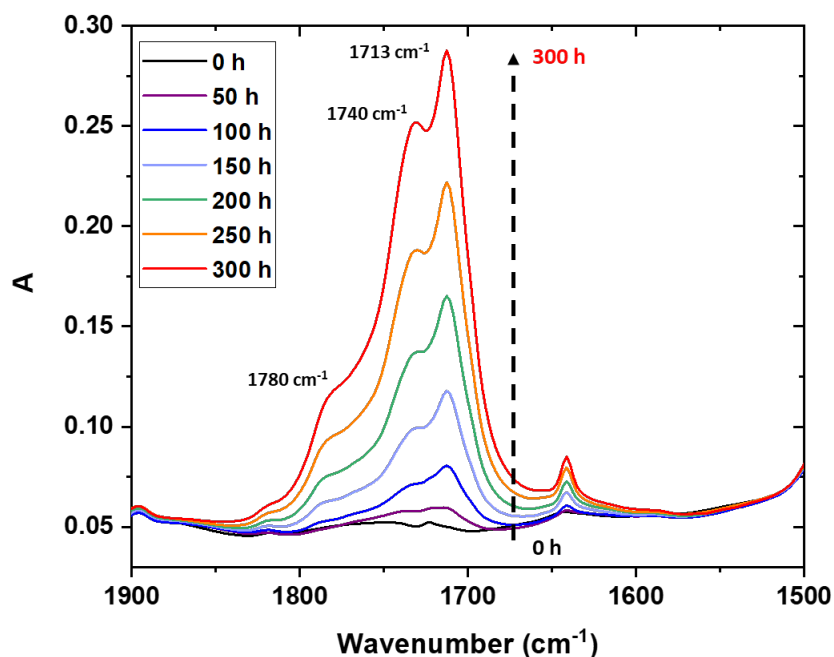


Figure 4.1. Transmission FTIR spectra in the $1900 - 1500 \text{ cm}^{-1}$ region for a PE film ($30 \mu\text{m}$) upon photooxidation. $I = 90 \text{ W.m}^{-2}$, $T = 55 \text{ }^\circ\text{C}$.

As clearly shown, new polar functions are progressively generated upon photoaging, more particularly carbonyls (C=O stretching at 1713 cm^{-1} for carboxylic acids, 1740 cm^{-1} for esters and 1780 cm^{-1} for lactones) and hydroxyl ones (O-H stretching at 3430 cm^{-1}). Owing to these changes, the initial non-polar PE undergoes a significant increase of polarity. Moreover, the formation of vinyls is also detected at 909 cm^{-1} . The corresponding photooxidation kinetics (Figure 4.2) can be

deduced by subtracting the initial absorbance at 1713 cm^{-1} from that obtained at a certain irradiation time.

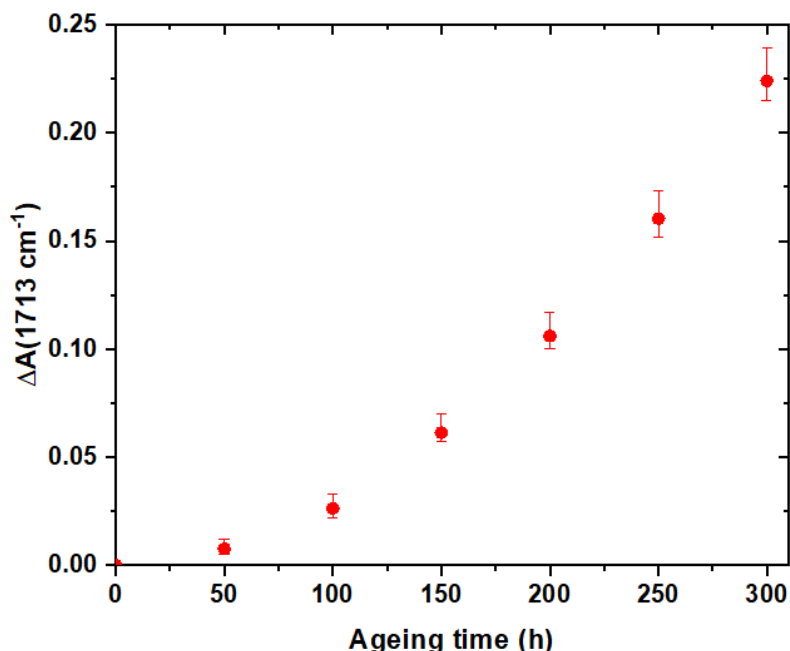


Figure 4.2. Difference of absorbance at 1713 cm^{-1} with respect to unexposed PE film ($30\text{ }\mu\text{m}$) upon photooxidation – $I = 90\text{ W.m}^{-2}$, $T = 55\text{ }^{\circ}\text{C}$. Results are an average from 3 samples, minimum and maximum values are also indicated to show the reproducibility.

It can be seen that the photooxidation, represented here by the formation of carboxylic acids, proceeds up to 300 h. Dark control experiments were realized at $55\text{ }^{\circ}\text{C}$ over the same time in an oven without any light. No change of the FTIR spectra was observed, which clearly indicates the photochemical origin of the oxidation process. However, films whose photoaging time is higher than 200 h become too fragile to be easily handled for transmission rate measurements, so it was decided to limit the photoaging to 200 h in the following parts of the work. It should be pointed out that the same results were obtained for 60 and $90\text{ }\mu\text{m}$ films.

When considering the permeability of a film, both surface and depth are clearly important parameters. Some polymers present an oxidation profile over depth as a result of a light absorption

profile (e.g. polycarbonate [19]), and/or an oxygen diffusion profile, which hinders replenishment of oxygen into the core of the sample (as for 1 mm thick PE slabs in Reference [20]). Occurrence of the possible oxidation profile can be assessed by recording FTIR mapping of cross-sectional samples of photoaged films (200 h), as for example in Figure 4.3a. As it was not possible to obtain a clear cutting with 30 μm films, microtoming was realized on 90 μm films. Thus, if no in-depth oxidation profile is observed for this thickness, it can be assumed the same for thinner films.

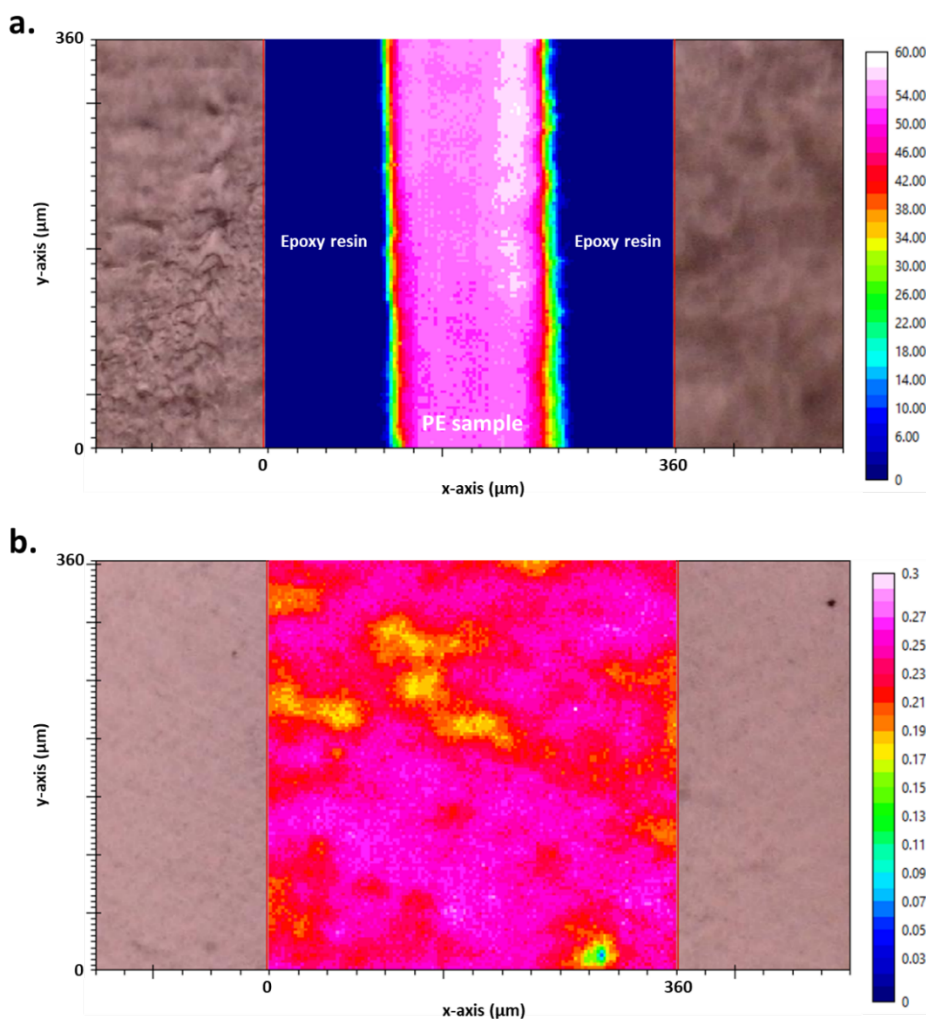


Figure 4.3. Transmission FTIR mappings (360 $\mu\text{m} \times 360 \mu\text{m}$, surface integration of the 1850 – 1650 cm^{-1} area, colour represents the value of the area surface integration) of: a. the cross-sectional sample of a 90 μm photoaged (200 h) PE film, b. a 30 μm photoaged (200 h) PE film.

As clearly shown, under our experimental conditions, no in-depth oxidation profile was observed for the 90 μm PE films used here. The oxidation is clearly observed with the same level within the entire thickness of the polymer film. Thus, it can be assumed the same for thinner films (30 and 60 μm). FTIR transmission microspectrometry was also employed to assess the homogeneity of photooxidation by recording mappings (360 $\mu\text{m} \times 360 \mu\text{m}$) at several positions on 30 μm films, as for instance in Figure 4.3b. All the mappings show that the distribution of oxidation products over the recording area is homogeneous. It can then be concluded that the extent of photooxidation is homogeneous in the whole sample (surface and depth) for all considered films (30, 60 and 90 μm). The increased polarity of PE that is caused by the photooxidation could result in a modification of its permeability. Indeed, it modifies the cohesive energy of PE (stronger polymer-polymer interactions) as well as its interactions with the permeating molecule, depending on the polarity of the latter [16].

In addition to the formation of polar groups, photooxidation could also increase the crystallinity rate of PE through the chemicrystallization process: smaller chains resulting from chains scission may potentially organize into new crystallites [18]. This would have an effect on the polymer permeability since crystalline areas are so densely packed that they are considered impermeable [21]. This restricts permeability to the amorphous regions, where photooxidation is also occurring [22]. DSC experiments shown that, under our experimental conditions, the crystallinity rate of PE slightly increases upon photoaging (+8 %) after roughly 200 h of irradiation (Figure S4.11).

2.2.2. Transmission rate measurements

The transport of molecules through polyethylene films of thickness d in methanolic solution was deeply investigated using the experimental setup described in the experimental section. Our concern was to measure the transmission rate of a given permeant and to evaluate the effect of the polymer photoaging on such rate. This mass transfer, followed in-line by fluorescence or UV spectroscopy, is naturally triggered by the concentration gradient between the upper ($c = 4.0 \times 10^{-2}$ mol.L $^{-1}$) and the lower ($c_0 \sim 0$) parts of the experimental system. Figure 4.4 shows a typical curve obtained for a 150 mL solution of carbazole (C $_{12}$ H $_9$ N) at room temperature (approximately 20 °C) and a polyethylene film with a thickness of 150 μ m, using fluorescence detection.

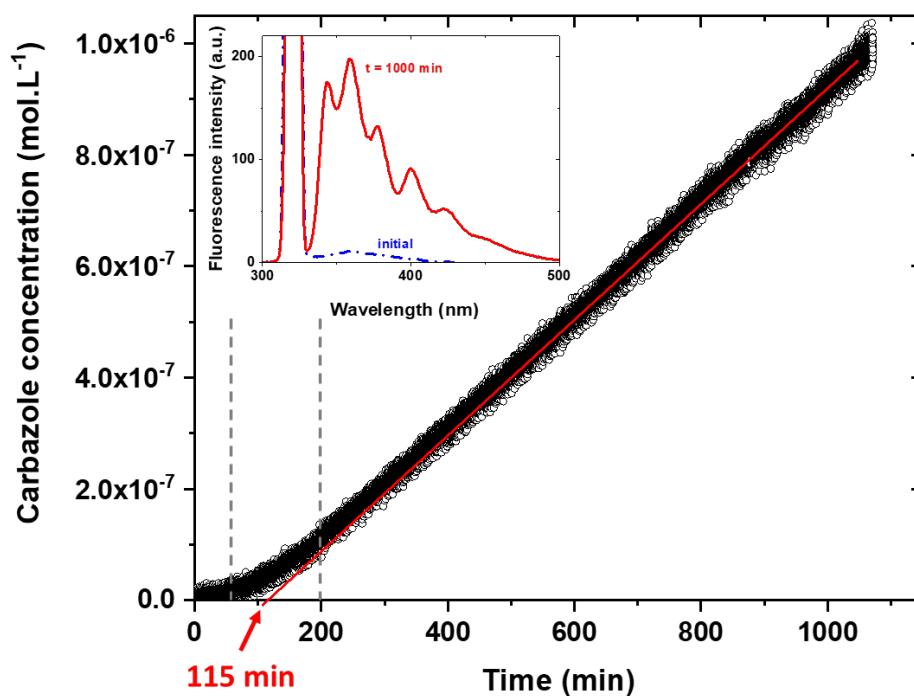


Figure 4.4. Typical curve obtained for the transmission of carbazole in methanolic solution (4.0×10^{-2} mol.L $^{-1}$) through a 150 μ m PE film at room temperature by using in live measurement of fluorescence ($\lambda_{exc} = 320$ nm, $\lambda_{em} = 360$ nm). Insert: fluorescence emission spectra before and after 1000 min of carbazole introduction into the upper part.

Recording fluorescence emission spectra prior to the introduction of carbazole into the upper part of the system and at the end of the experiment (1000 min) clearly indicates the occurrence of its transfer through the thickness of the polymer (Insert of Figure 4.4). The obtained curve for the transfer can be clearly divided in three well defined regions: 1. from 0 to 60 min as the penetration region where carbazole is adsorbed at the feed side of the polymer and starts diffusing within the thickness of the polymer film without any sign for its presence on the other side giving rise to the appearance of a time-lag period, 2. from 60 to 200 min as a transient region where carbazole leaves the polymer at the lower side, leading to a progressive increase of the transmission rate until it becomes constant, 3. after 200 min, the third region named as a stationary state domain where the evolution of the concentration as a function of time is perfectly linear (constant flow of carbazole) and from which the permeate transmission rate can be estimated using the corresponding slope. Under our experimental conditions, this was estimated to 1.0×10^{-9} mol.L⁻¹.min⁻¹. As shown in Figure 4.4, the above-named time-lag (t_L) may be obtained from the intersection of the linear region with the time axis. This is found to be equal to 115 minutes. Even though the liquid-phase experiments performed, the obtained curve perfectly correlates with those largely reported for gas and water vapour permeability in polymers [15].

Similar experiments were performed for different thicknesses of PE films, namely 30, 60, 90 and 150 μm (Figure S4.12). Transmission rate and time-lag were determined and are reported in Table 4.1. They obviously and significantly depend on the polymer film thickness: the time-lag shows a strong increase with d while the transmission rate drastically decreased, owing more likely to the fact that thicker polymers offer more resistance to the diffusion of the permeant. Under our experimental conditions, the transmission rate seems to be linear with $1/d$ (Figure S4.12).

The activation energy of the transmission process was determined for carbazole in the case of a 30 μm film by evaluating the transmission rate at different temperatures. This refers to the energy

barrier that should be overcome for carbazole to pass through PE film. From the Arrhenius plot (Figure S4.13), this activation energy was evaluated to 89.1 kJ.mol⁻¹ under our experimental conditions.

Table 4.1. Time-lag and transmission rate of carbazole in methanolic solution for PE films of different thicknesses at room temperature, minimum and maximum values are also indicated in parenthesis to show the reproducibility.

Thickness (μm)	Time-lag (min)	Transmission rate (mol.L⁻¹.min⁻¹)
30	21 (14.2-27.8)	6.6×10^{-9} ($6.43-6.78 \times 10^{-9}$)
60	35 (25.3-44.7)	2.4×10^{-9} ($2.16-2.63 \times 10^{-9}$)
90	68 (64.7-71.0)	1.6×10^{-9} ($1.43-1.76 \times 10^{-9}$)
150	115(94.3-135.6)	1.0×10^{-9} ($0.94-1.05 \times 10^{-9}$)

In order to find out the effect of PE photooxidation on its barrier properties, these three parameters, namely transmission rate, time-lag, and activation energy, were analysed upon photoaging up to 200 h. The transmission rate will be particularly used for the analysis of the chemical or/and physical changes of the polymer upon light exposure.

Figure 4.5 shows the transmission curves obtained for carbazole through PE films of 30 μm at different times of photoaging, and Table 4.2 summarizes the corresponding transmission rates.

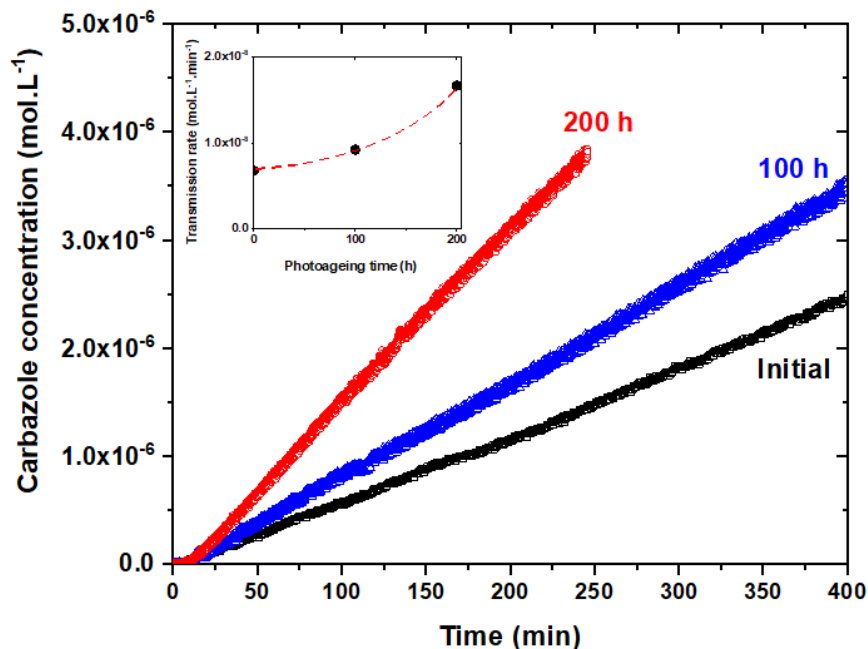


Figure 4.5. Transmission curves of carbazole in methanolic solution ($4.0 \times 10^{-2} \text{ mol.L}^{-1}$) through a $30 \mu\text{m}$ PE film at room temperature for different photoaging times. Insert: change of the transmission rate as a function of the photoaging time.

Table 4.2. Transmission rate of carbazole in methanolic solution at room temperature for PE films at different stages of photoaging, minimum and maximum values are also indicated in parenthesis to show the reproducibility.

Photoaging time (h)	Transmission rate ($\text{mol.L}^{-1}.\text{min}^{-1}$)
0	6.6×10^{-9} ($6.43\text{-}6.78 \times 10^{-9}$)
100	9.2×10^{-9} ($9.15\text{-}9.23 \times 10^{-9}$)
200	16.6×10^{-9} ($16.2\text{-}17.0 \times 10^{-9}$)

It is clear that the transmission rate increased significantly when the photoaging time increased. However, no linear relationship between the transmission rate and the photoaging time can be found (Insert of Figure 4.5).

This clearly demonstrates that the chemical and/or physical changes within the polymer structure caused by the photooxidation process affect the transmission of carbazole through it. It should be pointed out that similar findings were obtained for higher thicknesses of the polymer film, namely 60 and 90 μm (Figure S4.14). Concerning the time-lag, even though a small decrease is observed, the difference with the non-photoaged polymer appears to be too small to be used for further analysis.

The activation energy was also determined for 200 h photoaged polymer. This was found roughly similar to that obtained for no photoaged PE (Figure S4.13).

The change in the transmission rate of carbazole upon photoaging of PE may be owing to several factors such as: cross-linking, change in the crystallinity, appearance of cracks and/or changes in the polarity of the polymer. Cross-linking was not evidenced in our experimental conditions, while the crystallinity rate slightly increased (+8 %, *vide supra*). Anyhow, these two effects would more likely lead to a decrease of the transmission rate. The observed increase in our experiments could be explained by the appearance of cracks upon photoaging. However, AFM imaging (Figure S4.15) did not reveal any cracking process. The change in the polymer polarity could then be invoked here. As stated earlier, the photooxidation of the initially non-polar PE leads to an increase of its polarity due to the homogeneous photogeneration of polar groups (mainly carbonyl and hydroxyl ones) within its whole thickness. Thus, this photoinduced polarity of PE will determine its ability to interact with polar molecules such as carbazole ($\mu = 1.77 \text{ D}$) through dipole-dipole interaction or/and other intermolecular forces. Such effect will end up with a higher solubility of carbazole at the feed side of the polymer, which leads without any doubt to an increase in the number of permeant molecules diffusing within the thickness of the polymer film. Such process permits then a significant increase of the transmission rate of carbazole in the photoaged PE film. In order to

confirm such statement, the transmission rate was determined using a non-polar permeant such as naphthalene ($C_{12}H_8$).

Figure 4.6 shows the curves obtained for naphthalene in methanolic solution ($4.0 \times 10^{-2} \text{ mol.L}^{-1}$) through a $30 \mu\text{m}$ PE film prior to and after 200 h of photoaging. The transmission rate was found equal to 5.2×10^{-7} and $4.0 \times 10^{-7} \text{ mol.L}^{-1}.\text{min}^{-1}$ for the initial and photoaged polymer respectively.

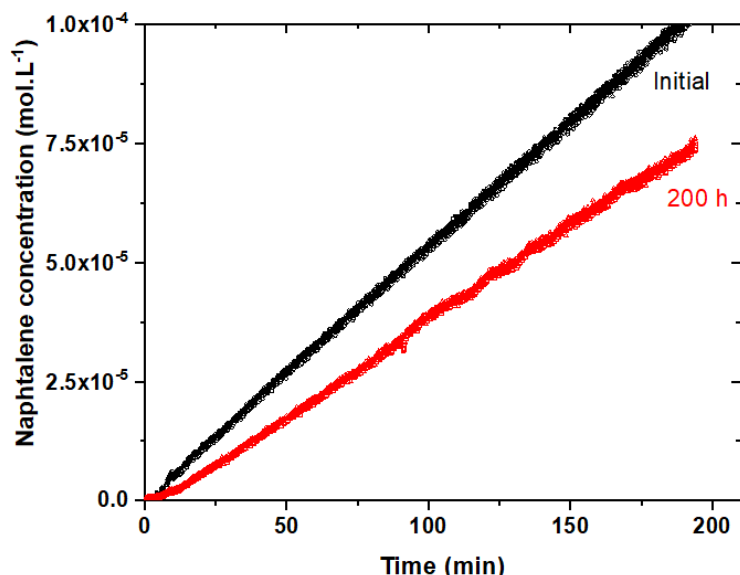


Figure 4.6. Transmission curves of naphthalene in methanolic solution ($4.0 \times 10^{-2} \text{ mol.L}^{-1}$) through a $30 \mu\text{m}$ PE film at room temperature prior to photoaging and after 200 h of photoaging.

Two main conclusions and findings may be extracted from these results: 1. the transmission rate for the non-polar permeant, namely naphthalene, was found to be much higher than that obtained for the polar carbazole, by roughly two orders of magnitude (respectively 5.2×10^{-7} and $6.6 \times 10^{-9} \text{ mol.L}^{-1}.\text{min}^{-1}$ before photoaging), 2. the transmission rate appears to slightly decrease upon photooxidation for naphthalene, which is the opposite result to that obtained for carbazole. The fact that naphthalene presents a higher transmission rate is more likely owing to the statement that non-polar permeant is highly soluble in a non-polar polymer, which is the case for the non-photoaged PE. The change in the polymer polarity upon photoaging could then be the main reason for the observed slight decrease of the transmission rate.

To confirm these results, the transmission experiments were extended to several permeants of different dipole moment by taking care to roughly maintain the main chemical structure (derivatives of naphthalene). From this set of experiments (Table 4.3), one can clearly conclude that polar permeants present smaller transmission rates that significantly increase when photoaged polymers are used by approximately a factor 2.5 - 3.5. The opposite findings were obtained for non-polar permeants, namely higher transmission rates and no significant changes are observed when PE is photoaged (Figure S4.14).

Table 4.3. Transmission rates of various permeants in methanolic solutions ($4.0 \times 10^{-2} \text{ mol L}^{-1}$) in non-photoaged and 200 h photoaged PE films ($30 \mu\text{m}$) at room temperature, minimum and maximum values for transmission rates are also indicated in parenthesis to show the reproducibility.

Permeant	Dipole moment (D)	Transmission rate ($10^{-9} \text{ mol.L}^{-1}.\text{min}^{-1}$)		Ratio $\text{TR}_{200}/\text{TR}_0$
		Non-photoaged polymer TR_0	Photoaged polymer (200 h) TR_{200}	
Naphthalene (C_{10}H_8)	0	520 (503-538)	400 (394-407)	0.77
1,4-dimethyl naphthalene ($\text{C}_{12}\text{H}_{12}$)	0.06	195 (182-207)	190 (183-196)	0.97
2,6-dimethyl naphthalene ($\text{C}_{12}\text{H}_{12}$)	0	760 (783-735)	960 (947-973)	1.26
1-methyl naphthalene ($\text{C}_{11}\text{H}_{10}$)	0.37	210 (207-214)	320 (311-339)	1.52
1-naphthol ($\text{C}_{10}\text{H}_8\text{O}$)	1.29 - 1.49	1.51 (1.47-1.56)	5.30 (4.81-5.60)	3.5
1,4-naphthoquinone ($\text{C}_{10}\text{H}_6\text{O}_2$)	1.36	31 (30.1-33.6)	93 (86.5-98.7)	3.0
2-hydroxynaphthoquinone ($\text{C}_{10}\text{H}_6\text{O}_3$)	2.99	5.0 (4.95-5.27)	12 (11.6-12.5)	2.4
Carbazole ($\text{C}_{12}\text{H}_9\text{N}$)	1.77	6.6 (6.43-6.78)	16.6 (16.2-17.0)	2.5

These results support the fact that the change in the polarity of the polymer upon light irradiation, through the generation of polar functional groups, play an important effect in the alteration of the permeability in liquid phase of polymers. This can vary depending on the polarity of the permeants. As clearly demonstrated, the no photoaged PE, namely non-polar material, was less permeable to polar permeants but the transmission rate increased by a factor of roughly 3 when PE when photoaged for 200 h. This can be explained by the higher solubility of the polar permeants at the surface and/or inside the polymer since the presence of polar functional groups in a polymer can create sites for hydrogen bonding or dipole-dipole interactions. In contrary, for non-polar permeants, the transmission rate was drastically high when no photoaged PE was used and the photoaging leads to small or no change of the permeability in liquid phase (see Figure S4.16). Thus, one should carefully take into consideration the interplay between polarity and of course chemical and physical structures of a polymer for specific intended applications.

2.3. Conclusion

The excitation of Polyethylene, PE, within the range 300 - 420 nm for roughly 300 hours, under our experimental conditions, permits the oxidation of the polymer with the generation of several polar functional groups as monitored by FTIR. Among these groups carbonyls from carboxylic acids esters and lactones and also hydroxyl group. These photoinduced changes in the chemical structure of the initial no polar PE lead more likely to the increase of the dipole moment of the polymer. The transmission FTIR mapping together with the FTIR transmission microscopy permits to deduce that no oxidation profile is seen, and a perfect homogeneous distribution of the polar functional groups is obtained within the thickness of the polymer. The photooxidation of PE shows also a slight increase in the crystallinity (+8%) but no cracks were revealed by AFM imaging experiments.

The transmission rates of several permeants were determined in methanolic solution with a self-designed system and via on-line variation of fluorescence intensity and/or UV-visible absorbance. With initial no polar PE, the transmission rate for no polar permeants was high by a factor of roughly two orders of magnitude when compared to polar permeants. This is more likely linked to the difference in their solubility in the polymer at the feed side of the polymer. When PE is photoaged for 200 hours, an important increase in the transmission rate was observed for polar permeant, by a factor of 2.5 - 3, while for no polar permeant the transmission rate remains roughly constant. This is more likely linked to the increase of the polarity of PE during the photoaging process via the generation of polar functional groups. Thus, the slight increase in the polarity of the polymer permits the establishment of various interactions permeant/polymer leading to the unavoidable increase of the solubility at the feed side of the polymer resulting the in the increase of the transmission rate.

2.4. Acknowledgments

The authors wish to thank the *Université Clermont Auvergne* for financial support (PhD scholarship of Zhouyun Chen). The authors would like also to thank David Bourgoigne Mohammed Houssat for FTIR and AFM imaging and Prof. Jean-Luc Gardette, Dr. Sandrine Therias and Prof. Pierre Olivier Bussiere for the fruitful and helpful discussions.

2.5. Supplementary Information

FTIR transmission spectra of PE films upon photooxidation

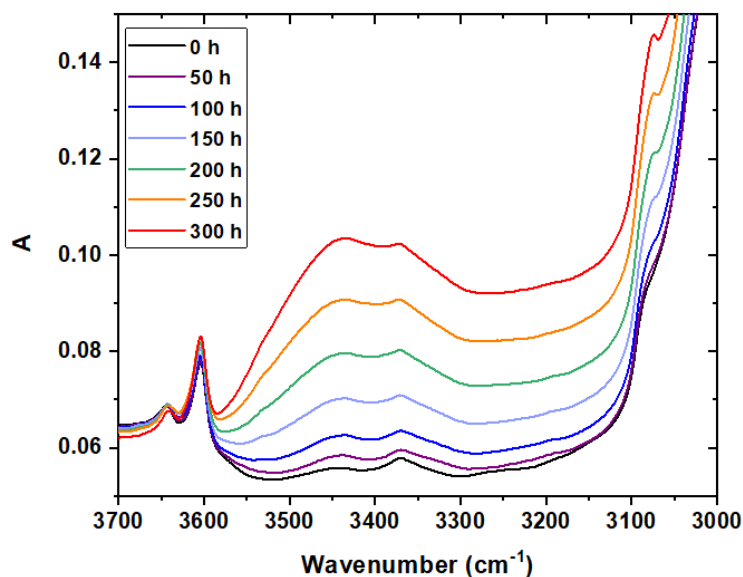


Figure S4.7. Transmission FTIR spectra in the 3700-3000 cm^{-1} region for a PE film (30 μm) upon photooxidation – $I = 90 \text{ W.m}^{-2}$, $T = 55 \text{ }^\circ\text{C}$.

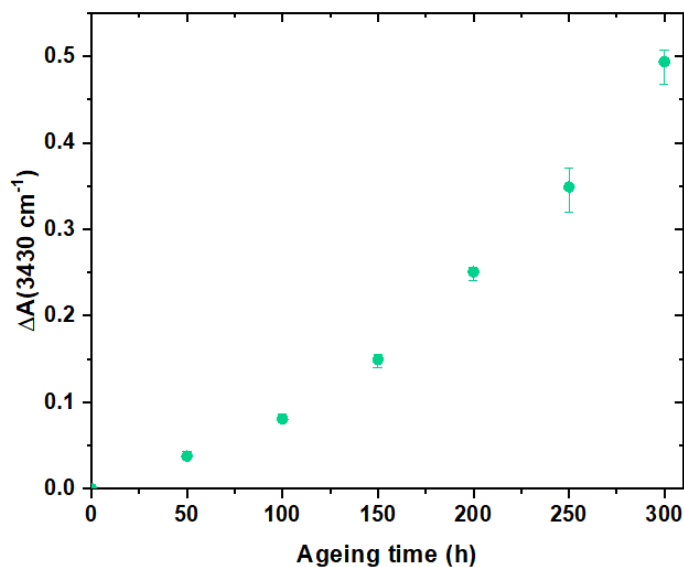


Figure S4.8. Difference of absorbance at 3430 cm^{-1} with respect to unexposed PE film (30 μm) upon photooxidation – $I = 90 \text{ W.m}^{-2}$, $T = 55 \text{ }^\circ\text{C}$. Results are an average from 3 samples, minimum and maximum values are also indicated to show the reproducibility.

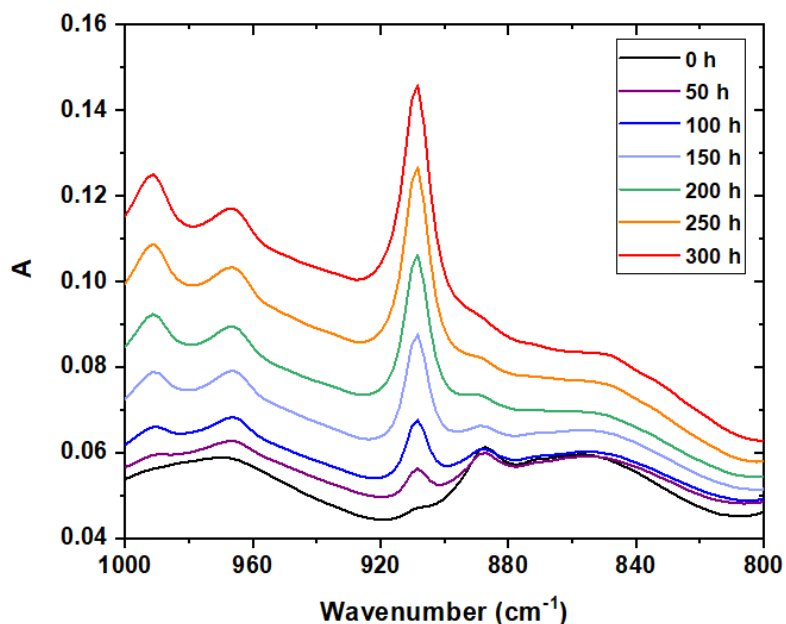


Figure S4.9. Transmission FTIR spectra in the 1000-800 cm^{-1} region for a PE film (30 μm) upon photooxidation – $I = 90 \text{ W.m}^{-2}$, $T = 55 \text{ }^\circ\text{C}$.

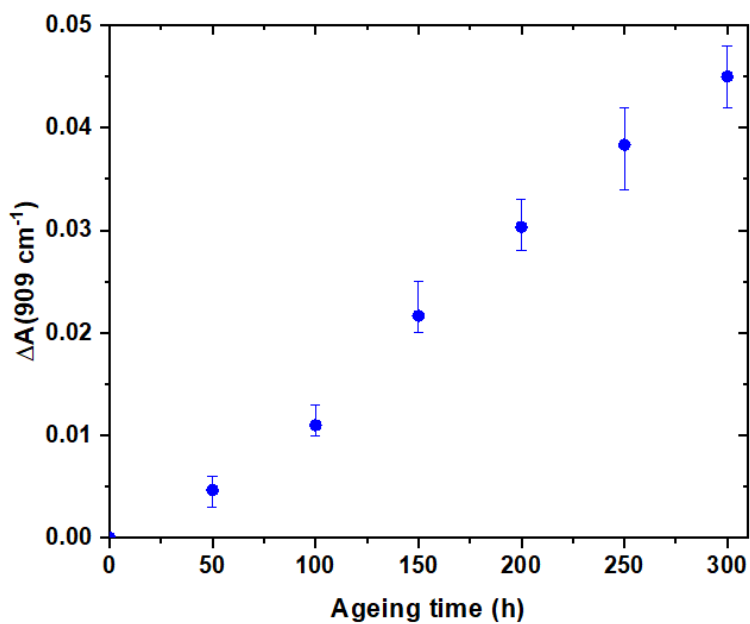


Figure S4.10. Difference of absorbance at 909 cm^{-1} with respect to unexposed PE film (30 μm) upon photooxidation – $I = 90 \text{ W.m}^{-2}$, $T = 55 \text{ }^\circ\text{C}$. Results are an average from 3 samples, minimum and maximum values are also indicated to show the reproducibility.

Change in crystallinity rate upon photooxidation

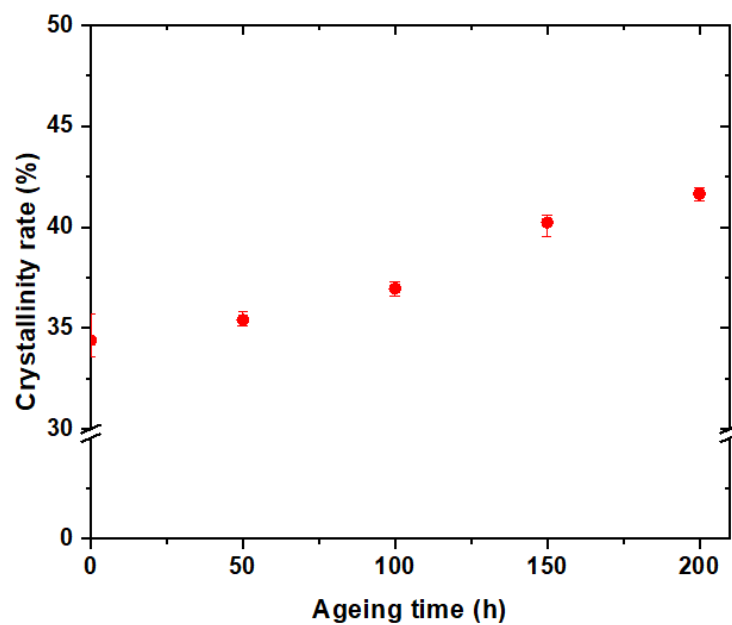


Figure S4.11. Crystallinity rate of PE films (30 μm) upon photooxidation – $I = 90 \text{ W.m}^{-2}$, $T = 55 \text{ }^\circ\text{C}$. Results are an average from 3 samples, minimum and maximum values are also indicated to show the reproducibility.

Transmission rate of carbazole at different PE thicknesses d

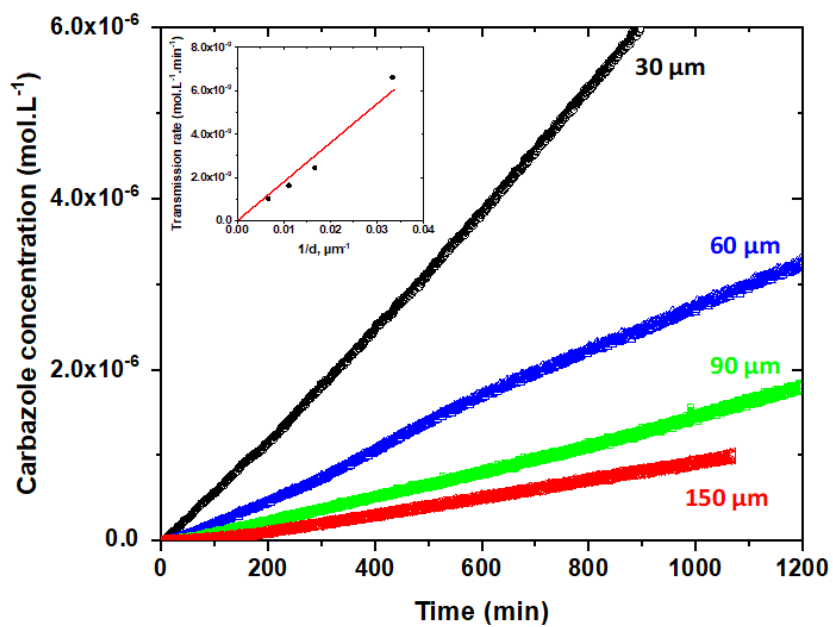


Figure S4.12. Transmission curves of carbazole in methanolic solution ($4.0 \times 10^{-2} \text{ mol.L}^{-1}$) through PE films of different thicknesses d at room temperature. Insert: change of the corresponding transmission rate as a function of d^{-1} .

Transmission activation energy for carbazole in initial and photoaged PE

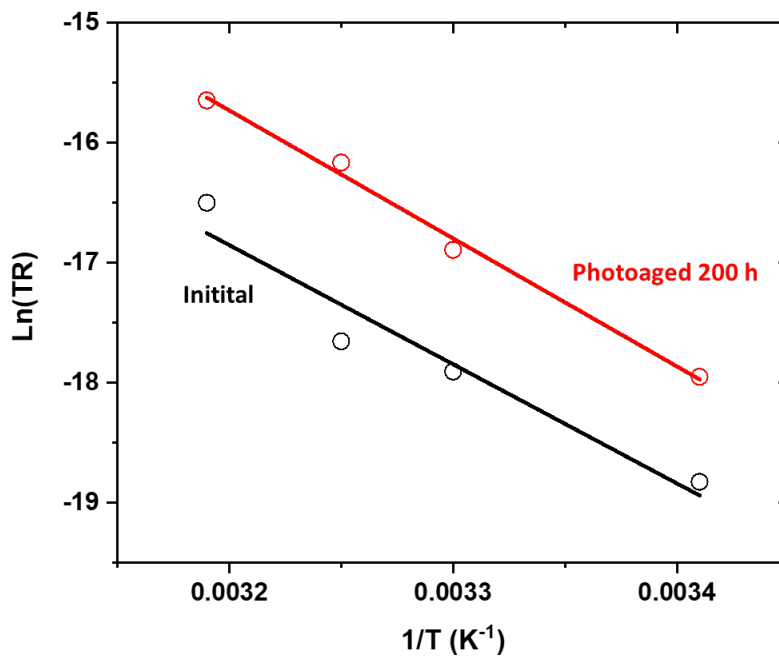


Figure S4.13. Arrhenius plot for the transmission of carbazole in methanolic ($4.0 \times 10^{-2} \text{ mol L}^{-1}$) solution through a $30 \mu\text{m}$ PE film prior to photooxidation (black) and after 200 h of photooxidation (red).

Change in the transmission rate upon photoaging for different thicknesses

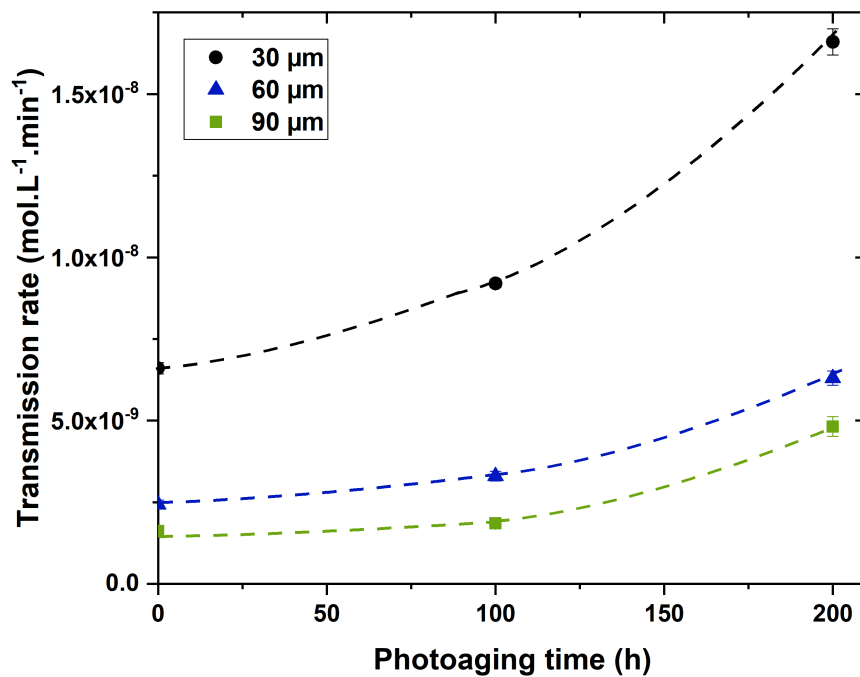


Figure S4.14. Change of the transmission rate of carbazole as a function of photoaging time in methanolic solution ($4.0 \times 10^{-2} \text{ mol L}^{-1}$) through PE films of different thicknesses at room temperature. Results are an average from at least 2 independent samples, minimum and maximum values are also indicated to show the reproducibility.

AFM images of initial and photoaged PE films

Atomic Force Microscopy (AFM) images were obtained in tapping mode with an Innova® atomic force microscope (Bruker), using RTESPA 300 permeants (Bruker) with a nominal tip radius of 8 nm, a spring constant of 40 N.m⁻¹, and a resonance frequency on the order of 300 kHz.

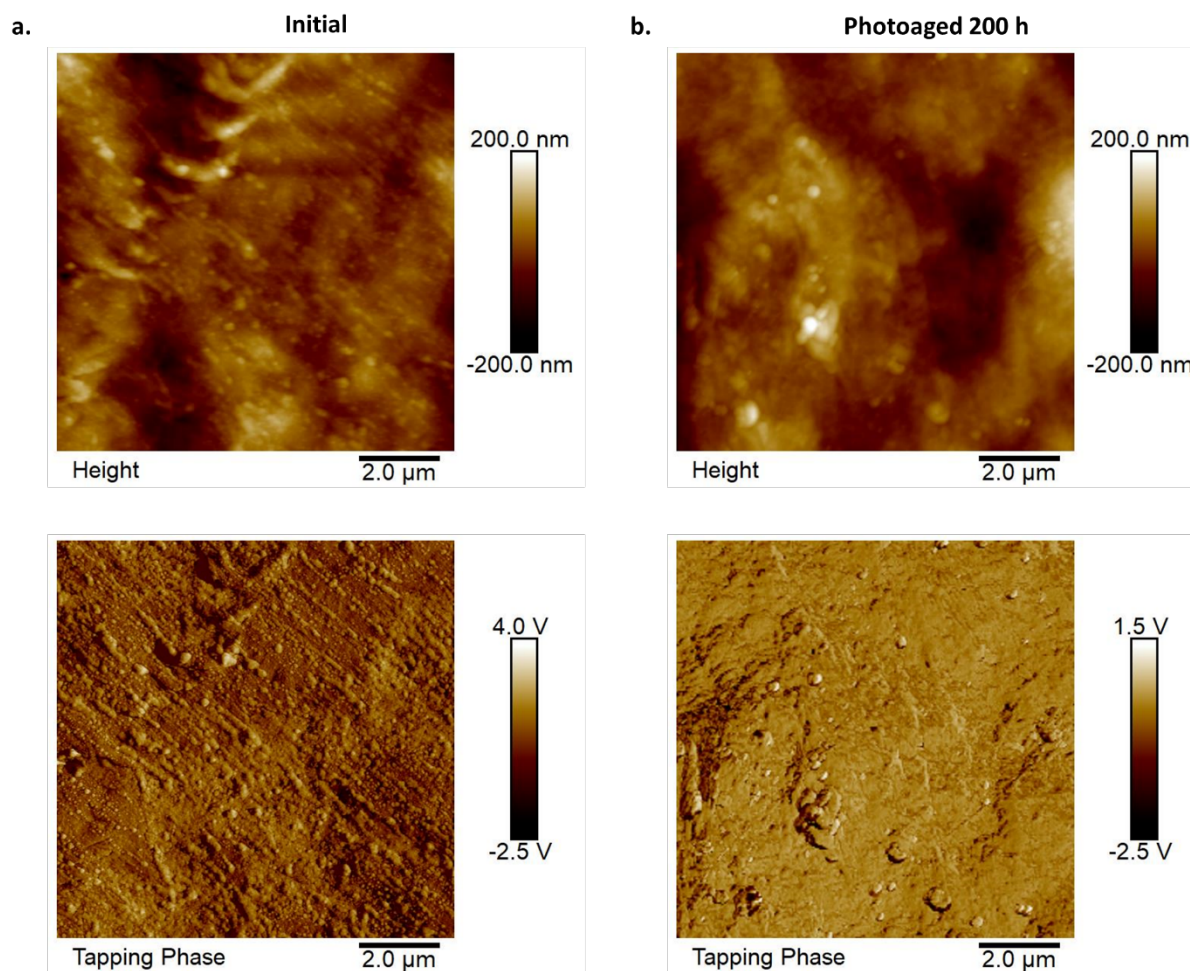


Figure S4.15. Height and phase AFM images of a 30 μm PE film: a. prior to photooxidation, b. after 200 h of photooxidation.

Ratio of transmission rate for the different permeant molecules

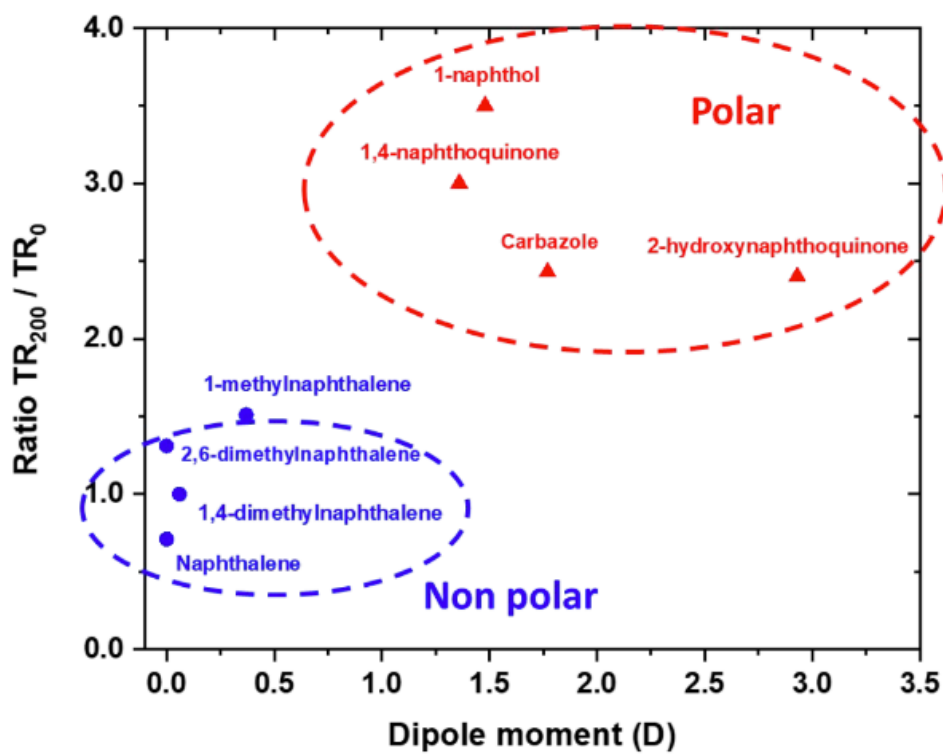


Figure S4.16. TR_{200}/TR_0 ratio (TR_{200} = transmission rate for 200 h photoaging and TR_0 = transmission rate for non-photoaged polymer) for a methanolic solution ($4.0 \times 10^{-2} \text{ mol L}^{-1}$) through a $30 \mu\text{m}$ PE film at room temperature.

References

1. Plastics - the Facts 2022, Plastics Europe, 2022, <https://plasticseurope.org/knowledge-hub/plastics-the-facts-2022> (accessed 2023-05-05).
2. Peacock A. Handbook of polyethylene: structures: properties, and applications. CRC press, 2000.
3. Paxton N C, Allenby M C, Lewis P M, et al. Biomedical applications of polyethylene. European Polymer Journal, 2019, 118: 412-428.
4. SCOTT G. Mechanisms of photodegradation and stabilization of polyolefins. 1976.
5. Ginjac J M, Gardette J L, Arnaud R, et al. Influence of hydroperoxides on the photothermal oxidation of polyethylene. Die Makromolekulare Chemie: Macromolecular Chemistry and Physics, 1981, 182(4): 1017-1025.
6. Gugumus F. Photo-oxidation and Stabilization of Polyethylene//Mechanisms of polymer degradation and stabilisation. Dordrecht: Springer Netherlands, 1990: 169-209.
7. Guadagno L, Naddeo C, Vittoria V, et al. Chemical and morphological modifications of irradiated linear low density polyethylene (LLDPE). Polymer degradation and stability, 2001, 72(1): 175-186.
8. Rivaton A, Gardette J L, Mailhot B, et al. Basic aspects of polymer degradation//Macromolecular Symposia. Weinheim: WILEY-VCH Verlag, 2005, 225(1): 129-146.
9. Gardette M, Perthue A, Gardette J L, et al. Photo-and thermal-oxidation of polyethylene: comparison of mechanisms and influence of unsaturation content. Polymer Degradation and Stability, 2013, 98(11): 2383-2390.

10. Rabek J F. Polymer photodegradation: mechanisms and experimental methods. Springer Science & Business Media, 2012.
11. Socrates G. Infrared and Raman characteristic group frequencies: tables and charts. John Wiley & Sons, 2004.
12. Briassoulis D, Aristopoulou A, Bonora M, et al. Degradation characterisation of agricultural low-density polyethylene films. *Biosystems engineering*, 2004, 88(2): 131-143.
13. Klopffer M H, Flaconnèche B. Transport properties of gases in polymers: bibliographic review. *Oil & Gas Science and Technology*, 2001, 56(3): 223-244.
14. Cussler E L. Diffusion: mass transfer in fluid systems. Cambridge university press, 2009.
15. Robertson G L. Food packaging: principles and practice. CRC press, 2005.
16. George S C, Thomas S. Transport phenomena through polymeric systems. *Progress in Polymer science*, 2001, 26(6): 985-1017.
17. Siracusa V. Food packaging permeability behaviour: A report. *International Journal of Polymer Science*, 2012, 2012.
18. Fayolle B, Richaud E, Colin X, et al. Degradation-induced embrittlement in semi-crystalline polymers having their amorphous phase in rubbery state. *Journal of materials science*, 2008, 43: 6999-7012.
19. Collin S, Bussière P O, Therias S, et al. Physicochemical and mechanical impacts of photo-ageing on bisphenol a polycarbonate. *Polymer degradation and stability*, 2012, 97(11): 2284-2293.
20. Moisan J Y. Effects of oxygen permeation and stabiliser migration on polymer degradation//Polymer permeability. Dordrecht: Springer Netherlands, 1985: 119-176.
21. Michaels A S, Parker Jr R B. Sorption and flow of gases in polyethylene. *Journal of Polymer Science*, 1959, 41(138): 53-71.

22. Rabek J F. Photodegradation of polymers: physical characteristics and applications. Springer Science & Business Media, 2012.

Chapter 5: Permeability in gas phase on polyethylene

1. Introduction

The fifth chapter of this thesis is dedicated to the study of the gas permeability of given organic vapours through polyethylene (PE) and the possible effect of the photoaging on such process. In contrast to the study undertaken in Chapter 4, this part of the study will rule out any implication of the solvent in the permeability process, and thus the results will then be directly connected to the permeant in its gas state. The study was performed using permeants of various polarities, sizes, and structures. The chosen permeants are methanol, ethanol, hexane, and cyclohexane and the gravimetric approach was used to evaluate the transmission rate of the permeant. A high-precision balance was then used for the determination of the mass loss at a given time and at a constant temperature. The gravimetric measurements offer a relatively robust method for the evaluation of the permeability and to study the dynamics of permeant flow in the polymer. However, it is essential to perform multiple experiments under highly controlled conditions to ensure the reliability of gravimetric experiments and avoid issues such as leaks (that represent a usual problem for these kinds of experiments).

This chapter will then present, first, the results obtained for the permeability of polar compounds (methanol and ethanol) and, second, that for non-polar permeants (cyclohexane and hexane) in polyethylene. The effect of photoaging on such permeability was considered. However, it should be noted that this study is still preliminary, and the discussion will be limited and reasoned based on the obtained results. Nevertheless, presenting this part in the manuscript will permit us to have better knowledge concerning the transmission rate of some permeants in the absence of the solvent, since the latter plays without any doubt a significant role in this type of process.

2. Results and discussion

2.1. Transmission rates of polar vapours

The measurements of the permeability for methanol and ethanol in their gas phase through polyethylene (PE) were performed using bottles of a total volume of 40 mL (as thoroughly presented in [Chapter 2 4.2.3](#)). The surface of the polymer film (30 μm thickness) that covers the entire open part of the bottle was roughly 3.14 cm^2 . The total amount of the liquid phase (methanol or ethanol) was constant at approximately 33 mL and created, when the bottle was sealed with the polymer, a given vapour pressure that depends on the temperature. Such pressure represents the driving force for the permeant to diffuse through the thickness of the polymer and escape from the bottle at the opposite side. The gravimetric experiment appears then to be appropriate for such a study, at a constant and controlled temperature of 40 $^{\circ}\text{C}$.

Under these precise conditions, the mass loss of methanol (or ethanol) as a function of time was followed as represented in Figure 5.1. This shows the typical change observed under the used experimental conditions. It clearly demonstrates that for both permeants (methanol and ethanol), the mass loss is effective but relatively small. Moreover, two key points can be extracted from this experiment: 1. no lag period was observed under our experimental conditions; 2. the dynamic equilibrium was rapidly reached, giving rise to linear plots that permit the determination of the transmission rate for both permeants. These were evaluated to 5.6×10^{-3} and 3.5×10^{-3} $\text{g}\cdot\text{h}^{-1}$ for methanol and ethanol, respectively. Owing to the difference in their vapour pressure (Table 5.1) and chemical structure, as well as the difference in interactions between the polymer and the

permeants, the obtained transmission rates cannot be compared directly. However, they will be compared for each permeant with their corresponding values obtained with photoaged PE.

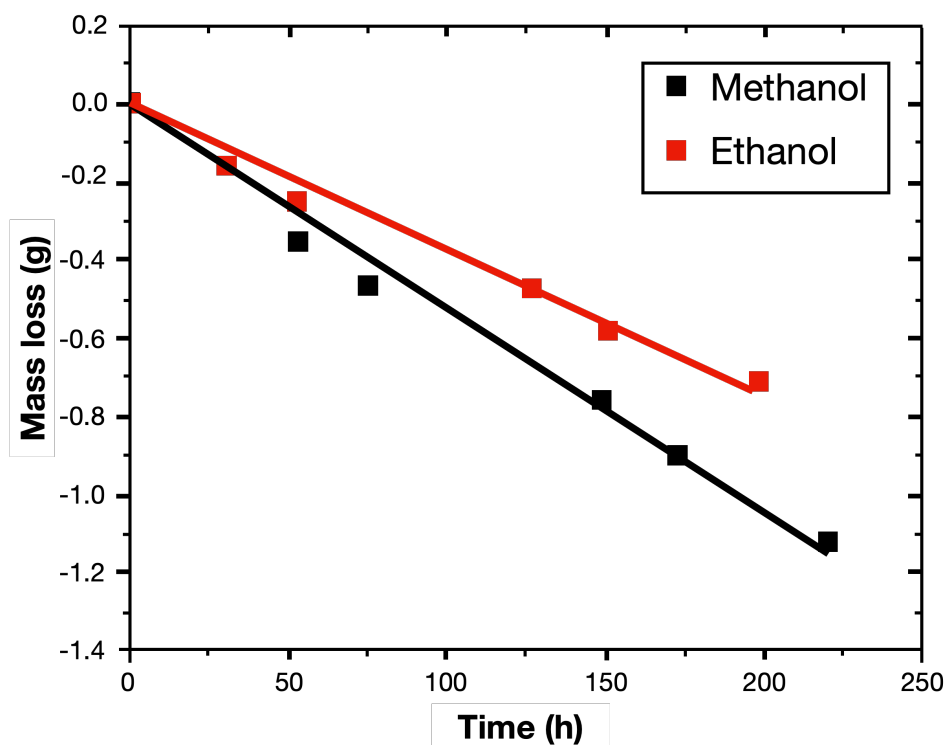


Figure 5.1. Mass loss versus time for the transmission of methanol and ethanol through non-photoaged PE (thickness = $30\mu\text{m}$) at $40\text{ }^\circ\text{C}$.

Table 5.1. Transmission rate through non-photoaged PE, and vapour pressure for methanol and ethanol; minimum and maximum values are also indicated in parenthesis to show the reproducibility.

Permeant	Transmission rate ($\text{g}\cdot\text{h}^{-1}$)	Vapour pressure [1] (kPa)
Methanol	5.6×10^{-3} ($4.8\text{-}6.1\times 10^{-3}$)	35.1
Ethanol	3.5×10^{-3} ($3.1\text{-}3.8\times 10^{-3}$)	19.1

To explore the effect of PE photooxidation on its barrier properties, the experiments were performed after 100 hours of photoaging to keep the film strong enough. The results for methanol, given in Figure 5.2, clearly show that the transmission rate increased by roughly 20 % when compared to the value obtained for non-photoaged polymer ($6.7 \times 10^{-3} \text{ g.h}^{-1}$). For ethanol, the increase was slightly higher: 28.5 %. ($4.5 \times 10^{-3} \text{ g.h}^{-1}$) (Table 5.2).

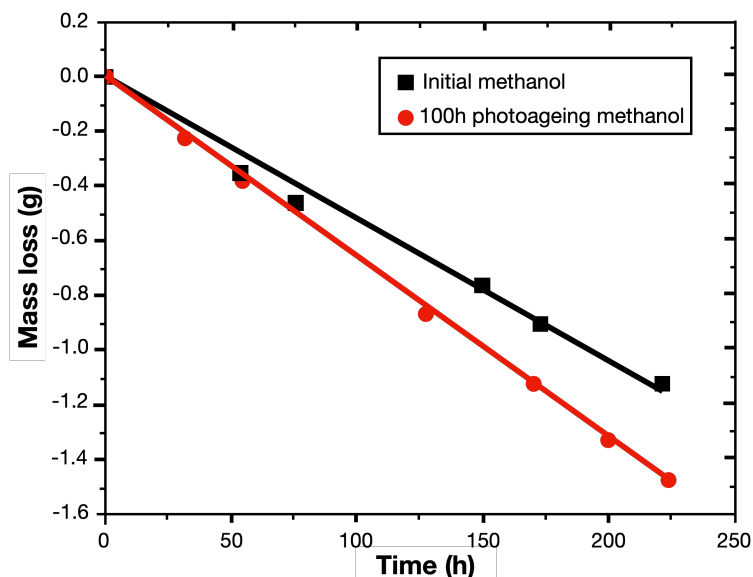


Figure 5.2. Mass loss versus time for the transmission of methanol through non-photoaged and photoaged PE (100 hours; $30\mu\text{m}$) at 40°C .

Table 5.2. Dipole moment and transmission rate through PE for methanol (MeOH) and ethanol (EtOH) upon photoaging of PE; minimum and maximum values are also indicated in parenthesis to show the reproducibility.

Photoaging time (hours)	Permeant	Dipole moment [2], D	Average transmission rate (g.h^{-1})
0	MeOH	2.37	5.6×10^{-3} ($4.8\text{-}6.1 \times 10^{-3}$)
100			6.7×10^{-3} ($6.3\text{-}7.3 \times 10^{-3}$)
0	EtOH	2.64	3.5×10^{-3} ($3.1\text{-}3.8 \times 10^{-3}$)
100			4.5×10^{-3} ($4.2\text{-}5.0 \times 10^{-3}$)

Such increases in the transmission rate for methanol and ethanol clearly reveal a change in the polymer permeability upon photoaging. As demonstrated experimentally in [Chapter 4 2.2.1](#), the polarity of the permeants would be here the guideline for the discussion of the results. The photooxidation of the initially non-polar PE leads to an increase in its polarity via the generation of chemical groups such as carbonyls and hydroxyls within the whole thickness of the polymer. Thus, this photogenerated PE polarity will favour polar molecules' interaction with the polymer's at the feed surface through dipole-dipole interaction and/or other intermolecular forces. This will undoubtedly lead to the increase of the solubility and thus to the rise in the number of molecules diffusing throughout the polymer thickness. To confirm such findings, experiments were undertaken using two non-polar permeants, hexane and cyclohexane.

2.2. Transmission rates of non-polar vapours

As shown in Figure 5.3, the mass loss obtained for hexane and cyclohexane using non-photoaged PE was significantly higher than that obtained with polar permeants. The transmission rates were estimated from the slopes of the linear plots and found to be equal to 0.159 and 0.101 g.h⁻¹ for hexane and cyclohexane, respectively. The high transmission rates are clearly explained by the higher solubility of the non-polar permeant in non-photoaged PE (non-polar). This clearly indicates the effect of the polarity of both the permeant and the polymer on the permeability.

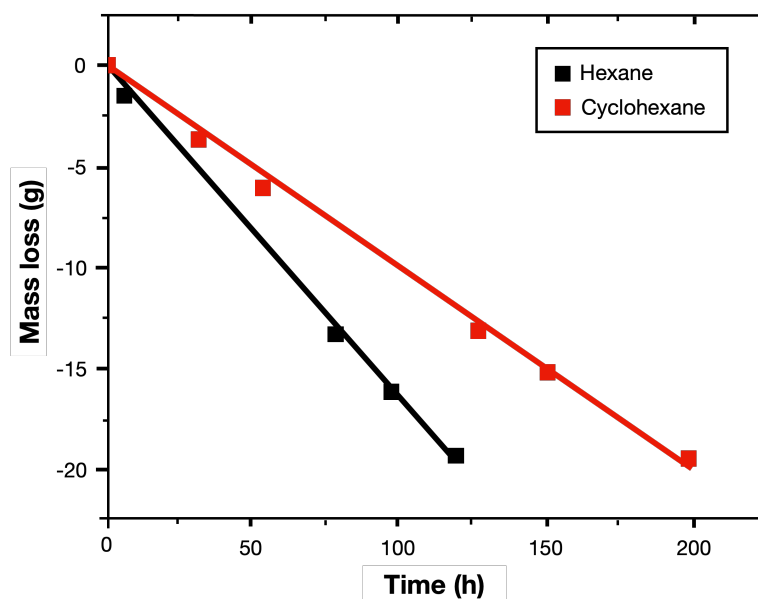


Figure 5.3. Mass loss versus time for the transmission of hexane and cyclohexane through non-photoaged PE (thickness = 30 μ m) at 40 °C.

When photoaged PE is considered, a decrease in the transmission rate for hexane, as shown in Figure 5.4, was observed. Similar results were also found for cyclohexane. The decrease was evaluated to 13 % and 17 % for hexane and cyclohexane, respectively (Table 5.3). This is more likely owing to the slight increase of the polarity of photoaged PE which prevents non-polar permeant from being attracted by the polymer at its feed side. This leads then to a decrease in the number of molecules diffusing through the polymer thickness.

Such conclusions perfectly fit with the results extracted from the transmission rate in the liquid phase ([Chapter 4 2.2.2](#)).

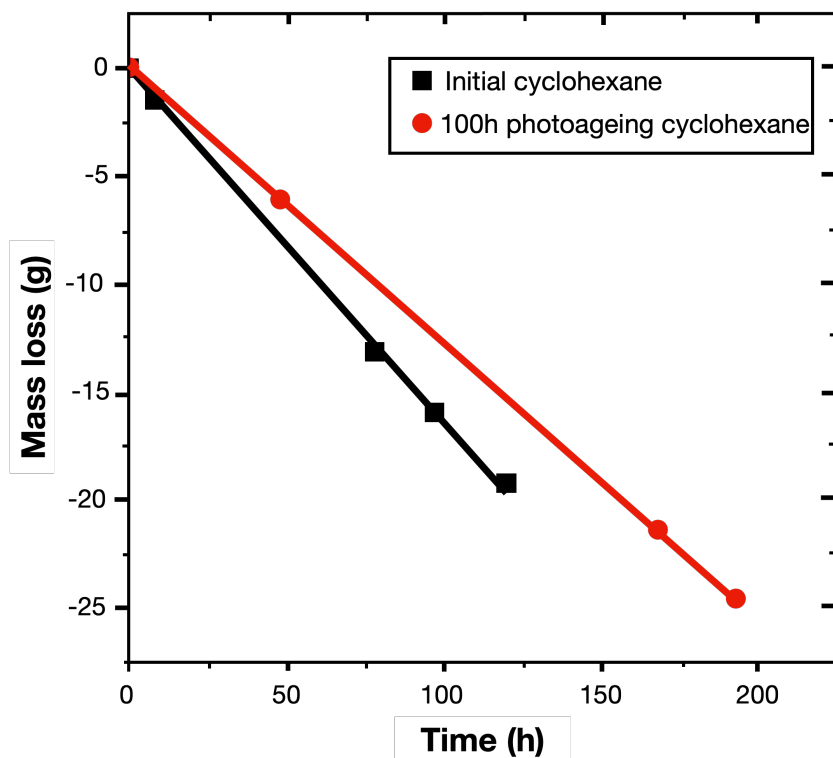


Figure 5.4. Mass loss versus time for the transmission of cyclohexane through non-photoaged and photoaged PE (100 hours; 30 μ m) at 40 °C.

Table 5.3. Dipole moment and transmission rate through PE for hexane and cyclohexane upon photoaging of PE, minimum and maximum values are also indicated in parenthesis to show the reproducibility..

Photoaging time (hours)	Permeant	Vapour Pressure [1] (kPa at 40 °C)	Average transmission rate (g.h ⁻¹)
0	Hexane	39.6	0.159 (0.151-0.173)
100			0.137 (0.127-0.143)
0	Cyclohexane	23.6	0.101 (0.096-0.120)
100			0.0832 (7.20-8.90 $\times 10^{-2}$)

It should be pointed out that the shape of the permeants also plays an important role in the permeation process (as demonstrated in [Chapter 1 2.3.3](#)). It is known that the n-alkanes, elongated or flattened molecules, present higher diffusivity [3] and solubility [4] than the spherical molecules with similar size and mass. This effect may partly explain why hexane presents a higher transmission rate than cyclohexane, however, the higher vapour pressure of hexane may also be a positive factor for this. Therefore, further study is warranted to determine the roles of multiple factors, including permeant's vapor pressure and shape, in influencing the transmission rate.

It is clear here, particularly after these preliminary findings, that more experiments should be performed using various gases of various polarities on different polymer structures. These experiments will represent a decent guideline for us to draw general and relevant conclusions.

3. Conclusion

When dealing with a permeant in its gas state, the permeation process is only owing to the interactions between the polymer and the permeant. In the case of PE, where the polymer turns polar after photoaging, distinct conclusions can be drawn for polar and non-polar permeants. Transmission rates are lower for polar vapours for all aging times, owing to the low affinity between them and PE. However, such rates increase upon photooxidation for polar molecules, while they decrease for non-polar ones. This is attributed to the increase in PE polarity caused by the photooxidation process. These experiments showed that among the various factors, the increase of the polarity of the polymer during photoaging is clearly one of the factors that play a role in the change of the permeability of the polymer.

References

1. Yaws C L. The Yaws handbook of vapor pressure: Antoine coefficients. Gulf Professional Publishing, 2015.
2. Jorge M, Gomes J R B, Barrera M C. The dipole moment of alcohols in the liquid phase and in solution. *Journal of Molecular Liquids*, 2022, 356: 119033.
3. Berens A R, Hopfenberg H B. Diffusion of organic vapors at low concentrations in glassy PVC, polystyrene, and PMMA. *Journal of Membrane Science*, 1982, 10(2-3): 283-303.
4. Rogers C E. Permeation of gases and vapours in polymers//Polymer permeability. Dordrecht: Springer Netherlands, 1985: 11-73.

General conclusion & perspectives

General conclusions

This thesis project tries to reveal the relationship between the photoaging and permeability of polymers. It focuses on the oxygen permeability as well as the permeability of various other permeants in liquid and gas states.

The polymers of the study are polycarbonate (PC) and polyethylene (PE), both of which are commonly used in scenarios where they are exposed to light-induced degradation. After exposure to light, these polymers undergo photochemical degradation, leading to irreversible changes in their properties (chemical, mechanical, and optical), which should also affect their permeability. The techniques used to measure permeability, in addition to commercially available methods, have also been developed using an experimentally self-designed setup, which has been proven to be reliable and convenient for permeability measurements. The thesis project fills the blank of polymer material science by studying this relationship in a fairly methodical approach.

The first part of the project (Chapter 3) consists of the study of photoaging of PC and PE, and the oxygen permeability changes:

- Infrared spectra (FTIR) in transmission mode shows changes upon exposure of sequential photoaging of PC samples, with the appearance and growth of carboxylic acids, anhydrides, and hydroxyl compounds. UV-visible spectra confirms the limit of photooxidation due to sample yellowing, hindering further light penetration. The cross-linking occurrence has been observed by the increase of Vickers micro-hardness and gel fraction during photoaging. ATR-FTIR spectra and transmission FTIR microscopy demonstrate that oxidation products are

predominantly formed on the exposed surface, confirming the surface-based nature of photooxidation. The estimated oxidation depth in PC films is approximately $30 \pm 5 \mu\text{m}$.

- When side #1 of PC underwent photoaging, the permeation coefficient P decreases significantly (-49 %) within 500 hours. This decrease results from a reduced solubility coefficient S (-47 %) rather than that of the diffusion coefficient D (-8 %). This is due to localized oxidation at the surface, affecting dissolution. Two effects from photooxidation contribute to P reduction: the appearance of polar groups and cross-linking, both decreasing polymer-oxygen interactions and oxygen solubility. Polar groups, which reduce interactions between the polymer and oxygen, decrease oxygen solubility. The interactions further enhance the polymer-polymer cohesive energy, leading to a decrease in oxygen diffusivity. Cross-linking reduces available absorption sites and limits oxygen diffusion. The photoaging of side #2 leads to similar consequences as observed for side #1, in terms of the appearance of extra polar groups and cross-linking. However, P does not result in a further decrease. This can be explained by the "funnel effect", where the oxidation of side #1 already limits the entire permeation process, primarily through a reduction in solubility at its surface. The degradation of side #2 to the same extent as side #1 did not significantly modify the measured value of P.
- PE photoaging, limited to 200 hours due to the risk of film rupture, leads to increased polarity due to the formation of polar functional groups such as carbonyls (C=O) and hydroxyl functions (O-H). This alters the material's interactions with permeants and its cohesive energy. Cross-sectional FTIR mappings reveal homogeneity in oxidation across the thickness of $90 \mu\text{m}$ film samples. DSC analysis shows an 8 % increase in PE crystallinity rate after 200 hours of photoaging, potentially impacting permeability. AFM measurements confirm the absence of crack formation during the process.

- P (oxygen permeability coefficients) of PE at different temperatures (from 10 to 50 °C) and photoaging times show a typical increase in permeability with rising temperature. The decrease in P during photoaging may be attributed to the combined effects of polar oxidation products and increased crystallinity. Simultaneous decreases (15 %) in D and S confirm the homogeneity of PE photoaging.

This part correlates primarily with the oxygen permeability and changes during photoaging. Notably, changes in polarity exert a substantial influence on the permeation of non-polar oxygen molecules. Factors such as changes in crystallinity, the occurrence of cross-linking, and variations in surface morphology are pertinent aspects to consider when explaining the mechanisms of permeability alterations.

The second part of the project (Chapter 4) focuses on exploring the permeability of PE in the liquid phase. It corresponds to evaluating the transmission rate using carbazole (a highly fluorescent compound) with non-photoaged PE samples to validate the custom-designed equipment. The study is extended to the impact of parameters like polymer thickness on lag period and transmission rate. It is also extended to the analysis of how photoaging affects the transmission rate of carbazole, particularly in terms of polarity changes. Furthermore, the influence of photoaging with various permeants (naphthalene derivatives with different dipole moments) on the transmission rate is also explored:

- The transmission rate of permeants in methanol solutions depends on their polarity. Initially, with non-polar PE, non-polar permeants exhibit higher transmission rates, likely due to higher solubility at the feed side of non-polar polymer.

- After 200 hours of photoaging, polar permeants' transmission rate significantly increase (2.5 - 3 times), while non-polar permeants showed minimal changes. This increase is attributed to the enhanced polarity of PE after photoaging, enabling various permeant-polymer interactions and increasing solubility at the feed side of the polymer. Photooxidation of PE generates polar functional groups, potentially increasing the polymer's dipole moment. Additionally, a slight increase in crystallinity (+8 %) is observed without crack formation.

This part of the study demonstrates that photoaging of PE leads to changes in its chemical structure, increased polarity, and enhanced transmission rates for polar permeants, highlighting the significance of polarity in permeation processes.

The third part of the project (Chapter 5) concerns the evaluation of the permeability of four organic vapours through PE using a gravimetric method. This study could also rule out the role played by the solvent while studying the permeability in solutions. This part focuses on the polarity changes during PE photoaging and their consequences on permeability. Two polar and two non-polar gases are used to evaluate and predict the gas transmission rate preliminarily:

- In the case of PE, which changes from non-polar to polar after photoaging, the transmission rates of the two polar gases are initially low with a slight increase following photoaging. Conversely, the transmission rate of non-polar gases is initially higher but decreases after photoaging. This would be attributed to the change in polarity of PE upon photoaging.

These preliminary experiments provide clues about the influence of polymer photoaging, polarity differences in polymers, and the properties of the permeating substances on transmission rates.

In conclusion of these chapters, this study tries to answer the question of "How does the photoaging of polymer affect its permeability?" The study uses three approaches in general. Firstly, change the polymers by selecting two polymers of PC and PE that differ in initial polarity, crystallinity rate, and photoaging mechanism. In both of them, the formation of carbonyl and hydroxyl groups, upon photoaging, changes the polarity. Cross-linking in PC and crystallinity rate increase in PE are presented. Funnel effect is presented for the results of the oxygen permeability in PC during sequential photoaging.

Secondly, change the permeants. In this study, the focus lies on the polarity of the permeant properties. By changing different polarities in gas and liquid phases, the permeants and polymers with similar polarity show high permeability.

Last but not least, change the environment. The temperature was modified in the oxygen and liquid permeability experiments in PE. Oxygen permeability increases with temperature for PE. 38 kJ.mol⁻¹ activation energy was calculated in PE oxygen permeation.

Finally, during this study, the processes of analysing permeability for PC and PE would be a good workflow for the other polymers that could be analysed with different permeabilities. Moreover, this study fairly addresses a gap in this subject, which has the potential to enhance the understanding of polymer applications and modifications, such as medical devices and packaging. The techniques employed throughout this study, including fluorescence spectroscopy, UV-visible spectroscopy and GC-MS in analysing various permeants, hold substantial value for advancing the field of permeability measurements. These methodologies can serve as valuable tools for future research and development in this area, offering insights and data that can contribute to refining and optimizing polymer-related applications and modifications.

Perspectives

Despite the different answers provided by this study, numerous perspectives and areas of work can be proposed to promote further improvement and innovation of polymer materials and permeability studies.

- Analysis of activation energy of permeation

The experiments involving the Arrhenius plot in Chapter 3, which focused on the oxygen permeability of PE, did not reveal any significant changes in activation energy during the photoaging process. However, this intriguing observation warrants further investigation. Considering the observed changes in PE during photoaging, it is reasonable to suspect that the activation energy may vary under specific conditions.

To delve deeper into this phenomenon, a potential way could involve using PE samples subjected to more extended photoaging times, notably thicker samples. This approach may provide more conclusive insights into the activation energy of permeation and how it evolves during the photoaging process. Additionally, exploring alternative methods to measure the energy associated with different permeation steps could offer a valuable perspective.

- Analysis of time-lag of the permeant transmission of PE in the liquid phase

The concept of time-lag was introduced in Chapter 4, but its systematic exploration was limited due to the extended duration required for testing and visualizing time-lag effects. Nonetheless, investigating time-lag is crucial because it can offer a comprehensive understanding of the permeation process and provide valuable insights when comparing experiments. Hence, a more comprehensive and systematic study of time-lag is warranted, as it has the potential to illuminate critical aspects of the permeation phenomenon and its behaviour under varying conditions.

- Analysis of gas transmission rate in PC

To further solidify the findings in Chapter 5, additional experiments involving a more comprehensive range of gases and varying polymer thicknesses should be conducted. Expanding the scope of the research to encompass more results and a greater diversity of gases will enhance the reliability and comprehensiveness of the analysis. Additionally, investigating how different polymer thicknesses impact the photoaging process can provide valuable insights into the phenomenon.

- Other factors towards the permeability

Generally speaking, this study focused more on the polarity of the permeants' and polymers' influence on permeability. However, it is essential to analyse other factors, such as molecule size and shape, and/or vapor pressure for permeants; cross-linking, and/or crystallinity rate for polymers, and their influences on the permeability.

Abstract

Polycarbonate (PC) and polyethylene (PE) are common daily polymers. In their typical usage scenarios, these materials can undergo the phenomenon of photoaging. Photooxidation can lead to various consequences, including property degradation and surface changes. This study aims to take a comprehensive approach to investigate photoaging's impact on PC and PE's permeability. Several testing methods (oxygen permeability, transmission rate determination, and Arrhenius plots) were employed to describe and measure permeability during the photoaging of PC and PE. The consequence of PC and PE photoaging was verified using different approaches (micro-hardness, infrared microscopy, DSC, etc.). "Funnel effect" of oxygen permeability was observed in sequential photoaged PC, relating to the surface oxidized layer in the sample. Arrhenius plot of the permeation process was verified (from 10 to 50 °C) throughout the photoaging of PE. A self-designed experimental system was constructed and proven reliable for measuring permeability in the liquid phase. The effects of the permeant were also observed in both liquid and gas phase permeability.

Keywords: Photooxidation, Permeability, Polymer degradation, Permeation, Diffusion, Sorption

Résumé

Le polycarbonate (PC) et le polyéthylène (PE) sont deux polymères courants dans la vie quotidienne. Dans leurs scénarios d'utilisation habituels, ces matériaux peuvent subir le phénomène de photovieillissement. La photooxydation peut entraîner diverses conséquences, notamment la dégradation des propriétés et des modifications de surface. Cette étude vise à adopter une approche globale pour étudier l'impact du photovieillissement sur la perméabilité du PC et du PE. Plusieurs méthodes d'essai (perméabilité à l'oxygène, détermination du taux de transmission et tracés d'Arrhenius) ont été utilisées pour décrire et mesurer la perméabilité pendant le photovieillissement du PC et du PE. Les conséquences du photovieillissement du PC et du PE ont été vérifiées en utilisant différentes approches (microdureté, microscopie infrarouge, DSC, etc.). Un « effet entonnoir » de la perméabilité à l'oxygène a été observé dans le PC photovieilli de manière séquentielle, en relation avec la couche oxydée en surface de l'échantillon. Le tracé d'Arrhenius du processus de perméation a été vérifié (de 10 à 50 °C) tout au long du photovieillissement du PE. Un système expérimental a été construit et s'est avéré fiable pour mesurer la perméabilité en phase liquide. Les effets du perméant ont également été observés dans la perméabilité en phase liquide et gazeuse.

Mots-clés: Photooxydation, Perméabilité, Dégradation des polymères, Perméation, Diffusion, Sorption